FINAL REPORT

THEORETICAL AND EXPERIMENTAL STUDY OF LOW-VELOCITY PENETRATION PHENOMENA

Contract No. DA 19-129-AMC-150(X)

UTAH RESEARCH & DEVELOPMENT CO., INC.

SALT LAKE CITY, UTAH

Subsidiary of Interstate Engineering Corporation, Anaheim, California

SPONSORED BY:

Advanced Research Projects Agency
U. S. Army Natick Laboratories
Natick, Massachusetts

ARPA Order No. 267

FINAL REPORT

THEORETICAL AND EXPERIMENTAL STUDY OF LOW-VELOCITY PENETRATION PHENOMENA

Contract No. DA 19-129-AMC-150(X)

UTAH RESEARCH & DEVELOPMENT CO., INC.
1820 South Industrial Road
Salt Lake City, Utah 84104

Phone: 801/486-1301

The findings in this report are not to be construed as an official Department of the Army position, unless so designated by other authorized documents.

Citation of trade names in this report does not constitute an official indorsement or approval of the use of such items.

DDC AVAILABILITY NOTICE

Distribution of this document is unlimited.

DISPOSITION INSTRUCTIONS

Destroy this report when no longer needed. Do not return it to the originator.

TABLE OF CONTENTS

TABLE OF CONTENTS (Continued)

TABLE OF CONTENTS (Continued)

LIST OF FIGURES

PART I.

LIST OF FIGURES (Continued)

LIST OF FIGURES (Continued)

LIST OF FIGURES (Continued)

LIST OF TABLES

PART I.

PART II.

LIST OF TABLES (Continued)

APPENDIX

LIST OF TABLES (Continued)

LIST OF TABLES (Continued)

ABSTRACT

This final report on Contract DA 19-129-AMC-150(X) reports the development of a computer code for solving impact problems. The code uses moving mass points which have all the field variables such as pressure, energy, and stress associated with the points. The fields and their gradients determine the forces on the masses and change as the points move. The code was tested in a one-dimensional problem where it was found to produce correct results. The ideas embodied in this work appear to have sufficient value to justify research to extend them to three-dimensional impact problems.

An investigation was carried out on equations of state for materials of interest in armor development. A summary of existing data is given. A simple equation is given for the shock compression of metals and other materials and a computer code is given for calculating adiabatic expansions from a shock-compressed state.

A complete report is given on an experimental program to measure material properties. The emphasis in the work is on measuring the energy involved in large-scale deformation of materials. Measurements were made by crushing disks of the test material in testing machines and by ballistic impacts. Measurements were also made on rod-to-rod impacts and on impacts of steel balls on thin plates of the test materials. Ultimate strength of materials was measured by measuring maximum acceleration of a free surface in rod-to-rod impact. Techniques and results of the research are reported.

INTRODUCTION

This final report on Contract DA 19-129-AMC-150(X) covers the period from May 1964 to August 1966. All research from May 1964 to December 1965 has been previously reported in semiannual technical reports dated November 1964, May 1965 and December 1965. The present report covers the period January 1966 to August 1966. A Table of Contents and an Abstract are given in Appendix A for each of the previous semiannual reports. They will be summarized here in a general way where necessary to serve as background for the portion of the work covered in detail in this report.

The purpose of the research conducted under Contract DA 19-129-AMC-150(X) has been to develop methods for predicting the behavior of complex materials under the impact of high-speed projectiles. The velocity range of interest is from a few hundred to a few thousand feet per second. This covers the range of shell-fragment and bullet velocities and excludes the hypervelocity range associated with space vehicles and meteors.

To meet this goal, the work has centered around the development of a theoretical model which describes the transient motion and state of the materials under impact conditions. Because of the velocity range, effects associated with strength of materials, viscosity, and elasticity are important as well as the inertial effects which predominate at higher velocities. The mathematical models used are put in forms suitable for computer solution.

To support this theoretical work, an investigation of material properties under dynamic conditions has been conducted. This has consisted of an investigation of the work of others and original experimental measurements of some material properties. From this work, suitable equations of state have been developed for the computer program. These are simplified but appear to adequately represent material behavior in impact. In the experimental program, the greatest emphasis has been placed on measuring the energy required for deformation of materials well beyond the initial linear range. For materials showing simple behavior (no fracture or extreme changes in properties) the results have been usable in the computer program.

Much of the research in this program has been original and exploratory. Some has led to dead ends which were abandoned. The over-all goal of providing a complete, three-dimensional theoretical model for predicting impact behavior has not been met; however, a method of computer solution of the flow equations, which is new and

unique as far as can be determined, was developed and partially tested in a simple one-dimensional problem. This work is worthy of further attention and may provide the method to achieve the ultimate goal of a complete description of impact phenomena in complex materials.

In this report, past theoretical work in the contract and the work of others is briefly reviewed for comparison with the present mathematical model and computer program. The present model and computer code (abbreviated PIF for "Particle In Field") are discussed in detail and the results of one-dimensional computations are examined. The direction of possible future work is outlined.

A separate section is included on the work of describing material properties in forms suitable for the computer program.

Part of the experimental work on material-property measurements has been previously published in the semiannual reports. Since this was a continuing effort and early interpretations of results have been modified, the experimental research on energy involved in deformation is collected and discussed in this report.

The report is divided into two self-contained parts: I. THEORETICAL RESEARCH, II. MEASUREMENT OF MATERIAL PROPERTIES.

PART I. - THEORETICAL RESEARCH

1. MATHEMATICAL MODELS AND COMPUTER CODES

1.1 Review of Past Work

The first approach to solving the problem of material motion in impact was made from the point of view of nonlinear elasticity theory. The problem was formulated in tensor notation and approximations were made to form appropriate difference equations to allow computer solution of the problem. This work was reported in the semiannual technical report dated November 1964. The same approach was continued during the next six-month period and preliminary computer runs were made. Results were reported orally to personnel at U. S. Army Natick Laboratories. In practice, tensor theory has proved to be impractical if not unusable when large deformations occur. The particular approximations used to go from the tensor formulation to the computer code were not strictly valid and may have caused the program to fail. The program did not progress far enough to determine whether this would occur.

The attack on the solution of the impact problem via nonlinear elasticity and tensor theory was abandoned and work began on developing a model and computer code based on hydrodynamic theory coupled with elasticity at low deformations. The first efforts to use hydrodynamic theory are reported in the semiannual technical report dated December 1965. A simplified form of the equations was used merely to test the equation of state and to observe the general behavior of the model. The mathematical model chosen consisted of separate mass points separated by springs having spring constants determined by the equation of state (pressure a function of energy and density). In the one-dimensional model, density was determined from the spacing between particles, and energy was determined from the energy equation involving pressure, density, viscosity, and velocity gradients. This method can be contrasted with the approach of elasticity where "pressure" is determined from the strain.

This model was successful in predicting shock-wave velocities and pressure jumps across a shock wave. This gave encouragement that the method should be pursued and refined. The details of this work will not be repeated here. Many of the ideas and computational techniques are similar to those used in the latest work which will be discussed in Section 2.3.

1.2 Comparison of Computer Codes

Before beginning the work of refining this preliminary model, the results of others were investigated to see if similar work had already been done or if other formulations of the problem would be more successful. Existing codes have been applied to some cratering and penetration problems, but we could find no applications to the problem of the penetration of complex armor by a low-velocity projectile (military-rifle or shell-fragment velocities). In this section we will compare existing codes and indicate some of the problems which have prevented the successful solution of the impact problem.

An extensive review of existing codes is contained in Methods in Computational Physics, by Berni Alder (editor), Vol. 3, Fundamental Methods in Hydrodynamics, Academic Press, New York (1964). This probably contains the most complete discussion of the work of the large groups at Los Alamos and Livermore as well as that of other groups. The work of Riney at General Electric, Walsh at General Dynamics, and Bjork of Shock Hydrodynamics is based on this work. By this time, successful methods may have been developed for the low-velocity impact problem since several groups are working on techniques that might apply. However, as of the 7th Hypervelocity Impact Symposium, February 1965, such methods had not yet been discovered.

The different codes are primarily distinguished by the coordinate system used to describe the material and the techniques used for making the computer follow the material motion and solve the equations of motion.

Lagrangian. The moving material is described by a mesh of intersecting lines which move with the fluid. The forces on a fluid element are ordinarily determined by the distortion of the mesh.

Eulerian. The material is described by a fluid moving through a fixed mesh, and the forces on a fluid element are determined by the transport of mass, momentum and energy into a mesh cell.

Combination Formulations. Various combinations of Lagrangian and Eulerian systems have been used. Usually the coordinate system is made up of streamlines which are attached to the moving fluid and with fixed Eulerian grid lines crossing the streamlines.

PIC Code. The PIC code is a combination code and deserves special mention because of its successful use in hypervelocity impact

problems. The material is represented by a number of mass points which move through a fixed Eulerian mesh. The points are not connected. The mesh is used in the calculation of average field quantities which determine the forces acting on the mass particles.

In general, each formulation or code is suited to a particular type of problem. The mathematics involved in transforming the problem to difference equations and obtaining computer solutions are not completely understood. Much of the behavior of the mathematics is only brought to light as the computer produces numbers. This situation is expected since the underlying nonlinear differential equations are not understood --- particularly as applied to the complicated situations found in impact or other transient-flow problems.

Lagrangian Codes. Lagrangian codes have proved useful in smooth hydrodynamic problems and those involving elastic and plastic properties. The method is particularly good at keeping track of moving boundaries since initial accuracy is maintained throughout. The method works equally well with fast or slow, smooth flows.

With Lagrangian formulations, the quadrilaterals or triangles of the initial mesh must remain quadrilaterals or triangles; as a result, large distortions are not handled successfully. Turbulence, necking, thinning, slippage and cavitation are almost impossible to handle. Remapping has proved unsuccessful and instabilities develop. Shocks are difficult to handle and special artificial conditions have to be inserted.

Eulerian Codes. Eulerian codes are particularly good for problems involving large distortions and high-speed flow. (They are unstable if speeds are far subsonic.) Since quantities are averaged over a mesh spacing, boundaries and interfaces become diffuse and small features are smeared. Viscosity is handled artificially since the equations, as used, are not translationally or rotationally correct. Strength cannot be used, except as an artificial viscosity. Only simple fluid-type equations of state can be used which makes Eulerian codes of limited applicability to subsonic solid-flow problems.

PIC Code. The PIC code has the advantage of the Eulerian of allowing large distortions and the advantage of the Lagrangian in keeping track of each mass point. Boundaries are better defined than in pure Eulerian code. The disadvantages are mostly related to the Eulerian codes. Strength of materials is not introduced successfully and viscosity is applied mainly by the skill of the operator. The artificial viscosities

inherent in the program, or introduced artificially, are useful in smoothing shock waves and allowing their computation but must be removed as expansion takes place. The method becomes unstable as flow velocity becomes subsonic.

New PIF Code. The difficulties inherent in previous codes encouraged the development of a new code with particular applicability to low-velocity, armor-penetration problems. The ability of the PIC code to handle large deformations suggests that the material be represented by freely moving mass elements which are not connected in a gridwork. The resulting formulation may then be represented as follows:

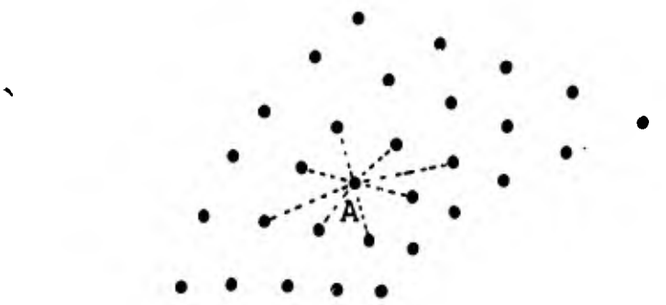

Each point represents a portion of the material, and all the field variables such as pressure, energy, density and stress are associated with each point. This is in contrast to the PIC code where fields are associated with the fixed mesh. The forces at a point, such as A, are determined by the fields and gradients generated by the point and its neighbors as indicated by the lines. Each point moves freely under the influence of these forces, and the immediate neighbors, new or old, determine succeeding forces. The essential differences between this code and others can then be summarized as the use of freely moving points with field quantities associated with the points. The code is basically Lagrangian since the motion of individual particles is followed.

1.3 Development of PIF Code

The general approach to solving the impact problem as outlined above has been applied to the case of two flat plates impacting. In this section, the general equations will be discussed. The equations will then be given for the one-dimensional case, and the computer program developed for this example will be discussed.

Equations. The hydrodynamic equations of motion can be

expressed in terms of the material derivative or the derivative following the motion. They can be written as follows:

Mass $$\frac{D\rho}{Dt} = -\rho \nabla \cdot \vec{v} \qquad (1)$$

Force $$\rho \frac{Dv}{Dt} = -\nabla \rho - \nabla \cdot \bar{\bar{\tau}} \qquad (2)$$

Energy $$\rho \frac{DU}{Dt} = -\rho (\nabla \cdot \vec{v}) - \bar{\bar{\tau}} : \nabla \vec{v} \qquad (3)$$

Where $$\frac{D}{Dt} = \frac{\partial}{\partial t} + v_x \frac{\partial}{\partial x} + v_y \frac{\partial}{\partial y} + v_z \frac{\partial}{\partial z}$$

Where ρ = density, $\vec{v}$ = velocity, p = pressure, $\bar{\bar{\tau}}$ is the stress tensor, U is specific internal energy and $\nabla \cdot \bar{\bar{\tau}}$ and $\bar{\bar{\tau}} : \nabla \vec{v}$ are tensor operations. In addition, the material equations relating pressure, density and energy, and stress, energy, velocity and density must be used. In the computations reported here, the equation of state used is

$$p = \frac{p_o \rho}{\rho_o} \left(\frac{U}{U_o} \right)^G \qquad (4)$$

where G is a constant depending on the material. This equation will be more fully discussed in Section 5 on material properties. The viscosity law used is given by

$$\tau = -\mu \frac{\partial v}{\partial x} \pm \tau_o \qquad (5)$$

where μ and τ_o are constants. This equation will be discussed in Part II., Section 5 on the experimental measurement of material properties.

Material Model. The material is represented in one dimension by mass points with quantities associated with each point such as position, velocity, etc. and with quantities depending on the relationship of one point to another such as $\partial v/\partial x$, ρ, etc. This model is illustrated in Table I.

Table I

List of variables used in PIF code. Subscripts p and t represent projectile and target. The mass points are shown numbered 1, 2 & ... . The variables listed in columns under the mass points are computed at the point or associated with the point. The variables listed in columns between the mass points are computed from the relationships between adjacent points.

	Projectile			Target		
	ō 1	ō 2	...	◙ 1	◙ 2	...
Position	x_{p1}	x_{p2}	...	x_{t1}	x_{t2}	...
Velocity	v_{p1}	v_{p2}	...	v_{t1}	v_{t2}	...
Velocity Gradient	$\left(\frac{\partial v}{\partial x}\right)_{p1}$	$\left(\frac{\partial v}{\partial x}\right)_{p2}$	...	$\left(\frac{\partial v}{\partial x}\right)_{t1}$		...
Density	ρ_{p1}	ρ_{p2}	...	ρ_{t1}		...
Internal Energy	U_{p1}	U_{p2}	...	U_{t1}		...
Pressure	p_{p1}	p_{p2}	...	p_{t1}		...
Stress	τ_{p1}	τ_{p2}	...	τ_{t1}		...
Pressure Gradient	$\left(\frac{\partial p}{\partial x}\right)_{p1}$	$\left(\frac{\partial p}{\partial x}\right)_{p2}$	...	$\left(\frac{\partial p}{\partial x}\right)_{t1}$	$\left(\frac{\partial p}{\partial x}\right)_{t2}$	...
Stress Gradient	$\left(\frac{\partial \tau}{\partial x}\right)_{p1}$	$\left(\frac{\partial \tau}{\partial x}\right)_{p2}$	...	$\left(\frac{\partial \tau}{\partial x}\right)_{t1}$	$\left(\frac{\partial \tau}{\partial x}\right)_{t2}$	

Difference Equations. With this model, and the above equations, the difference equations can be written as follows for any particle number i.

$$\Delta \rho_i = -\rho_i \Delta t \frac{(v_{i+1} - v_i)}{(x_{i+1} - x_i)} \tag{6}$$

$$\Delta v_i = -\frac{2\Delta t\,(p_i - p_{i-1})}{\rho_i\,(x_{i+1} - x_{i-1})} - \frac{2\Delta t\,(\tau_i - \tau_{i-1})}{\rho_i\,(x_{i+1} - x_{i-1})} \tag{7}$$

$$\Delta U_i = \frac{-p_i \Delta t}{\rho_i} \frac{(v_{i+1} - v_i)}{(x_{i+1} - x_i)} - \frac{\tau_i \Delta t}{\rho_i} \frac{(v_{i+1} - v_i)}{(x_{i+1} - x_i)} \tag{8}$$

Note that the factor 2 in the acceleration equation (Equation 7) comes because of the notation used. $\Delta\rho$ and ΔU are computed from the relationships between two points, i and i+1. Δv is computed using the average pressure in front of point i (p_i) and back of it (p_{i-1}).

Some care must always be exercised at the boundaries to make sure that gradients are taken properly and that other boundary conditions are met. In the computer program, boundary points are treated separately as special cases and all other points are handled by a standard routine.

After $\Delta\rho$, Δv, and ΔU are calculated, they can be added to the original ρ, v and U to get new values. From the density and energy, a new pressure can be calculated using Equation 4. A new velocity gradient can be calculated from the new v's and x's resulting from Equation 7; Equation 5 can then be used to obtain a new τ. New gradients of τ and p can be calculated by taking differences. After these calculations, we have a new value for all variables and the step can be repeated.

Computer Program. The actual computer program used for the preliminary results reported below is refined somewhat from the procedure described above. The above method may be called a simple marching method. Equations 1, 2, 3 or 6, 7, 8 give the slope of the curves of ρ, v, and U versus t. With an initial value for these quantities given, and the slope known, the estimated value of the function after a time interval Δt can be calculated. The slope at this new time is again calculated and another step in time is taken. The solution is produced in a step-wise fashion. All the equations interact, and under many conditions, the solution is stable and is close to the correct value. Some successful computer runs were made using the simple marching method.

A next simple step in refinement of this method of solution is to modify the simple marching method and use the initial value and slope of the function only to predict a new trial value. This trial value is used to calculate a new slope at the new trial value of the function. The original slope and the trial slope are then averaged, and the average slope is used to predict a new value of the function at the end of the time interval Δt. The well known Runge-Kutta method is a further refinement related to this "modified marching method" and could be applied to the set of equations used here. Only the "modified marching method" was used however. The computer program to accomplish a solution to these equations is outlined in Figure 1. A more detailed outline of the logic is given in Appendix A along with a list of variables and subroutines and a print-out of a particular program used.

This program is a preliminary version designed to test the main ideas embodied in the model and computational scheme. Many things were done to gloss over troublesome details in order to get the program working. Some discussion of these problems is necessary to allow the reader to make his own judgement as to the validity and utility of the work.

The equation of state given in Equation 4 was used for both compression and expansion. This equation is an accurate representation of the Hugoniot curve for shock compression and is one of the valuable contributions of this work. It is not valid for an adiabatic expansion. However, the Hugoniot is close to the adiabats for pressures up to several hundred kilobars, and the use of this equation was justified by the need to test the validity of the method. By using this equation in expansion, the material appears "stiffer" than it really is and more of the compressional energy is recovered in mechanical work. The heating effects of the shock process are lost. The viscosity law used partially offsets this, and shock heating effects due to viscosity are seen in the expansion waves.

No effort was made to include the effects of elasticity at low pressures. Equation 4 was used as a representation of the elastic behavior. This was troublesome when the material went into tension. Under certain conditions the energy would go negative when computing trial values. Instead of considering elasticity carefully and considering fracture, the pressure was arbitrarily set at the negative value indicated and the computations went on. This was not considered to be a serious problem because the averages between trial values and initial values did not go negative.

Where density went below preset limits, fracture was considered to occur. At this time, density and energy were set at initial values and stress was set at zero. This approximation to actual conditions caused spall effects to occur; the individual pieces were not followed

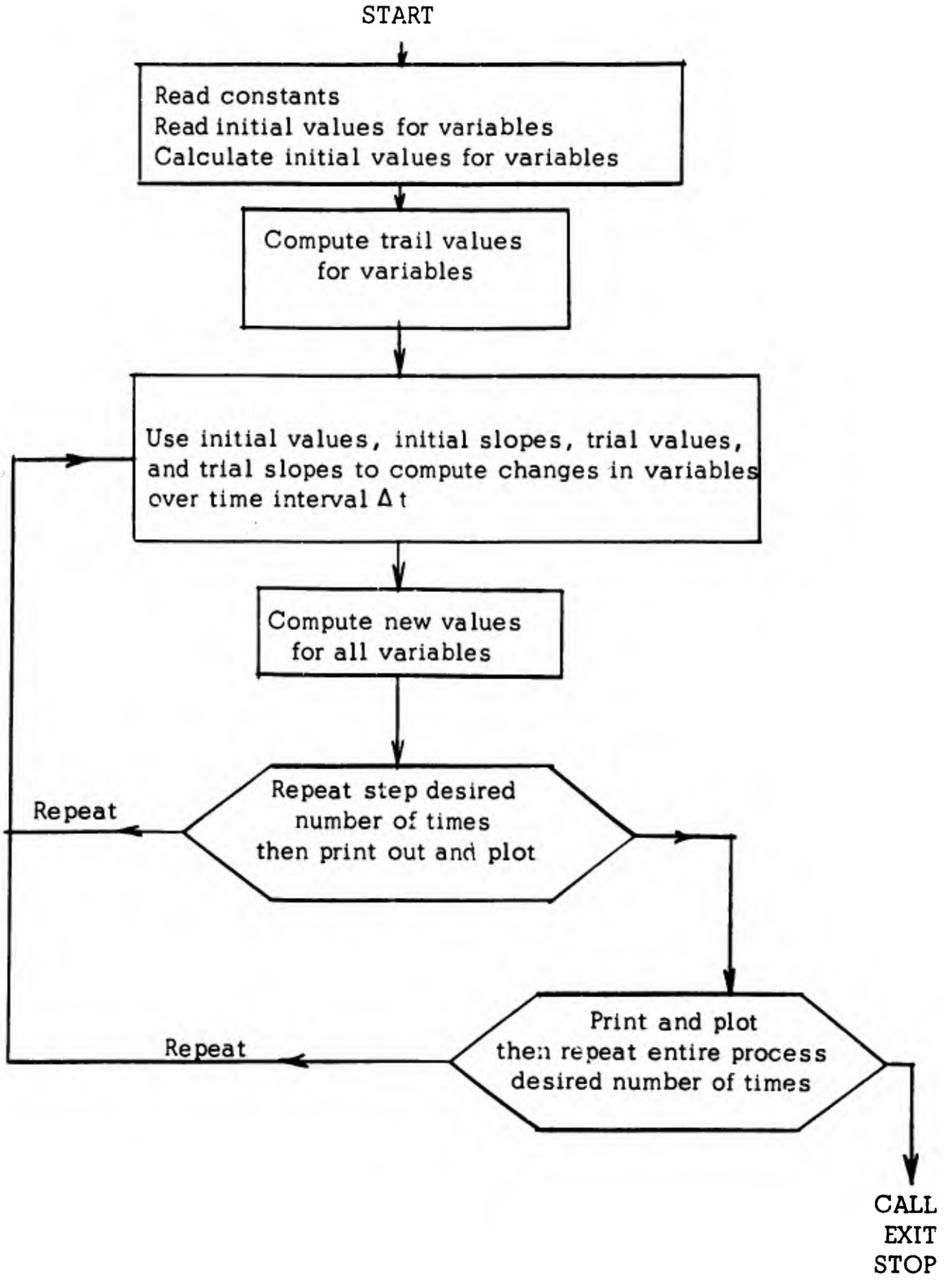

Figure 1. Outline of computing scheme used in PIF code for one-dimensional problem.

correctly but were merely reinserted into the regular program and started with the new conditions. This procedure invalidated many of the results in the low-pressure region after the expansion wave had passed, but probably had little effect on the main features of the initial rarefaction wave.

The exact details of handling the variables in a difference-equation scheme influenced the results. In the force equations (Equation 2 or 7), the density of point i may be considered to be an average of ρ_i and ρ_{i-1} or may be just ρ_i. Pressure jumps and wave velocities were correct when ρ_i was used, but symmetry of the problem was destroyed due to the particular notation used. In most computer runs, an average ρ was used to maintain symmetry and make it easier to monitor integrated momentum and energy as a check on over-all behavior of the computations.

The problems listed above appear to be the main ones encountered. Time did not permit a detailed mathematical analysis of them nor a thorough testing on the computer. All of these problems appear soluble, and the crude solutions applied here might be adequate for most practical applications. Considerable additional work was spent on the refinement of the equation of state to provide for correct adiabatic expansions. This is reported in Section 5. Time did not allow the incorporation of this into the main computer program.

2. RESULTS OF COMPUTER PROGRAM

A selection of typical results is shown in Figures 2 to 10. These are plots of pressure waves vs. distance, at different times, for the impact of two identical flat aluminum plates 3.0 cm thick moving at a relative velocity of 2.0 km/sec. The figures show the wave progressing from the center of symmetry at x = 0 into one plate. Figures 2 to 9 are plotted in a coordinate system with the center of mass stationary. The projectile plate is moving to the right with a velocity of 1 km/sec, and the target plate is moving to the left with a velocity of 1 km/sec. The wave is shown moving to the right in the target plate. Shock-wave velocity in the material is given by the distance-time relationship of the plot plus 1 km/sec. Figure 10 is plotted with the target plate stationary so that velocities can be computed from the indicated distances. These figures are not all strictly comparable because several conditions were being changed over the series of computer runs. Most are plotted on a linear scale which overemphasizes the overshoot and oscillations at the wave fronts. The low-level waves after the rarefaction are not seen. A logarithmic scale is used in Figure 10. Since the pressure changes over many decades, and since the pressure is such a strong function of energy and density, this gives a better visualization of the significance of deviations because it shows fractional changes rather than absolute values.

Figure 2 shows the shock wave progressing through the plate. The effects of the rarefaction are seen at t = 5 μsec. Figure 3 begins at 5 μsec and shows the rarefaction wave moving back toward the center at x = 0. The values of μ_o and τ_o are 0.543×10^{10} and 0.1×10^{5} respectively. These are the values chosen from the experimental data to fit Equation 5. The value of G used is 0.532 and gives agreement with the Los Alamos shock-wave data.

The behavior is generally correct: The pressure behind the wave is 1.9×10^{11} dyne/cm^2 after equilibrium is reached, and the velocity is 6.45 km/sec. The wave front is steep and is maintained. In this case, the overshoot grows slowly and the wave velocity may increase slightly. For comparison, an analytical solution using the Los Alamos data gives a pressure of 2.0×10^{11} dyne/cm^2 and a velocity of 6.8 km/sec. The rarefaction wave spreads as it should with the front moving at about 6.7 km/sec. This is close to the Los Alamos data on speed of sound in the compressed material.

Figures 4 and 5 show the behavior with viscosity increased by a factor of three. Results here show a little too much rounding of the wave front. A value of viscosity somewhere between the two extremes is probably best for this model. We believe it is more than coincidence that the

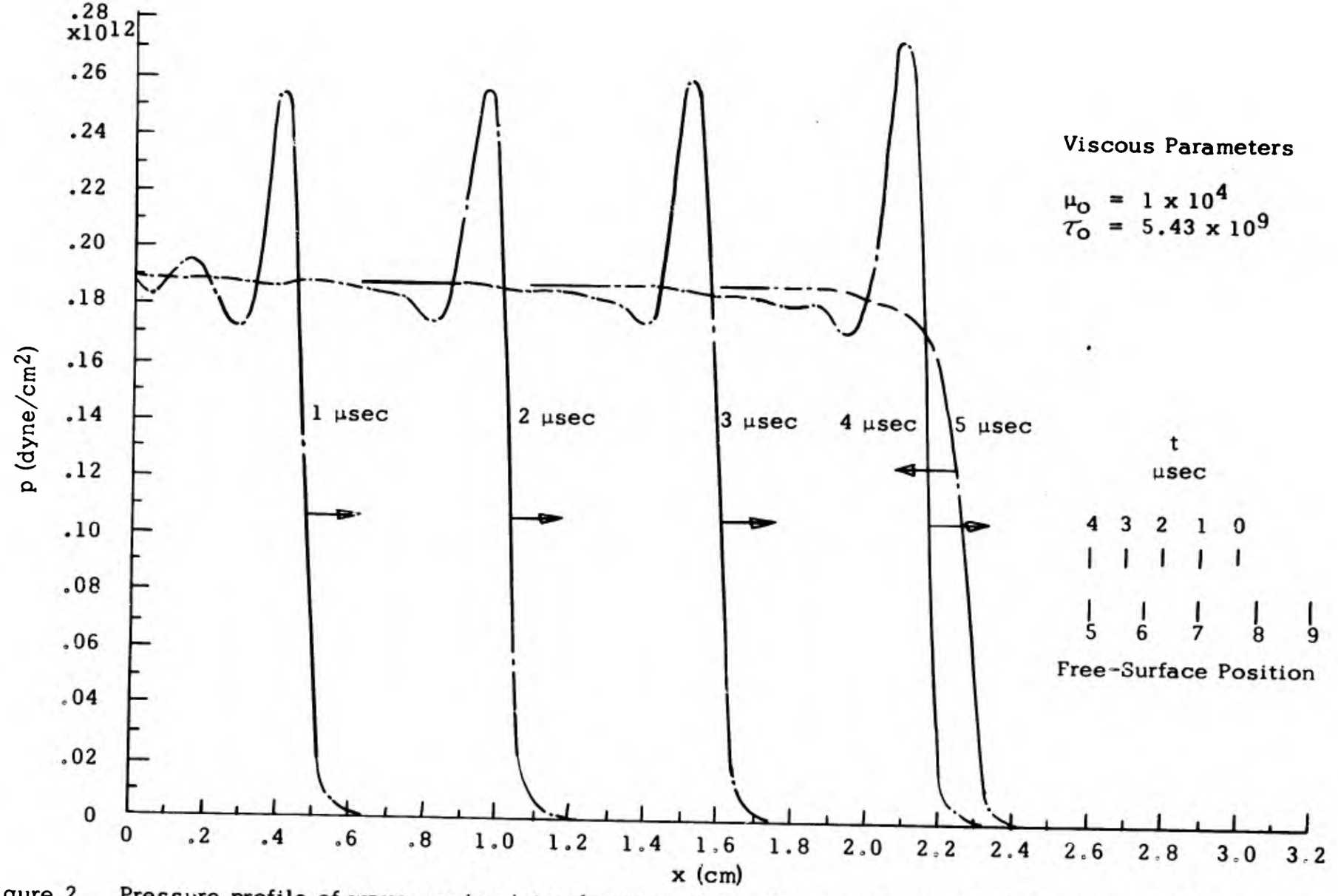

Figure 2. Pressure profile of wave moving into aluminum plate after impact at 2 km/sec. Reflected wave is shown at t = 5 μsec. The position of the free surface is shown. Wave velocity is approximately 6.45 km/sec.

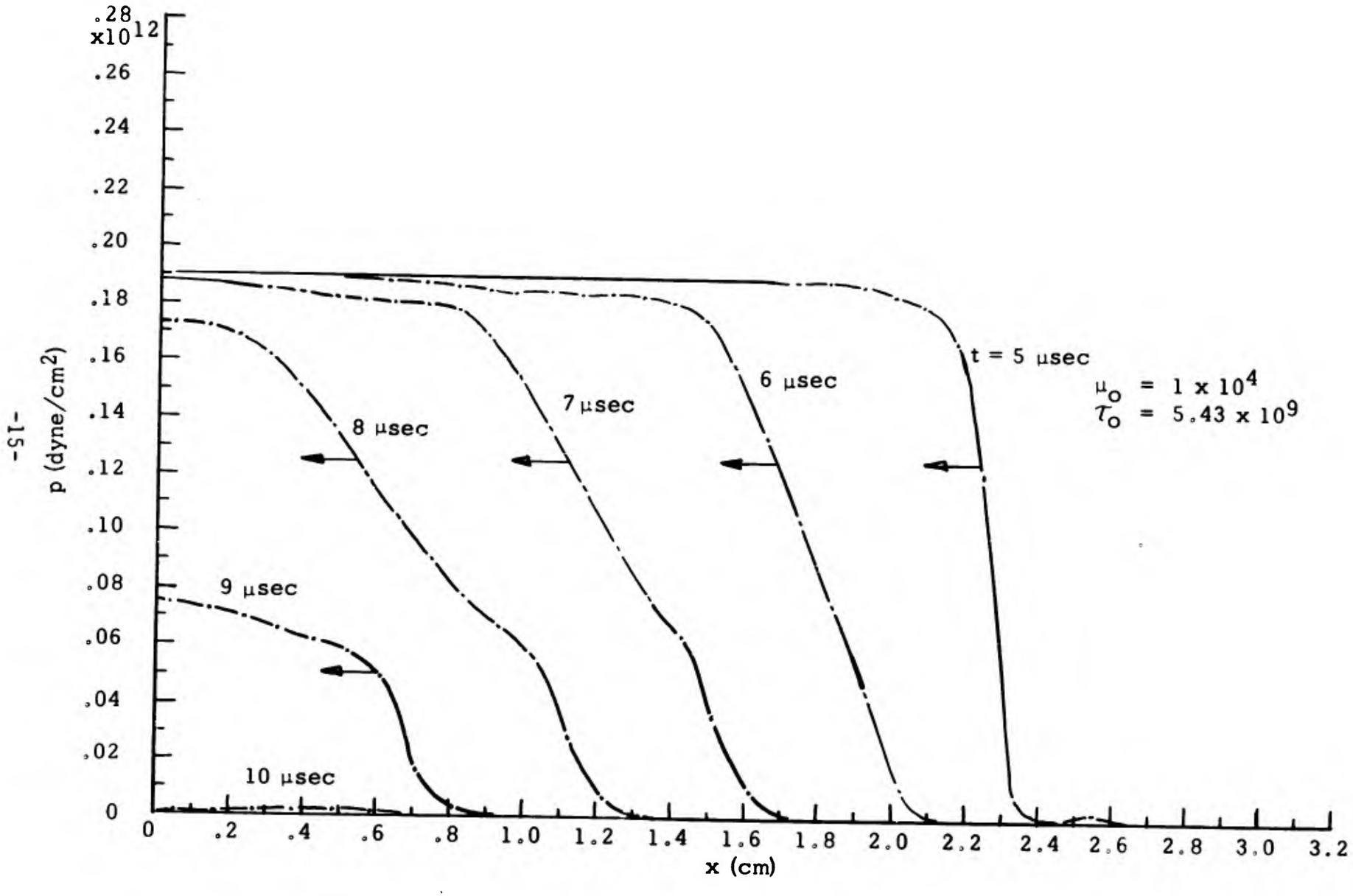

Figure 3. Continuation of Figure 2, showing progress of rarefaction wave. Velocity of wave front 6.7 km/sec decreasing with time to 6.4 km/sec.

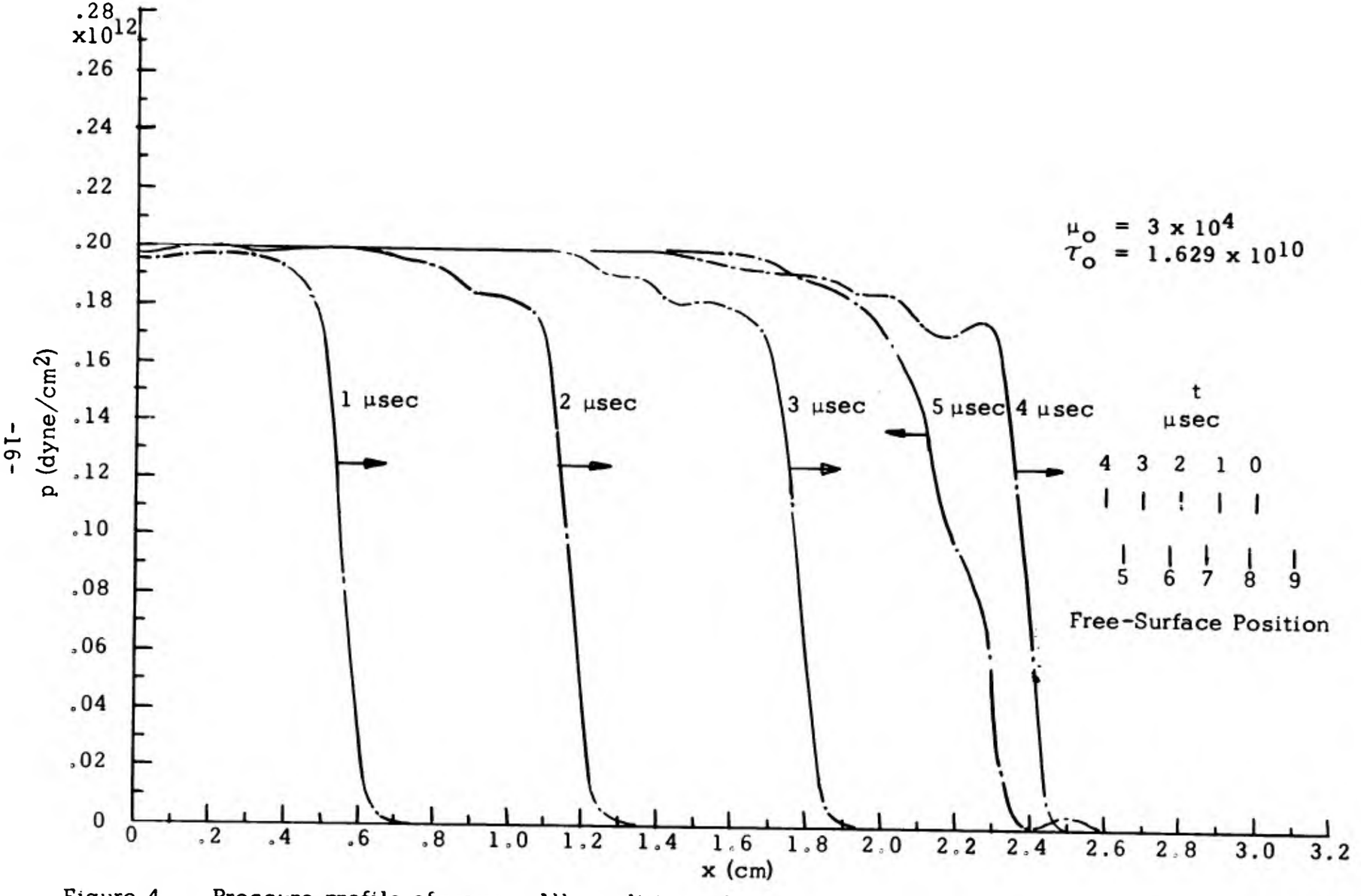

Figure 4. Pressure profile of wave. All conditions the same as in Figure 2 except τ_o and μ_o increased by a factor of 3. Wave velocity approximately 7.2 km/sec.

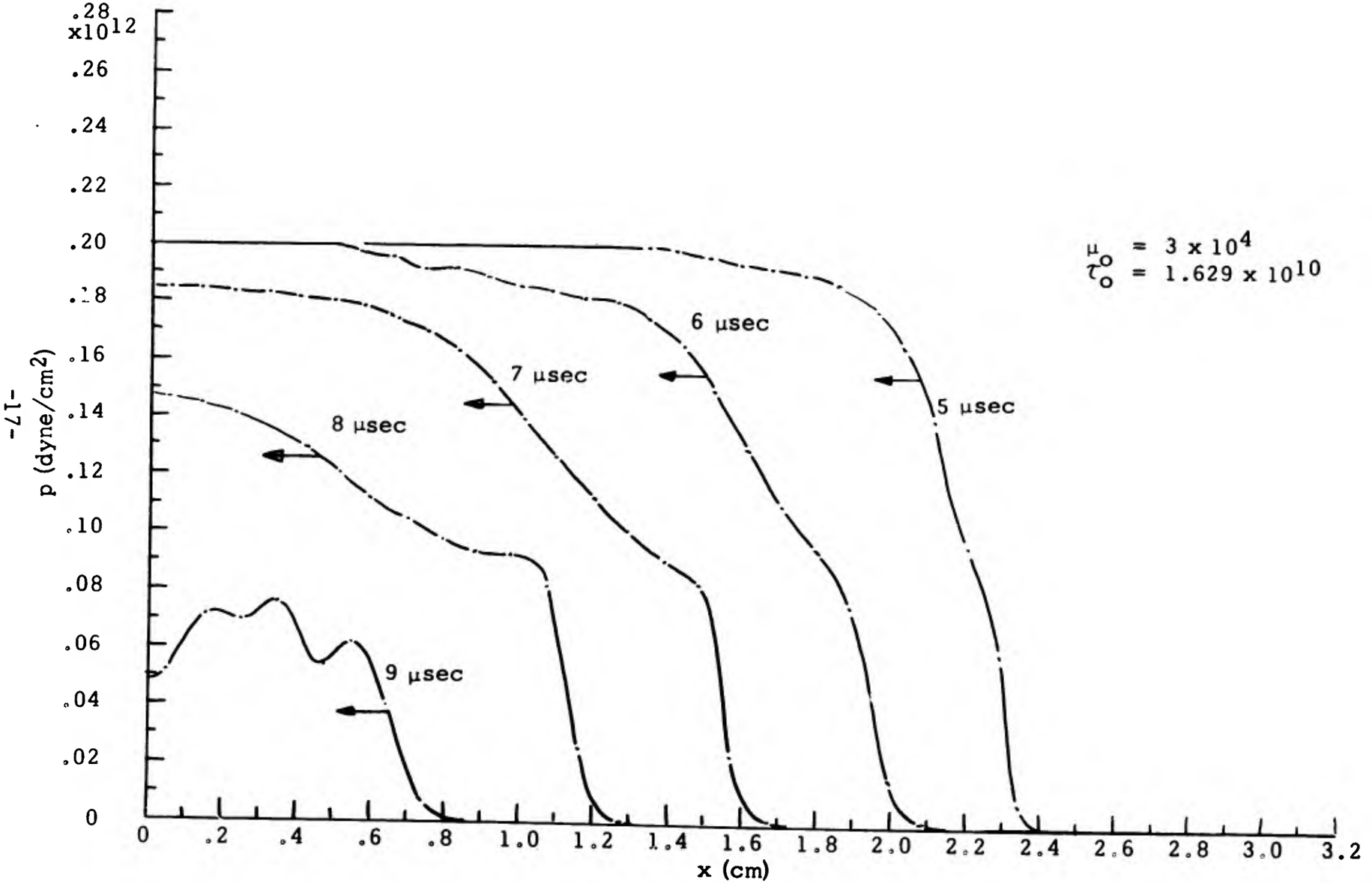

Figure 5. Continuation of Figure 4 showing progress of rarefaction wave. Velocity of wave front approximately 6.6 km/sec.

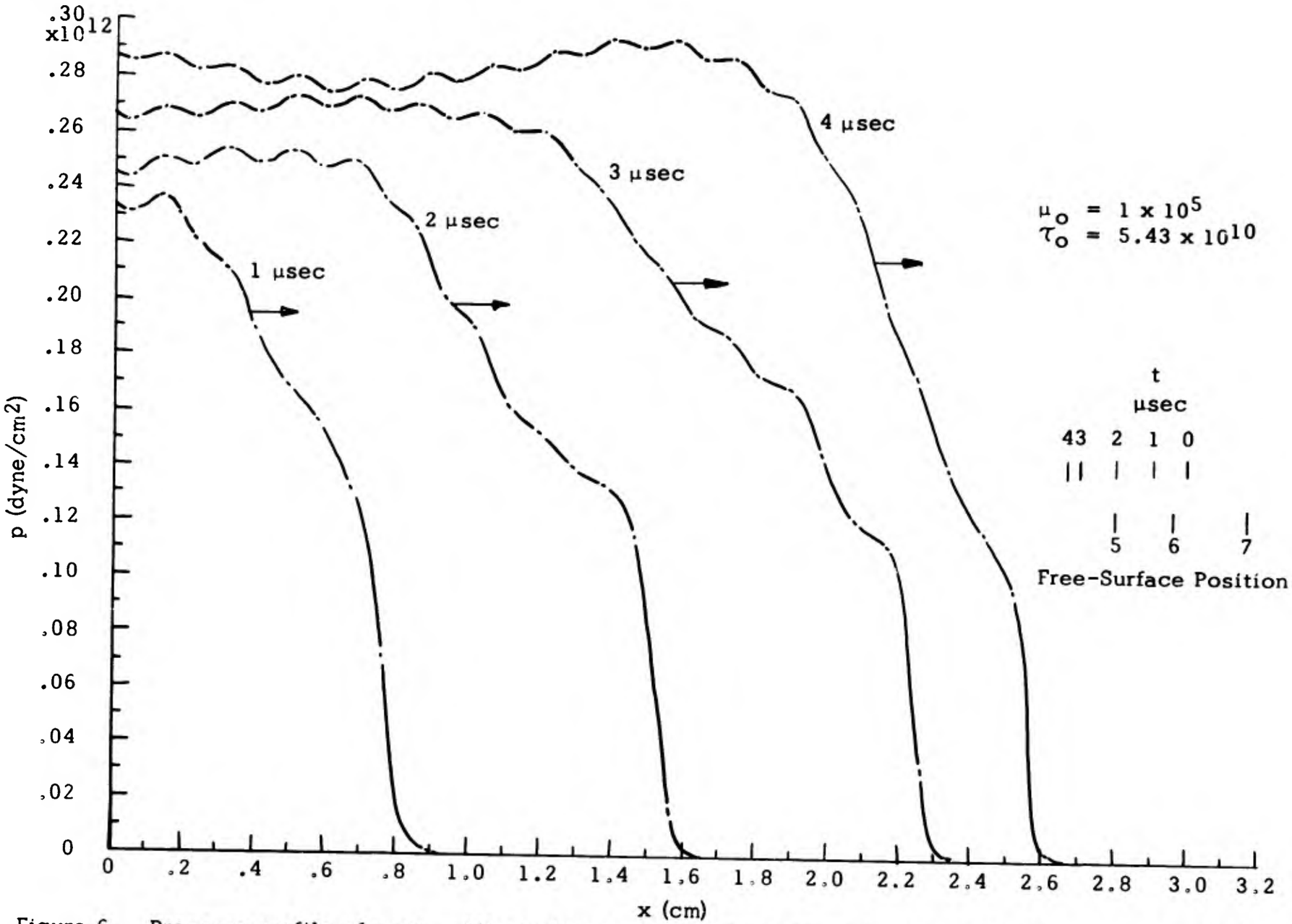

Figure 6. Pressure profile of wave. All conditions the same as Figure 2 except τ_o and μ_o are increased by a factor of 10. Wave velocity decreasing with time from 9.2 to 8.6 km/sec.

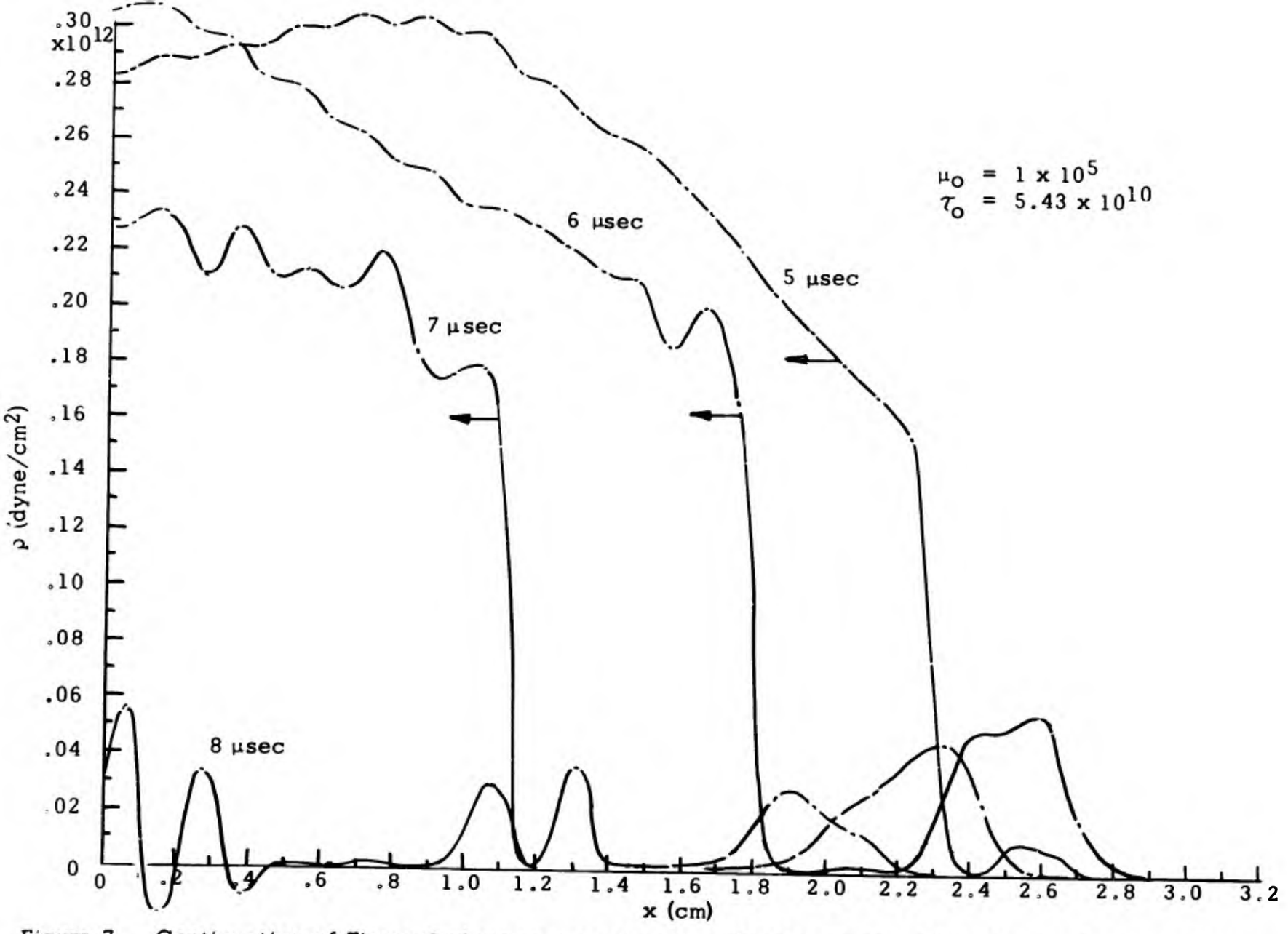

Figure 7. Continuation of Figure 6 showing progress of rarefaction wave. Wave front velocity approximately 7.5 km/sec.

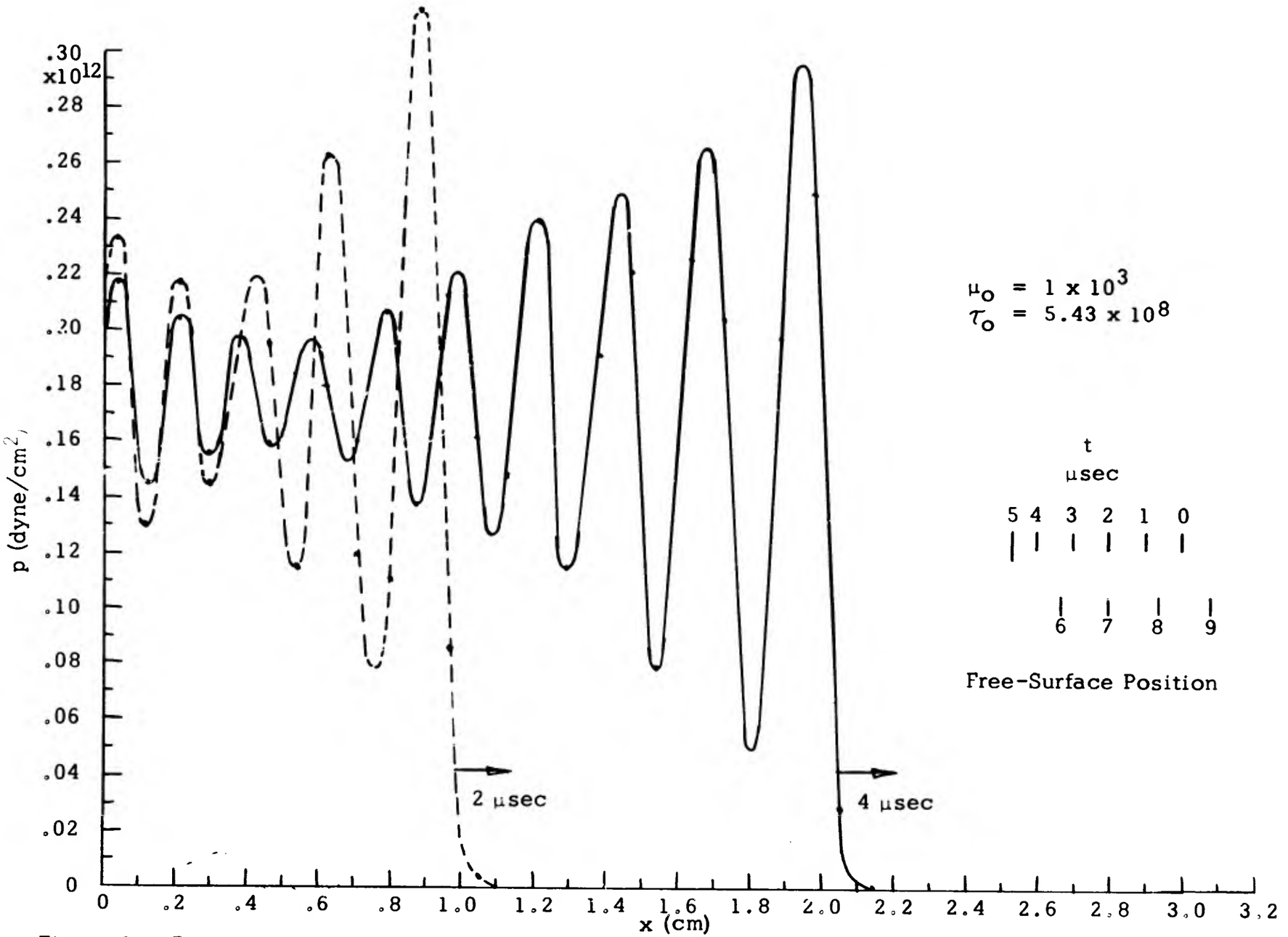

Figure 8. Pressure profile of wave. All conditions the same as Figure 2 except τ_o and μ_o are decreased by a factor of 1/10. Wave velocity approximately 6.1 km/sec.

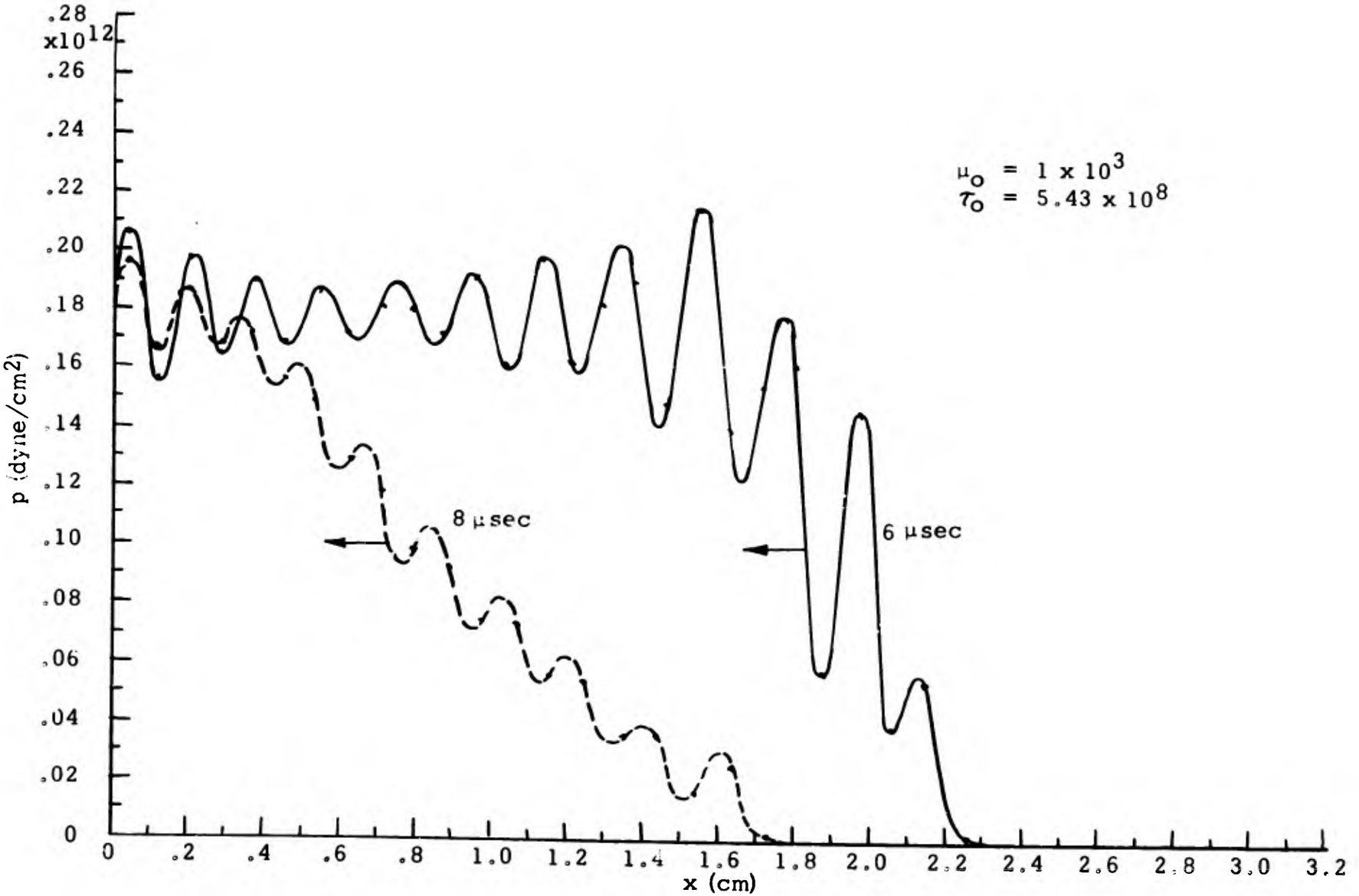

Figure 9. Continuation of Figure 8 showing progress of rarefaction wave. Wave front velocity approximately 6.3 km/sec.

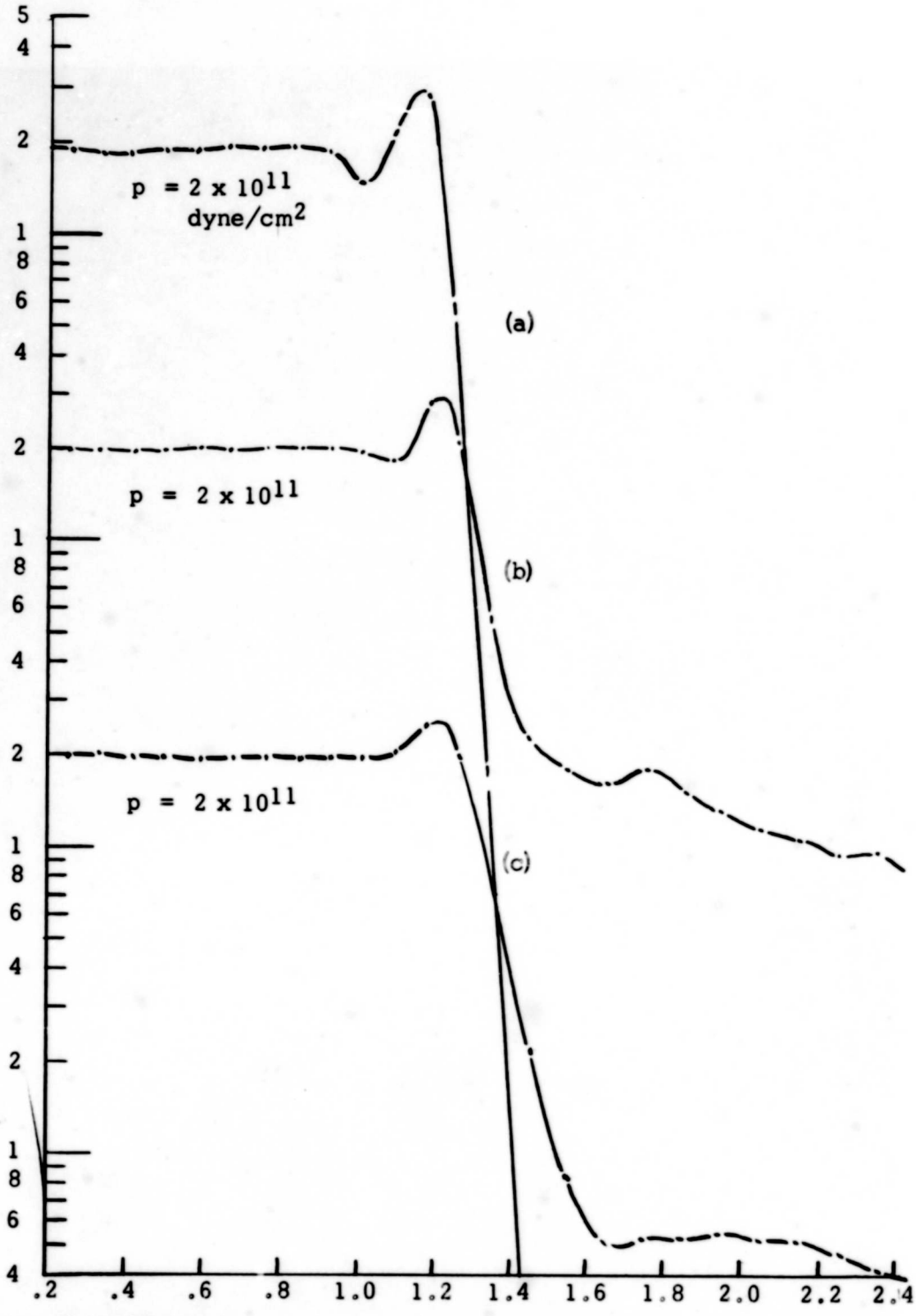

Figure 10. Effects of varying time interval Δt and low-level viscosity cut-off point.
(a) $\tau = 0$ when $\rho < \rho_o - .05\ \rho_o$. $\Delta t = 5 \times 10^{-9}$ sec
(b) τ used from Equation 5 for all conditions. $\Delta t = 5 \times 10^{-8}$
(c) τ used from Equation 5 for all conditions. $\Delta t = 5 \times 10^{-9}$
Wave profiles plotted at t = 2 μsec in coordinate system with target initially at rest. Pressure profiles are shown displaced for clarity.

experimentally chosen values of τ_o and μ_o were within a factor less than three of being the best in the theoretical code. Figures 6 to 9 show conditions with viscosity ten times and one-tenth the original. The strong effects of viscosity on wave shape and the lesser effects on pressure and velocity are seen. As the viscosity goes up, the initial shock-wave velocity increases. With the higher viscosities, the wave velocity decreases slightly as the wave progresses. With viscosity lower than normal, the shock-wave velocity is down. The rarefaction-wave velocity can be read directly from Figures 3, 5, 7, and 9 since it is shown moving into relatively stationary compressed material. This velocity varies from 6.3 km/sec in the lowest viscosity case up to possibly 7.5 km/sec for the highest viscosity.

In these examples, τ_o and μ_o were varied by the same factor. The effects of varying them separately should be examined. It should be noted that this model handles shock waves without artificial means for spreading the wave. Even without viscosity, the shock wave spreads over two or three mesh spaces. The reasons for this have not been explored, but it probably comes about because the solution is obtained in a step-by-step progression without iteration at each step.

In Figures 2 to 9, the time interval, Δt, was 5.0×10^{-8} sec. With a relative velocity of 2×10^5 cm/sec and a mesh spacing of 0.1 cm, the compression in the first cell after one time interval is 0.005. With a time interval of 5×10^{-9} sec, the results are smoother with less overshoot. This is shown in Figure 10. The shorter time interval spreads the wave more and the velocity of the initial rise in pressure is greater. The velocity of the peak pressure is about the same in the two cases. A much longer run with a larger number of mass points would be of interest to see if the solution is maintained over long distances. Note in Figure 10 that the coordinate system is for a stationary target so that the velocity is computed directly from the indicated distance.

The results of handling viscosity slightly differently are also shown in Figure 10. In Figures 2 to 9, the force term given by Equation 5 was set equal to zero until pressure or density reached a preset value. Below this value, only Equation 4, the pressure equation, was used. In Figure 10, Equation 5 was used down to zero pressure. This causes a small pressure (about 1 per cent of the shock-wave pressure), corresponding to τ_o, to be transmitted with high velocity through the mesh. The velocity is determined by the fact that the disturbance propagates one mesh space in each time increment. This figure is plotted with a logarithmic pressure scale to show the low-level pressure.

Figure 10 shows the results of handling density somewhat differently in the force equations (Equations 2 and 7). In Figures 2 to 9, the density used was the average of the cell before and after the mesh

point being considered. In Figure 10, the density is that of the cell to the right of the mesh point being considered (refer to Table II). This makes the scheme unsymmetrical for a left- and a right-going wave. This could be corrected, but was not. The differences in results are insignificant at this stage of progress although a slight pressure difference is noted when comparing Figures 10(a) and 2.

In the code used for these results, the problem of fracture was handled only crudely. The pressures and strains were computed by equations 4 and 5 in the low-pressure, low-velocity range where they are not valid. Better elastic-plastic behavior laws could have been used. When tensile stresses exceeded a certain limit, fracture was assumed to occur and pressures and energies were arbitrarily set at initial values. The computer then just used these new values and went on as before. No effort was made to follow the broken off parts separately. Evidence of spalled-off parts can be seen, particularly in Figure 7, in the maxima and minima of pressure after the release wave has passed. These are not necessarily correct but merely indicate the effects that are occurring.

In the computer runs, integrals of momentum and energy were taken. Momentum and energy were conserved in all symmetrical runs. The first hint of trouble in the accidentally nonsymmetrical runs was the non-conservation of momentum and energy. In the symmetrical runs, energy behaved properly in that all the kinetic energy was converted to internal energy then expansion converted some back to kinetic energy.

3. EVALUATION OF PIF CODE

The ultimate utility of this mathematical model and computer code cannot be judged completely on the basis of one simple test problem. However, the fact that solutions are stable and converge rapidly to values close to those computed analytically, using Los Alamos equation-of-state data, gives evidence that the ideas can be successfully applied to practical problems. The ideas are simply expressed so that parameters can be varied with some insight into the meaning of the results. Some of the achievements of the research may be listed as follows:

1. The mathematical concepts are relatively simple, coming directly from the hydrodynamic equations; thus, easily visualized changes can be made.

2. The computer program is simple and fast which allows changes to be made easily and makes the program inexpensive to run, test, debug and modify.

3. Material properties are easily handled.

4. The code is stable and converges rapidly under most conditions.

5. Wave shapes, velocities and magnitudes are approximately correct even though material properties in expansion were only roughly approximated.

6. The model predicts correct results when using experimentally determined equation-of-state data and energy-dissipation data (viscosity data).

7. Energy and momentum are conserved.

In evaluating the failings of the work, the two major areas of concern come under the heading of untried and untested work. They are first, the application of the ideas and methods described here to three-dimensional problems, and second, the use of a full description of material properties over the range of elastic, plastic, and hydrodynamic properties and including a careful description of fracture.

4. RECOMMENDED FUTURE THEORETICAL WORK

The problem of describing material properties for use in the computer program has not been seriously studied except for the case of development of a computer code for an adiabatic expansion from a shock compression. This will be discussed in Section 6. The all-important problems of material behavior in the lower pressure ranges have not been investigated and will not be discussed here other than to note that success in the over-all problem of describing low-velocity penetration depends on new methods of measuring and describing material properties.

Applying the above ideas of particles moving freely in force fields of their own making to three-dimensional problems has proved difficult. Much time was spent trying to produce a three-dimensional mathematical model (actually the problem tried was axially symmetrical with two space variables). Because of the failure to make significant progress on this problem, attention was turned to the one-dimensional case with the results described in this report.

The problem to be solved is that of finding gradients in a two-dimensional array of variables. The problem is simple if the mesh is undistorted (that is, if the variables are given in a rectangular array) and computer programs are available to do this. If the mesh is only slightly distorted, the neighbors of each point are known, along with their associated variables, and the problem is still solvable. In impact, large mesh distortions occur, the original neighbors of a point are far removed and new neighbors move in to determine the behavior of the functions at a particular point. No successful scheme was devised for having the computer decide which neighbors were important to a given point. The problem is particularly severe where large shears occur and where necking and cavitation occur. Here the over-all geometric shape of the mesh is strongly altered and relative spacing between points increases in one direction and decreases in another. The problem of determining meaningful gradients under these conditions is an important subject for research.

This problem appears solvable. The mind and eye can easily form approximate gradients and determine which points are significant in influencing each other. We feel that a computer can be programmed to search and form proper trial and error fits until good gradients are achieved. Probably the successful program will use the past behavior of points as well as their positions and values to make the decisions, determine the gradients, and compute forces. Although the problem is difficult, we feel that the positive results to be obtained in terms of having a working theoretical formulation of low-velocity penetration warrants a continuing effort at a two man-year level.

5. MATERIAL PROPERTIES

5.1 Shock-Wave Equation of State

The equation of state used in these computations is an accurate representation of the shock adiabat or the Hugoniot curve for many gases, liquids, and solids. In many cases, it serves as an adequate complete equation of state for all processes.

The equation as used here (Equation 4) is for relative conditions between two states, one of them an initial condition. The equation can be written

$$\frac{U}{pV} = mU^k \quad \text{or} \quad p = \frac{U^{1-k}}{mV} \tag{9}$$

where V is specific volume. The constants m and k are usually valid over wide ranges of conditions. For many metals which do not show phase changes, m and k are constant over a pressure range from 10 to 1000 kbar.

In a shock process, the conservation laws determine possible thermodynamic states so that we expect this equation to become one relating two variables. That this is true is shown by using the Hugoniot equation

$$U - U_o = 1/2\ (p-p_o)(V_o - V) \tag{10}$$

in Equation 9 to eliminate U/pV. If $U_o = p_o = 0$, Equation 10 becomes

$$U = 1/2\ p\ (v_o - v) = 1/2\ pV \left(\frac{V_o - V}{V}\right)$$

$$\text{or} \quad \frac{U}{pV} = 1/2 \left(\frac{V_o - V}{V}\right) = 1/2 \left(\frac{\rho}{\rho_o} - 1\right)$$

Substituting this into (9) gives

$$2mU^k = \left(\frac{V_o}{V} - 1\right) = \left(\frac{\rho}{\rho_o} - 1\right) \tag{11}$$

We thus have a relationship between U and ρ which is valid for shock compressions.

Other equations which adequately describe the Hugoniot conditions are available. The one described above was used because it is natural to use it with the hydrodynamic equations. Equations 1 and 2 give energy and density then Equation 4, which is obtained by solving Equation 9 for p, is used to obtain pressure. As shown by Equation 11, this is not a true equation of state, relating p, ρ, and U independently and is thus not valid for all processes. Other equations provide a better starting point for obtaining a computer program describing an adiabatic expansion from a shocked condition. The remainder of this section will describe the development of such an equation.

5.2 Summary of Equation-of-State Data

Hugoniot equation-of-state data have been obtained by several experimenters in pressure ranges up to 9 megabars. The most extensive data have been collected for metals, and much work has been done with rocks and other materials. A summary of the Hugoniot data available is given in Table II for the elements and Table III for alloys, rocks, and compounds. These tables list the materials, the pressure range of the data, and the source reference.

Since in the present studies the maximum velocity to be encountered is about 1 km/sec, the upper limit of the pressure range will be about 400 kilobars. This report will summarize the Hugoniot data up to about 2 or 3 times the 400 kilobar limit.

The shock wave conservation relations provide the basis for determining shock Hugoniot data experimentally. For a wave moving into a stationary material these relations can be written

$$\text{mass} \qquad \rho_o W_s = \rho_1 (W_s - W_p) \tag{12}$$

$$\text{momentum} \qquad \rho_o W_p W_s = p_1 - p_o \tag{13}$$

$$\text{energy} \qquad p_1 W_p = \rho_o W_s \left[1/2\ W_p^2 + (U_1 - U_o)\right] \tag{14}$$

where W_s and W_p are shock wave and particle velocities and subscripts o and 1 refer to conditions in front of and behind the wave. For measurement of shock-wave parameters, p_o and U_o can be considered zero. These equations then become

TABLE II

SOURCES OF EQUATION-OF-STATE DATA FOR THE ELEMENTS

Material	Pressure (megabars)	Reference
Aluminum (24ST)	0.15 to 0.34	1
Aluminum (24ST)	0.04 to 0.21	5
Aluminum	to 1.97	20
Aluminum (Porous)	0.7 to 9.0	11
Antimony	0.25 to 1.18	2
Beryllium	0.14 to 0.13	1
Beryllium		10
Bismuth	0.17 to 0.44	1
Bismuth	0.44 to 1.36	2
Bismuth	0.29 to 3.76	3
Cadmium	0.18 to 0.46	1
Cadmium	0.96 to 1.36	2
Cadmium	0.07 to 4.49	3
Cadmium		10
Cadmium	to 8.41	16
Carbon (Pyrolytic Graphite)	0.10 to 0.29	4
Chromium	0.23 to 0.48	1
Chromium	0.92 to 1.38	2
Chromium		10
Cobalt	0.24 to 0.51	1
Cobalt	1.12 to 1.60	2
Cobalt		10
Copper (Porous)	0.7 to 9.0	11
Copper	0.22 to 0.51	1
Copper	0.88 to 1.44	2
Copper	0.16 to 3.52	3, 20
Copper		10
Copper	to 9.07	16
Germanium		9
Gold	0.27 to 0.53	1
Gold	1.39 to 1.94	2
Gold	0.25 to 5.06	3
Gold		10
Indium	0.21 to 0.41	1
Iron	0.42 to 0.48	1
Iron	0.48 to 1.73	2
Iron	to 4.00	20
Iron	to 8.70	16
Iron	to 5.0	18

TABLE II (Continued)

Material	Pressure (megabars)	Reference
Lead	0.19 to 0.47	1
Lead	0.84 to 1.39	2
Lead	0.05 to 4.26	3, 20
Lead	to 9.15	16
Lead (Porous)	0.7 to 9.0	11
Magnesium	0.12 to 0.26	1
Molybdenum	0.36 to 0.54	1
Molybdenum	1.25 to 1.63	2
Molybdenum		10
Nickel	0.24 to 0.52	1
Nickel	1.01 to 1.50	2
Nickel		10
Nickel	to 9.18	16
Nickel (Porous)	0.7 to 9.0	11
Niobium	0.24 to 0.48	1
Palladium	0.26 to 0.53	1
Platinum	0.30 to 0.59	1
Rhodium	0.28 to 0.55	1
Silicon		9
Silver	0.21 to 0.51	1
Silver	1.11 to 1.53	2
Silver	0.12 to 5.01	3
Silver		10
Tantallum	0.27 to 0.55	1
Thallium	0.21 to 0.46	1
Thallium	0.86 to 1.52	2
Thallium		10
Thorium	0.19 to 0.43	1
Thorium	1.00 to 1.40	2
Thorium		10
Tin	0.17 to 0.43	1
Tin	0.79 to 1.38	2
Tin	0.05 to 3.77	3
Tin		10
Tin	to 7.52	16
Titanium	0.17 to 0.39	1
Titanium	0.76 to 1.06	2
Titanium		10
Tungsten	0.39 to 2.07	2
Tungsten		10
Uranium		13
Uranium (Spongy)		14

TABLE II (Continued)

Material	Pressure (megabars)	Reference
Vanadium	0.20 to 1.24	2
Vanadium		10
Xenon (Solid)		8
Zinc	0.18 to 0.45	1
Zinc	0.75 to 1.42	2
Zinc		10
Zirconium	0.21 to 0.41	1
Zirconium		10

TABLE III

SOURCES OF EQUATION-OF-STATE DATA
FOR ALLOYS, ROCKS, AND COMPOUNDS

Material	Pressure (megabars)	Reference
Brass	0.22 to 0.48	1, 17
Iron - Silicon Alloy		7
Steel (Low Carbon)		5
Quartz		6
Sodium Chloride (NaCl)		9
Paraffin		10
Magnesium Oxide (MgO)		9
Iron Oxide ($Fe_3 C_4$)		9
$Mg_2 Si O_4$		9
CO_2 (Solid)		10
Silica (Vitreous)		21
Marble		10, 12, 15, 17
Tuff		10, 15, 17
Quartzite	0.005 to 0.250	12
Sandstone	0.005 to 0.250	12, 17*
Calcite	0.005 to 0.250	12
Limestone	0.005 to 0.250	12, 17
Plagioclase	0.005 to 0.250	12
Basalt	0.005 to 0.250	12, 15, 17
Rock Salt		15
Granite		15, 17
Dolomite		15, 17*
Andesite		15, 17*
Taconite		15
Oil Sand		15
Oil Shale		15, 17
Gabbro		17
Gabbro	"several"	19
Anorthosite		17
Dunite		17
Olivine		17
Halite		17
Rhyolite		17*
Claystone		17*
Diorite		17*
Syenite		17*
Diabase		17*
Pyroxenite		17*
Lherzolite		17*

TABLE III (Continued)

Material	Pressure (megabars)	Reference
Dacite		17*
Trachyte		17*
Phonolite		17*
Granodiorite		17*
Nepheline Syenite		17*
Quartz Diorite		17*

* Hugoniot Synthesized

$$\rho_1 = \rho_o \frac{W_s}{W_s - W_p} \tag{12a}$$

$$p_1 = \rho_o W_p W_s \tag{13a}$$

$$U_1 = 1/2\, W_p^{\,2} \tag{14a}$$

Thus, density, pressure and internal energy in the shock wave can be obtained by measuring only wave speed and particle speed, W_s and W_p. The velocity terms may be eliminated simultaneously in Equations 12, 13 and 14 to obtain the Hugoniot relationship,

$$U_1 - U_o = \tfrac{1}{2}(p_1 + p_o)\left(\tfrac{1}{\rho_o} - \tfrac{1}{\rho_1}\right) = \tfrac{1}{2}(p_1 + p_o)(V_o - V_1) \tag{15}$$

where V_o and V_1 are the specific volumes before and after the shock wave.

Often in experiments, the particle velocity is determined indirectly from a measurement of the free surface velocity.

In Reference 1, an analytical fit to the data was made using a power series of the form

$$p_1 = A_1\mu + B_1\mu^2 + C_1\mu^3 \tag{16}$$

where

$$\mu = \frac{V_o}{V_1} - 1 = \frac{\rho_1}{\rho_o} - 1$$

From Equations 15 and 16, and assuming $p_o = 0$, the relation for internal energy on the Hugoniot curve is

$$U_1 = U_o + \frac{(A_1\mu^2 + B_1\mu^3 + C_1\mu^4)}{\left[2\rho_o(\mu+1)\right]} \tag{17}$$

Analytical fits were also made in Reference 1 for the Gruneisen ratio. The relationship of this parameter to the equation of state will be explained later. The equation for this parameter is given as

$$\gamma = \gamma_o + A_2\mu + B_2\mu^2 + C_2\mu^3 \qquad (18)$$

These constants are summarized in Table IV for several metals.

In Reference 2, a different form for the Hugoniot curve is derived. By assuming a straight line fit of the shock-velocity vs. particle-velocity curve, the equation

$$W_s = c + S W_p \qquad (19)$$

was obtained. From the shock-wave relations and Equation 19, the Hugoniot pressure was found to be

$$p_1 = c^2 (V_o - V_1) \Big/ \left[V_o - S (V_o - V_1)\right]^2 \qquad (20)$$

and the corresponding internal energy is given by

$$U_1 = U_o + \frac{1}{2} \left\{ c(V_o - V_1) \Big/ \left[V_o - S (V_o - V_1)\right] \right\}^2 \qquad (21)$$

The constants S and c are also summarized in Table IV for various metals. The density given in Table IV is the density of the metal at zero pressure. The constants for antimony, bismuth, and iron are considered to be approximations. In these metals, phase transitions occur at low pressures. The constants were obtained considering high-pressure data only and ignoring the transitions.

The Hugoniot data on rock materials in Table V were taken from References 15 and 17. The constants for Equations 19 - 21 are given in this table. Generally the scatter of the data in the rock experiments is much greater than in the metal experiments. Several of the rock Hugoniots were synthesized by the author of Reference 17. In this synthesis the chemical composition of the rock materials was determined; and the best Hugoniot data for the various elements was found. The Hugoniot of the elements and compounds in the rocks were weighted according to the molar fractions determined in the chemical analysis. The fractional Hugoniots were then summed to form the synthesized Hugoniot.

Data are scarce for several materials that are of particular interest in armor work. No data were found for plastics although some research is being conducted by Sandia Corp. and others on these materials. The data available on ceramics is limited. If calculations must be made

TABLE IV

CONSTANTS FOR SHOCK HUGONIOTS OF METALS

Metals	Density	Pressure Constants				Gruneisen Ratio Constants			Pressure Constants	
	(gms/cm^3)	A_1	B_1	C_1	γ_o	A_2	B_2	C_2	c	S
Aluminum (24ST)	2.785	765	1659	428	2.13	-7.245	24.707	32.577		
Antimony*	6.684								0.20	1.635
Beryllium	1.845	1185	1382	0	1.17	-2.523	12.990	-31.851		
Bismuth*	9.79								0.126	2.00
Cadmium	8.64	479	1087	2829	2.27	13.417	-75.631	72.965	0.2443	1.671
Chromium	7.13	2070	2236	7029	1.08	10.965	-54.874	49.000	0.5217	1.465
Cobalt	8.82	1954	3889	1728	1.99	-5.906	26.354	-48.076	0.4748	1.330
Copper	8.90	1407	2871	2335	2.04	-3.296	10.493	-19.264	0.3958	1.427
Gold	19.24	1727	5267	0	3.05	-21.876	115.18	-23.17	0.3075	1.560
Indium	7.27	496	1163	0	2.238	-9.431	27.392	-26.186		
Iron*	7.84								0.378	1.680
Lead	11.34	417	1159	1010	2.78	-8.406	22.791	-22.648	0.2028	1.517
Magnesium	1.735	370	540	186	1.46	-2.078	4.621	-4.840		
Molybdenum	10.20	2686	4243	733	1.58	-4.600	25.837	-61.398	0.5157	1.238
Nickel	8.86	1963	3750	0	1.91	-8.007	35.275	-59.812	0.4646	1.445
Niobium	8.604	1658	2786	0	1.679	-5.882	26.261	-49.145		
Palladium	11.95	1744	3801	15,230	2.183	26.824	-205.44	407.72		
Platinum	21.37	2760	7260	0	2.627	-16.911	100.10	-216.84		
Rhodium	12.42	2842	6452	0	2.265	-11.228	55.898	-109.85		
Silver	10.49	1088	2687	2520	2.47	-5.670	19.334	32.891	0.3243	1.586
Tantallum	16.46	1790	3023	0	1.689	-5.166	15.925	-18.991		
Thallium	11.84	317	938	1485	2.96	-3.617	2.264	-1.171	0.2132	1.278
Thorium	11.68	572	646	855	1.124	3.552	-14.223	15.552	0.2640	1.476
Tin	7.28	432	878	1935	2.03	9.4186	-52.133	66.016	0.4779	1.089
Titanium	4.51	990	1168	1246	1.18	2.225	-9.904	11.052		
Tungsten	19.17								0.4005	1.268
Vanadium	6.1			1242					0.5108	1.210
Zinc	7.135	662	1577	0	2.38	-6.087	18.626	23.535	0.3050	1.559
Zirconium	6.49	934	720	3275	0.771	-0.449	0.285	-0.102		
Brass	8.413	1037	2177		2.04	3.405	-26.304	38.692		

* Low pressure transitions occur in these metals. The constants are for approximate curves, and were taken from data above the transition pressures.

TABLE V

CONSTANTS FOR SHOCK HUGONIOTS OF ROCKS

Rock Materials	Density (gm/cm^3)	Constants c	S
Basalt	2.67	.26	1.60
Gabbro	2.98	0.35	1.32
Shale	2.00	0.36	1.34
Limestone	2.50	0.34	1.27
Granite	2.67	0.46	1.00
Anorthosite	2.75	0.30	1.47
Dunite	3.30	0.63	0.65
Olivine	3.00	0.50	1.14
Halite	2.16	0.35	1.33
Rock Salt	2.15	0.35	1.29
Tuff (dry)	1.70	0.136	1.085
Tuff (wet)	1.86	0.263	1.17
Taconite (iron)	4.25	0.325	1.44
Taconite (rock)	2.0	0.29	1.13
Oil Sand	1.90	0.305	1.13
Dolomite*	2.84	0.33	1.30
Rhyolite*	2.35	0.39	1.45
Sandstone*	2.00	0.43	1.34
Claystone*	1.00	0.58	1.32
Diorite*	2.84	0.37	1.38
Syenite*	2.76	0.37	1.38
Diabase*	2.97	0.36	1.41
Pyroxenite*	3.23	0.34	1.38
Lherzolite*	3.23	0.33	1.39
Dacite*	2.60	0.39	1.37
Andesite*	2.60	0.38	1.38
Trachyte*	2.60	0.37	1.37
Phonolite*	2.60	0.31	1.36
Granodiorite*	2.72	0.38	1.36
Nepheline Syenite*	2.61	0.37	1.38
Quartz Diorite*	2.81	0.37	1.38

* Synthesized Hugoniots from Reference 17.

on some of these materials for which no data are available, the synthesis approach could be used to determine the Hugoniot; but the accuracy of the results would be questionable.

5.3 Equation-of-State Calculations

The Mie-Gruneisen equation of state has been found to apply in the pressure range of interest in impact. At temperatures of several thousand degrees, electrons play an important role in the specific heat and pressure and the Mie-Gruneisen equation of state does not apply. In this range, equations considering the electronic components of pressure have been formulated. (Refs. 20, 22, and 23). Equations of this type must be used in problems involving hypervelocity impacts where very high pressures and temperatures result. In armor calculations the pressure is limited to about 400 kilobars, and the temperature is comparatively low in metals. Some typical temperature values on the Hugoniot at 400 kilobars are 311°C for copper, 1812°C for lead, 181°C for nickel, and 520°C for silver. Of the metals listed in Reference 1, the temperature of lead at 400 kilobars was the highest. In the range of interest, the electronic components of pressure are therefore negligible and the Mie-Gruneisen equation of state can be used.

The Mie-Gruneisen equation of state is

$$(p - p_h) = \frac{\gamma}{V}(U - U_h) \qquad (22)$$

p_h and U_h are the Hugoniot pressure and internal energy. They may be obtained from any of the equations giving shock wave pressure and energy and are ultimately based on experimental data. Both p_h and U_h are functions of specific volume as is the Gruneisen ratio, γ. Slater obtained the relation

$$\gamma = -\frac{V}{2}\left(\frac{d^2p/dV^2}{dp/dV} - \frac{2}{3}\right) \qquad (23)$$

for the Gruneisen ratio. Dugdale and MacDonald modified Slater's formula to obtain

$$\gamma = -\frac{V}{2}\left(\frac{d^2(pV^{2/3})/dV^2}{d(pV^{2/3})/dV}\right) - 1/3 \qquad (24)$$

The Dugdale-MacDonald relation for the Gruneisen ratio is considered to be the more accurate of the two. The analytical fits of the $\gamma(V)$ curves given in Table IV can be obtained using either Equation 22 or 24.

In calculations of impact phenomena, a shock compression will take place along the Hugoniot curve; then as the pressure is released the material begins to expand. If this expansion is considered to be adiabatic, the differential equation describing the expansion is obtained by differentiating Equation 22 as follows

$$\frac{V}{\gamma}\left(\frac{dp_A}{dV} - \frac{dp_h}{dV}\right) + (p_A - p_h)\frac{d}{dV}\left(\frac{V}{\gamma}\right) = \frac{dU_A}{dV} - \frac{dU_h}{dV} \quad (25)$$

Subscripts h and A refer to conditions along the Hugoniot curve and along the adiabat. For the adiabatic case, $dU_A/dV = -p_A$, and Equation 25 becomes

$$\frac{dp_A}{dV} = (p_H - p_A)\frac{\gamma}{V}\frac{d}{dV}\left(\frac{V}{\gamma}\right) - \frac{\gamma}{V}p_A - \frac{\gamma}{V}\left(\frac{dU_H}{dV} + \frac{dp_H}{dV}\right) \quad (26)$$

This is a first order equation in terms of the known $p_h(V)$, $U_h(V)$, and $\gamma(V)$. The differentiation was necessary to eliminate the unknown U_H.

For simplification we have approximated the Gruneisen ratio data of Reference 2 with straight lines as follows

$$\gamma = A + M(V/V_o) \quad (27)$$

Figures 11, 12, and 13 compare the data from Reference 2, indicated by the points, with the straight line approximations up to 400 kilobars. The constants, A and M, for the straight line approximations are given in Table VI. The straight line approximations should not be used beyond the 400 kilobar limit. In general, the straight line approximations in Figures 11, 12, and 13 compare better with the data of Reference 2 than do the data from Reference 1 in the range to 400 kilobars.

5.4 Computer Code for Adiabatic Expansion

To allow a comparison with the results of calculations in Reference 2 and to lay a foundation for using the Mie-Gruneisen equation of state in hydrodynamic flow calculations, a computer program was written to numerically solve Equation 26 for the adiabats using the Runge-Kutta method. This program calculated the adiabatic pressure by starting on the Hugoniot curve at a known pressure and volume. The adiabatic pressure was then calculated point by point at given intervals along the

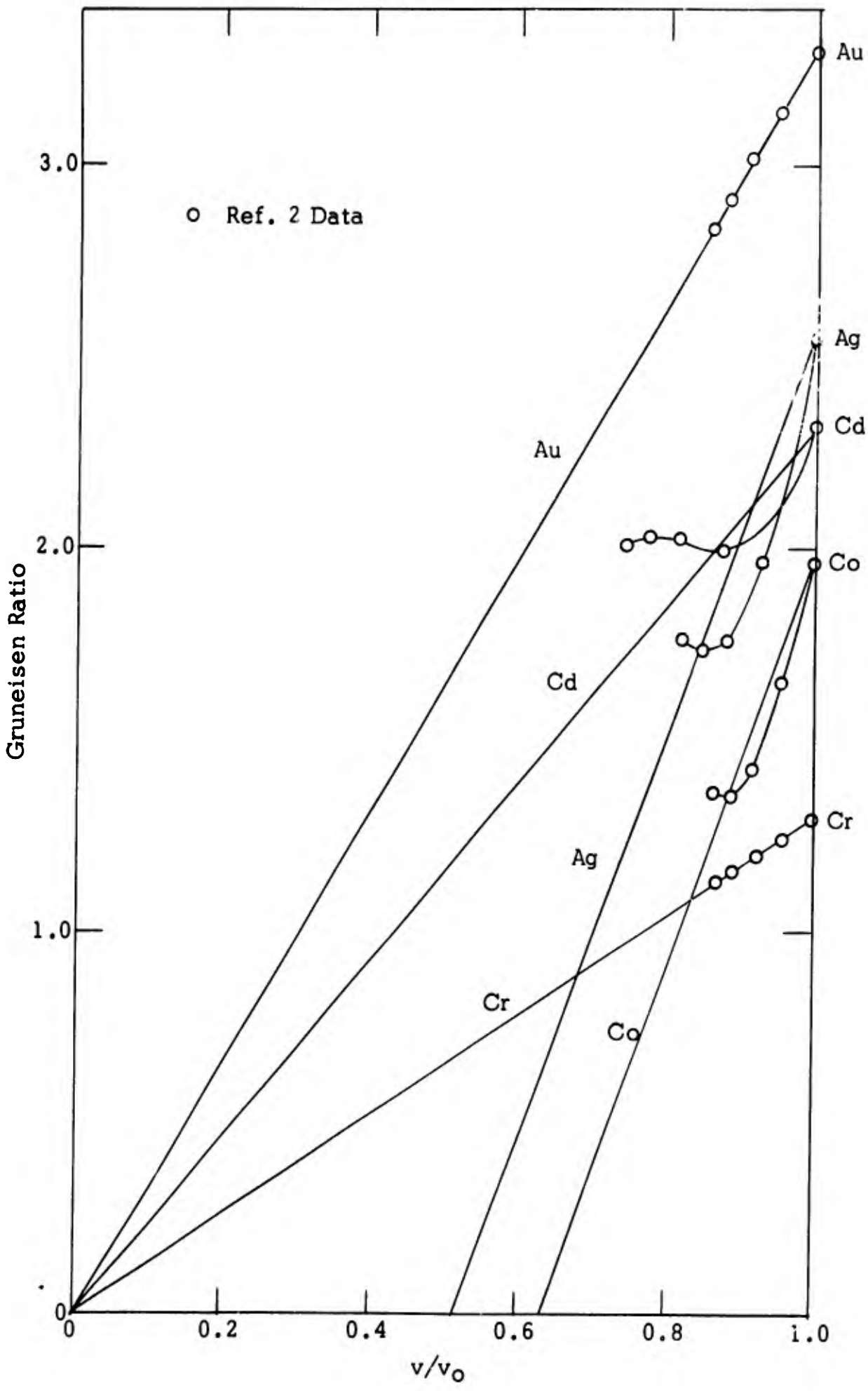

Figure 11. Gruneisen ratios from Reference 2 and straight line approximations for pressure range to 400 kilobars.

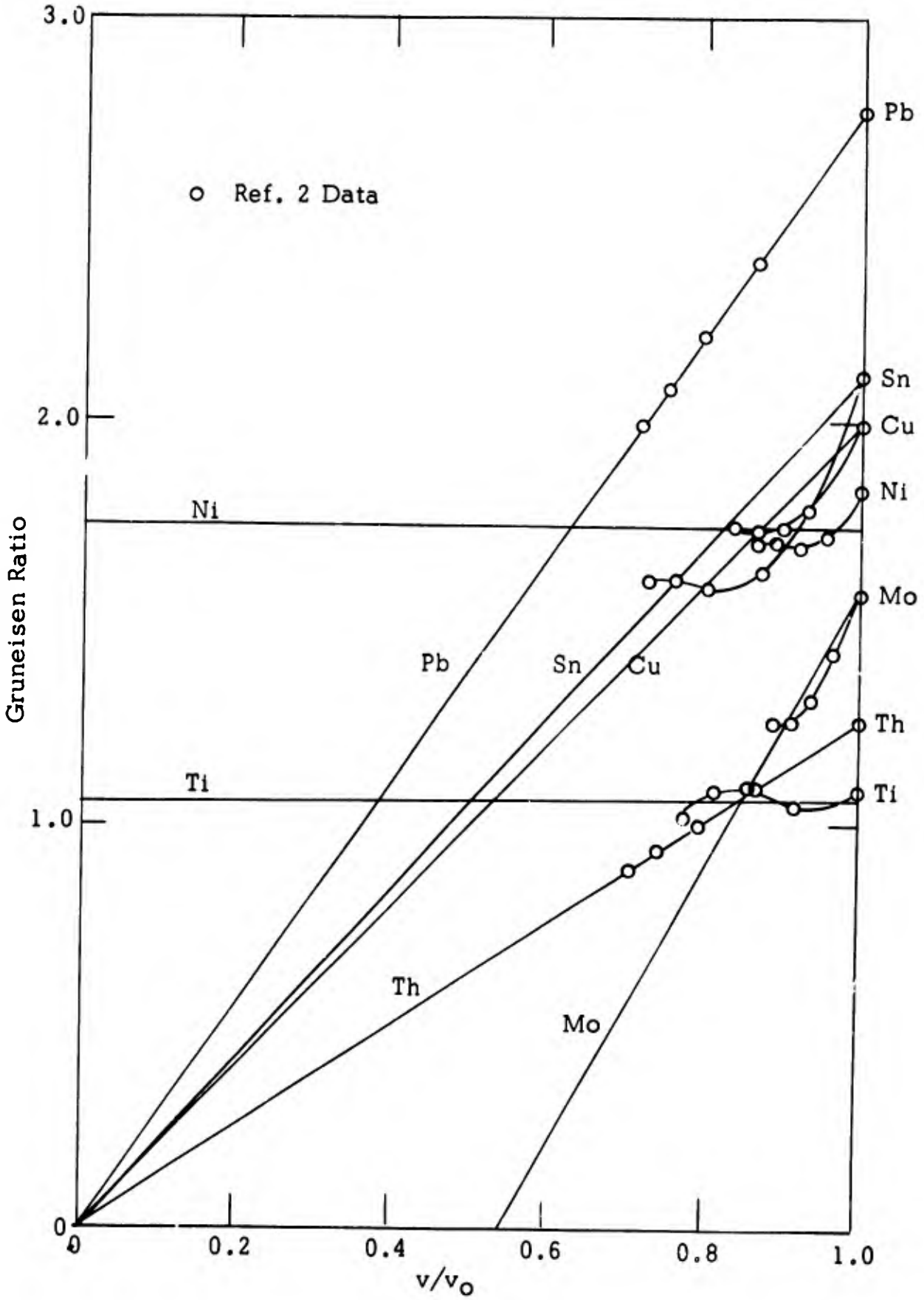

Figure 12. Gruneisen ratios from Reference 2 and straight line approximations for pressure range to 400 kilobars.

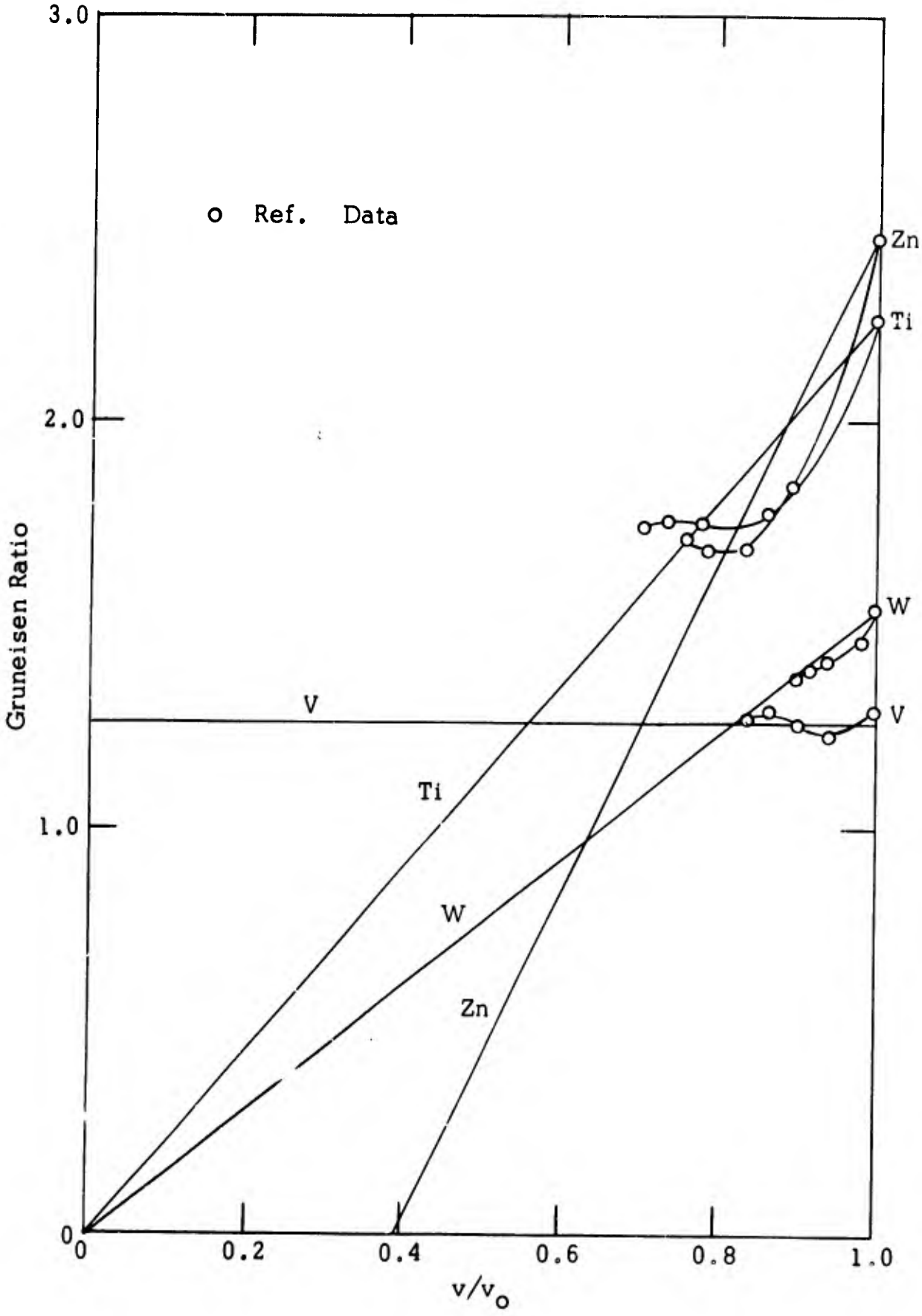

Figure 13. Gruneisen ratios from Reference 2 and straight line approximations for pressure range to 400 kilobars.

TABLE VI

CONSTANTS FOR APPROXIMATE GRUNEISEN RATIO
AND COMPARISON OF V/V_o VALUES
AT P = 0 FOR ADIABATIC EXPANSION
STARTING AT 400 KILOBARS ON HUGONIOT CURVE

			V/V_o at P = 0	
	A	M	Ref. 2	URDC Calc.
Cadmium	2.32	0	1.059	~1.050
Chromium	0	1.29	1.002	1.001
Cobalt	-3.26	5.47	1.003	1.004
Copper	0	2.00	1.006	1.006
Gold	0	3.29	1.005	1.005
Lead	0	2.77	1.071	1.057
Molybdenum	-1.86	3.44	1.001	1.001
Nickel	1.74	0	1.003	1.004
Silver	-2.68	5.15	1.013	1.012
Thallium	0	2.25	1.079	1.066
Thorium	0	1.26	1.027	1.033
Tin	0	2.11	1.054	1.055
Titanium	1.06	0	1.007	1.010
Tungsten	0	1.54	1.000	1.001
Vanadium	1.26	0	1.003	1.004
Zinc	-1.63	4.08	1.032	1.032

expansion curve. The Hugoniot pressure, Hugoniot energy, and Gruneisen ratio needed in the solution were obtained from Equations 20, 21, and 27. A flow diagram of the steps involved in the calculation is shown in Figure 14. The diagrammed procedure used the Runge-Kutta method. Four values of W(I) are calculated using the results from Equations 20 and 27, and the derivatives of Equations 20 and 21. The values of V and p_A used in the calculations are indicated. The adiabatic pressure is then calculated using the form W(I) terms and the initial pressure in Equation 28 (shown in the figure). The calculation is then repeated several times with the previous p(J) becoming the initial condition.

Note a few changes in notation in Figure 14. This reflects the usage in the computer program. p_A becomes P_A and U becomes E. H is the time interval and J is the step number. Calculations were made for the various metals in Reference 2. The adiabatic expansion was started at the 400 kilobar point on the Hugoniot curve. Our results for the volume ratio at zero pressure are compared with those of Reference 2 in Table VI. The comparisons are good and indicate that the approximation of the Gruneisen ratio is justified. A calculation was made for lead with the expansion from the 200 kilobar point on the Hugoniot curve. The ratio, V/V_O, was equal to 1.018 which is exactly the same as that given in Reference 2. In Reference 1, the value of V/V_O for an expansion from 204 kilobars was 1.020.

Conclusions. There is an abundance of Hugoniot data for metals which can be used in armor calculations. So far as plastics and ceramics are concerned, there are little data. This indicates a need of experimental studies to determine shock Hugoniots for plastics and ceramics.

The Mie-Gruneisen equation of state provides an adequate description of the states of materials up to the 400 kilobar limit of interest in armor calculations. With the straight-line approximations of the Gruneisen ratio it allows rather straightforward calculations of the states in the materials. The equation for adiabatic expansion has not yet been included in the PIF code computer program to calculate impact effects. In order to include these calculations in the hydrodynamic flow computer code, some additional steps must be taken. Energy may be added to or taken from the system by friction which leads to a deviation from the Hugoniot or adiabat. It seems appropriate that energy should be added or subtracted at incremental steps as the Hugoniot or adiabatic equations are applied. This requires adjustments in initial conditions at each step, but should give satisfactory results. This is a subject for future research.

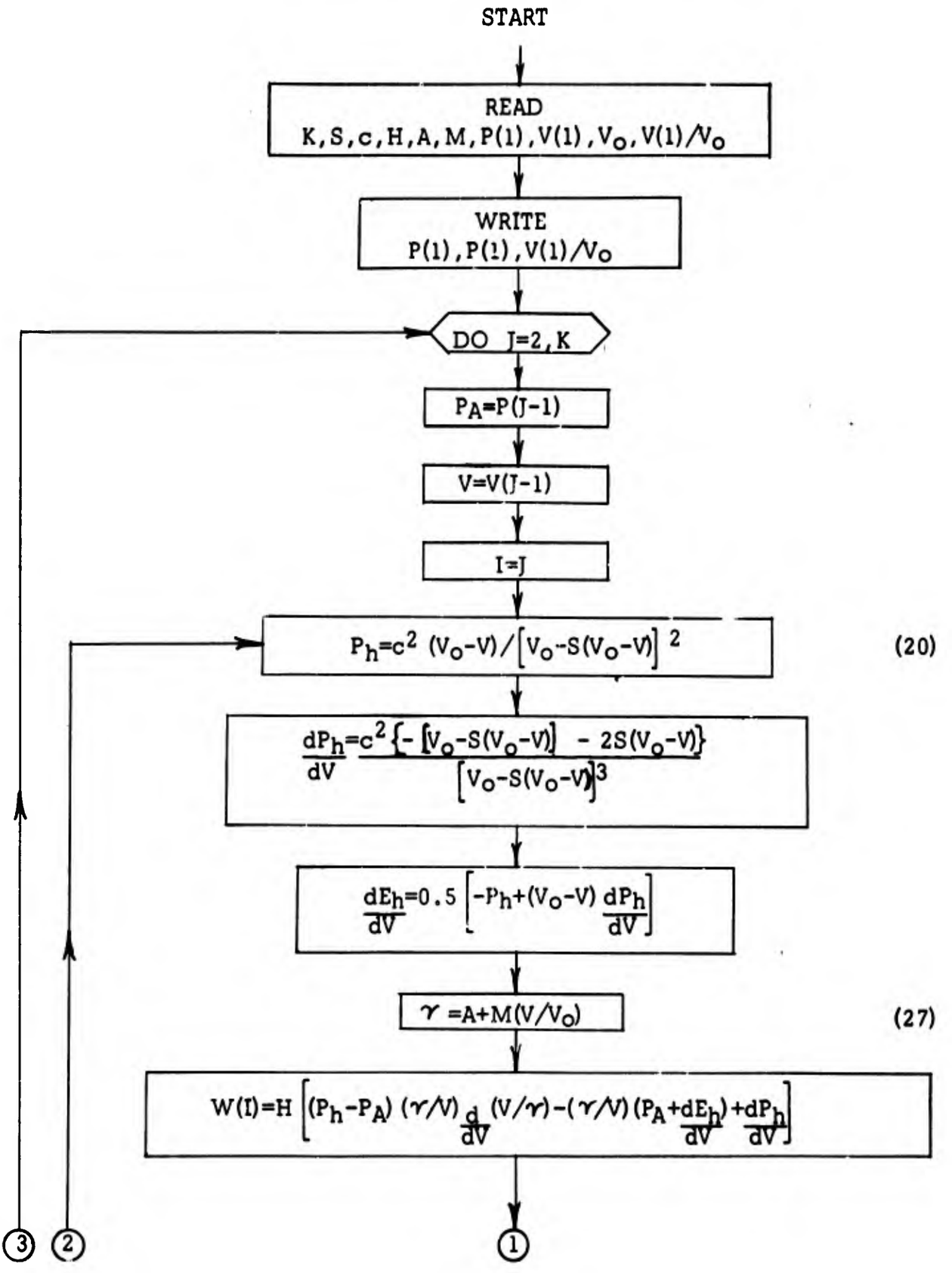

Figure 14. Flow diagram for computer calculations of adiabats.
(Continued on next page)

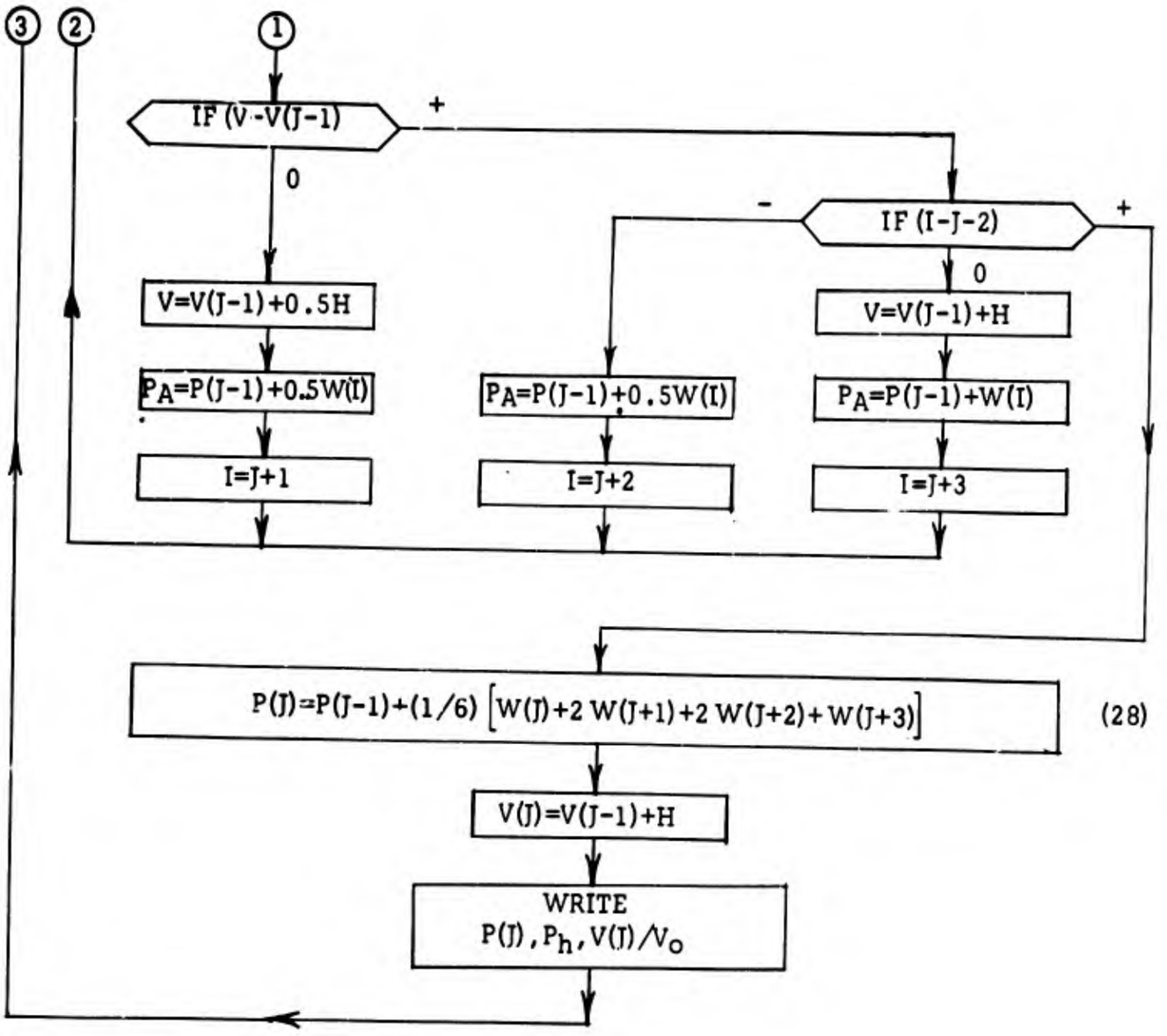

Figure 14. (Continued)

6. REFERENCES

1. J. M. Walsh, M. H. Rice, R. G. McQueen, and F. G. Yarger, "Shock-Wave Compressions of Twenty-Seven Metals - Equations of States of Metals," Phys. Rev., 108, 196 (1957)

2. R. G. McQueen and S. P. Marsh, "Equation of State for Nineteen Metallic Elements from Shock-Wave Measurements to Two Megabars," J. Appl. Phys., 31, 1253 (1960)

3. L. V. Al'tshuler, K. K. Krupnikov, and M. J. Brazhnik, "Dynamic Compressibility of Metals under Pressures from 400,000 to 4,000,000 Atmospheres," Soviet Physics JETP, 34 (7), 614 (1958)

4. D. G. Doran, "Hugoniot Equation of State of Pyrolytic Graphite to 300 Kbars," J. Appl. Phys., 34, 844 (1963)

5. J. Appl. Phys., 30, 568 (1959)

6. G. R. Fowles, "The Development of an Explosive Electric Transducer, Part I, Equation of State of Quartz," SRI, TID 11862

7. E. G. Zukar, C. M. Fowler, F. S. Minshall, and J. O'Rourke, "The Behavior of Iron-Silicon Alloys Under Impulsive Loading," Trans. Metall. Soc., AIME, 227, 746 (1963)

8. Packard and Swenson, "An Experimental Equation of State of Solid Xenon," J. Phys. Chem. Solids (G.B.), 24, 1405 (1963)

9. B. J. Davydon, "Equation of State for Solid Bodies," Transl. of Akademiya Nauk. SSSR, Iznestiya Seriya Geofizichesha (Ya), 1956, No. 12, pp 1411-1418, U. S. Gov. Res. Rep. Vol. 39, p. 149A, July 20, 1964, AD 600 614

10. V. M. Gogolev, V. G. Myrkin, and G. I. Yahlokova, "Approximate Equation of State of Solids," Zh. Prikl. Mekham. i Tekhm Fiz. 1963 (5), 93-8

11. S. B. Kormer, A. I. Funtikov, V. D. Urlin, and A. N. Kolesnikova, "Dynamic Compression of Porous Metals and the Equation of State with a Variable Specific Heat at High Temperature," Soviet Physics JETP, 15, 477 (1962)

12. V. G. Gregson, T. J. Ahrens, and C. F. Peterson, "Dynamic Properties of Rocks," NASA Doc. N63-20783, 88 pp (1963)

13. I. C. Skidmore and E. Morris, "Experimental Equations of State Data for Uranium and Interpretations in the Critical Regions," Thermodynamic Nuclear Materials, Proc. Conf. Vienna 1962, 173-216 (pub. 1963)

14. E. Morris, U. K. At. Energy Authority, At. Weapons Res. Estab. Rept. 0-61/62, 65 pp (1962)

15. D. B. Lombard, "The Hugoniot Equation of State of Rocks," UCRL 6311, Feb. 28, 1961

16. L. V. Al'tshuler, A. A. Bakanova, and R. F. Trunin, "Shock Adiabats and Zero Isotherms of Seven Metals at High Pressures," Soviet Physics JETP, 15, 65 (1962)

17. A. J. Chabai, "Synthesis of Shock Hugoniots for Rock Materials," Sandia Corporation Report No. SCR-555, May 1963

18. L. V. Al'tshuler, K. K. Krupnikov, B. N. Ledenev, V. I. Zhuchikhin, and M. I. Brozhnik, "Dynamic Compressibility and Equation of State of Iron under High Pressure," Soviet Physics JETP, 34(7), 606 (1958)

19. V. N. Zharkov and V. A. Kalinin, "Equation of State for Gabbro and Dunite at High Pressures," Isv. Akad. Nauk. SSSR, Ser. Geofiz, 1962, 298-306

20. L. V. Al'tshuler, S. B. Kormer, A. A. Bakanova, and R. F. Trunin, "Equation of State for Aluminum, Copper, and Lead in the High Pressure Region," Soviet Physics, JETP, 38(11), 573 (1960)

21. J. Viard, "Hugoniot Curve of Vitreous Silica and Crystallization under Shock," Comptes Rendus, 249, 820 (1959)

22. S. B. Kormer, A. I. Funtikov, V. D. Urlin, and A. N. Kolesnikova, "Dynamic Compression of Porous Metals and the Equation of State with Variable Specific Heat at High Temperatures," Soviet Physics JETP, 15, 477 (1962)

23. M. H. Wagner, N. B. Brooks, and R. L. Bjork, "Impact of a Porous Aluminum Projectile on Aluminum at 20 and 72 km/sec," Proceedings of the 7th Hypervelocity Impact Symposium, Vol. 3, February 1965

APPENDIX A

SEMIANNUAL REPORT - November 1964

TABLE OF CONTENTS

SUMMARY

The tensor formulation of the stress-strain relationships involved in finite time-dependent deformation of a solid has been changed from that previously reported. The new mathematical model is described along with a discussion of the applicable mathematics.

The computer code developed to calculate the flow field in impact has been modified to eliminate propagated error in the time dimension.

A system for high speed photographic analysis of deformation of wires and rods is described. Data from rod-to-rod impact are analyzed to determine the energies involved in metal deformation. Average energy per unit deformation is found to decrease with increasing impact velocity.

SEMIANNUAL REPORT - May 1965

TABLE OF CONTENTS

SUMMARY

A study of the strength of materials under large deformation has been conducted. The sample to be tested was in the form of a thin disk and was crushed between a fixed and a moving anvil. Velocities ranging from 10^{-3} to 10^{4} cm/sec were obtained by driving the anvil either by a testing machine or by a compressed-air gun.

A simplified analysis of the problem is given, and the assumptions used are discussed and compared with the experimental data. The

relationship between internal energy of the material and deformation is found to be $U = \tau \ln (z_o/z)$ where U is energy per unit mass, z_o and z are initial and final thickness of the disk and τ is a constant, the "strength" of the material. Variations in τ are discussed in terms of strain-rate effects and strain-hardening effects.

The materials tested were copper, 99.99 per cent pure aluminum, 6061-T4 and -T6 aluminum, nylon, Lexan, Teflon, polyethylene and polypropylene.

SEMIANNUAL REPORT - December 1965

TABLE OF CONTENTS

ABSTRACT

Progress is reported on the development of a computer code for describing the flow field during impact of solid on solid. A one-dimensional material model is used consisting of isolated mass points connected by springs with highly non-linear spring constants and viscous damping. The spring constant is derived from shock Hugoniot equation-of-state work,

and the viscosity comes from measurements of the energy involved in crushing discs of the material used. So far, aluminum has been the only material tested in the computer program. The results of varying the predictor/corrector scheme used to stabilize the solution and the results of varying viscosity are presented. It is shown that the solution gives the correct pressure jump across a shock front and gives correct wave velocities. Some oscillations and propagation of error are present. Methods of improving this are discussed.

A rod-to-rod impact experiment is described for measuring the maximum pressure gradient which a material can sustain under dynamic impact conditions. The method is suitable for measuring material strength properties for brittle materials which are not suited to the disc-crushing experiments previously used. Results are presented for nylon, polypropylene, plexiglass, Benelex, and glass. The plastics show a maximum pressure gradient, then a leveling off as impact velocity is increased. Glass increases continually up to the maximum velocities tested. Further work to increase the pressure used in the tests and to investigate geometric effects is outlined.

APPENDIX A

Variables Used in PIF Code Program

RHO	Density, ρ	RHOT	Trial Value
DVDX	$\partial v/\partial x$	DVDXT	" "
V	Velocity, v	VT	" "
DPDX	$\partial p/\partial x$	DPDXT	" "
DTDX	$\partial \tau/\partial x$	DTDXT	" "
U	Internal Energy	UT	" "
P	Pressure, p	PT	" "
TAU	Stress, τ	TAUT	" "
X	Position, x	XT	" "
PLOG	Log_{10} p		
NP	Number of pressure points plotted		
MAX	Maximum number of mesh points		
DXO	Initial spacing of points, Δx		
DT	Time interval, Δt		
RHOO	Initial density, ρ_o		
EM	Constant in equation of state, m		
AK	Constant in equation of state, k		
TAO	Constant in stress equation, τ_o		
EMU	Constant in stress equation, μ_o		
UO	Initial internal energy, U_o		
SMOM	Sum of momentum of all mass points		
SNRG	Sum of energy of all mass points		
SU	Sum of internal energy of all mass points		
T	Time, t		
NTINT	Index number. Number of time intervals computed or number of times program has repeated		
NPRINT	Index number. Number of print-outs since last plot		
NPRNT	Pre-set number. Number of time increments between print-out		
NPLOT	Pre-set number. Number of print-outs between plots		
MAXP	Maximum particle index in projectile		
NPRNT 2,	NPLOT2. Same as NPRNT and NPLOT. These allow changing print-out and plot interval during run.		
XO	Position of mass point with index 1		
VINP	Velocity of projectile mass points		
VINT	Velocity of target mass points		
TMAX	Time at which plotting and printing intervals are changed or time of stopping program		
TMAX2	Time at which program stops		

Other variables appearing in the program were not used in the particular versions shown. Other variables are derived in the program from the above in an obvious manner.

Flow Diagrams for PIF Program

No diagrams are shown where the flow does not branch. Refer to program listing for each program.

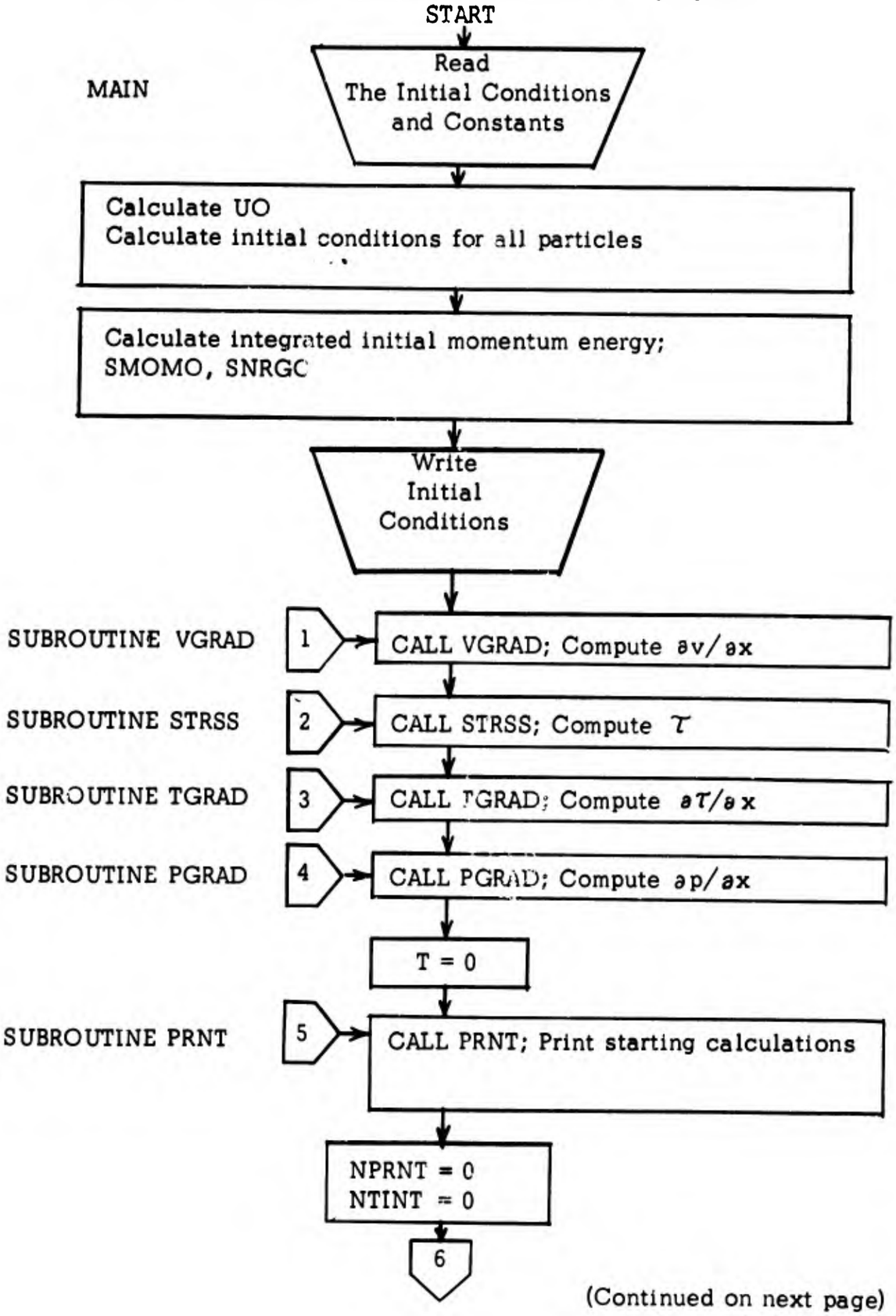

(Continued on next page)

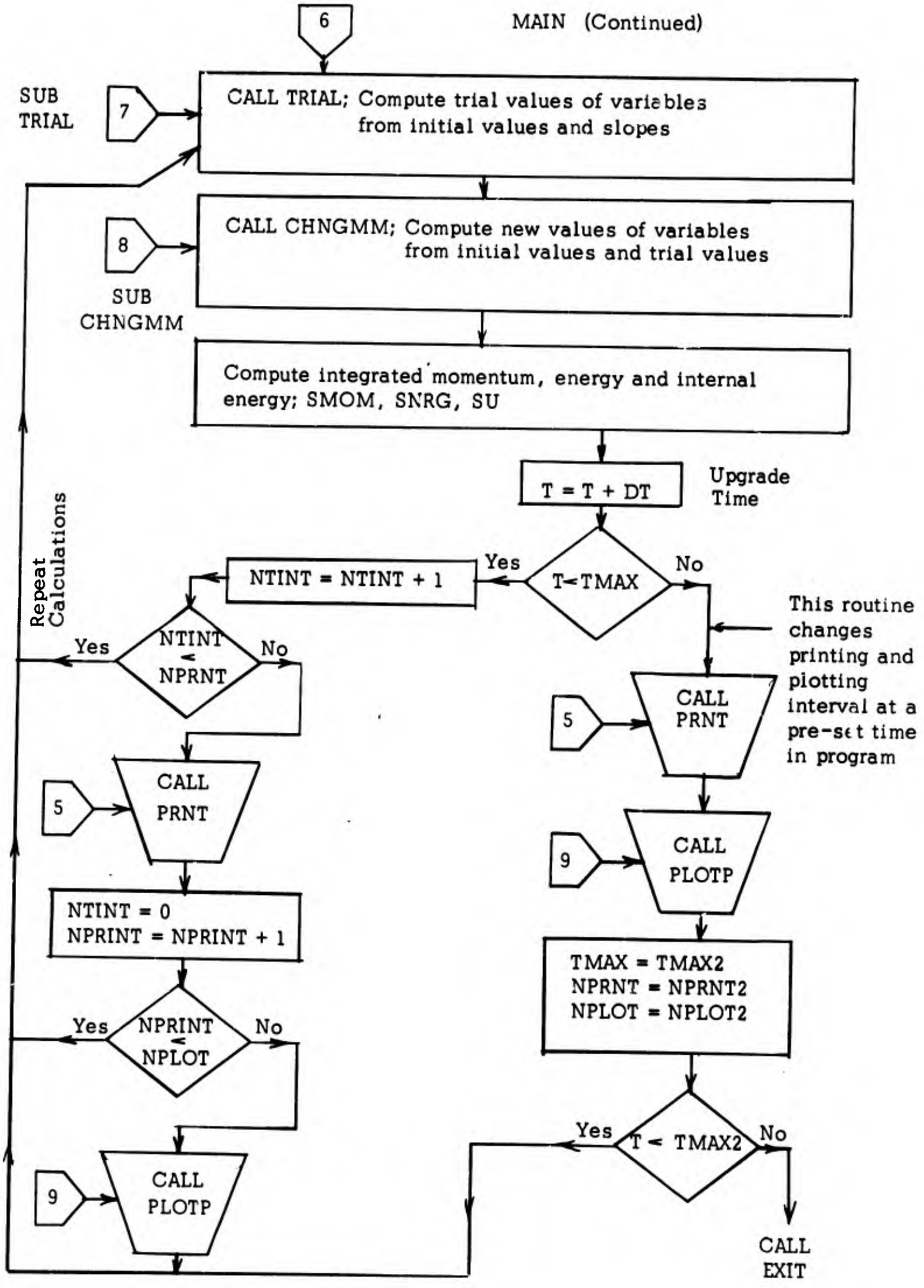
6
MAIN (Continued)
SUB TRIAL
7
CALL TRIAL; Compute trial values of variables from initial values and slopes
8
CALL CHNGMM; Compute new values of variables from initial values and trial values
SUB CHNGMM
Compute integrated momentum, energy and internal energy; SMOM, SNRG, SU
T = T + DT
Upgrade Time
T=TMAX
Yes
No
NTINT = NTINT + 1
Repeat Calculations
NTINT < NPRNT
Yes
No
This routine changes printing and plotting interval at a pre-set time in program
5
CALL PRNT
5
CALL PRNT
9
CALL PLOTP
NTINT = 0
NPRINT = NPRINT + 1
TMAX = TMAX2
NPRNT = NPRNT2
NPLOT = NPLOT2
NPRINT < NPLOT
Yes
No
T < TMAX2
Yes
No
9
CALL PLOTP
CALL EXIT

SUBROUTINE TRIAL

Trial values for ρ, U, and v are calculated for each particle using Equations 1, 2, and 3. A trial value for x is computed by XT = X + DT * V. Trial values are computed for $\partial v/\partial x$, τ, p, $\partial p/\partial x$, $\partial \tau/\partial x$.

SUBROUTINE CHNGMM

The initial values of the slopes for ρ, U and v are averaged with the trial values and this average slope is used to compute ρ, U, and v. Position is computed from X = X + (DT/2.) * (V + VT). From these new values, $\partial v/\partial x$, τ, $\partial \tau/\partial x$, p and $\partial p/\partial x$ are computed to prepare for a new step.

SUBROUTINE PRESS AND PRESST

Pressure is computed using Equation 4. If the energy is negative, pressure is computed using the absolute value of the ratio U/UO then setting P(I) = -P(I). This expedient allows the use of the simple equation of state into regions of tensile stress.

SUBROUTINES STRSS AND STRSST

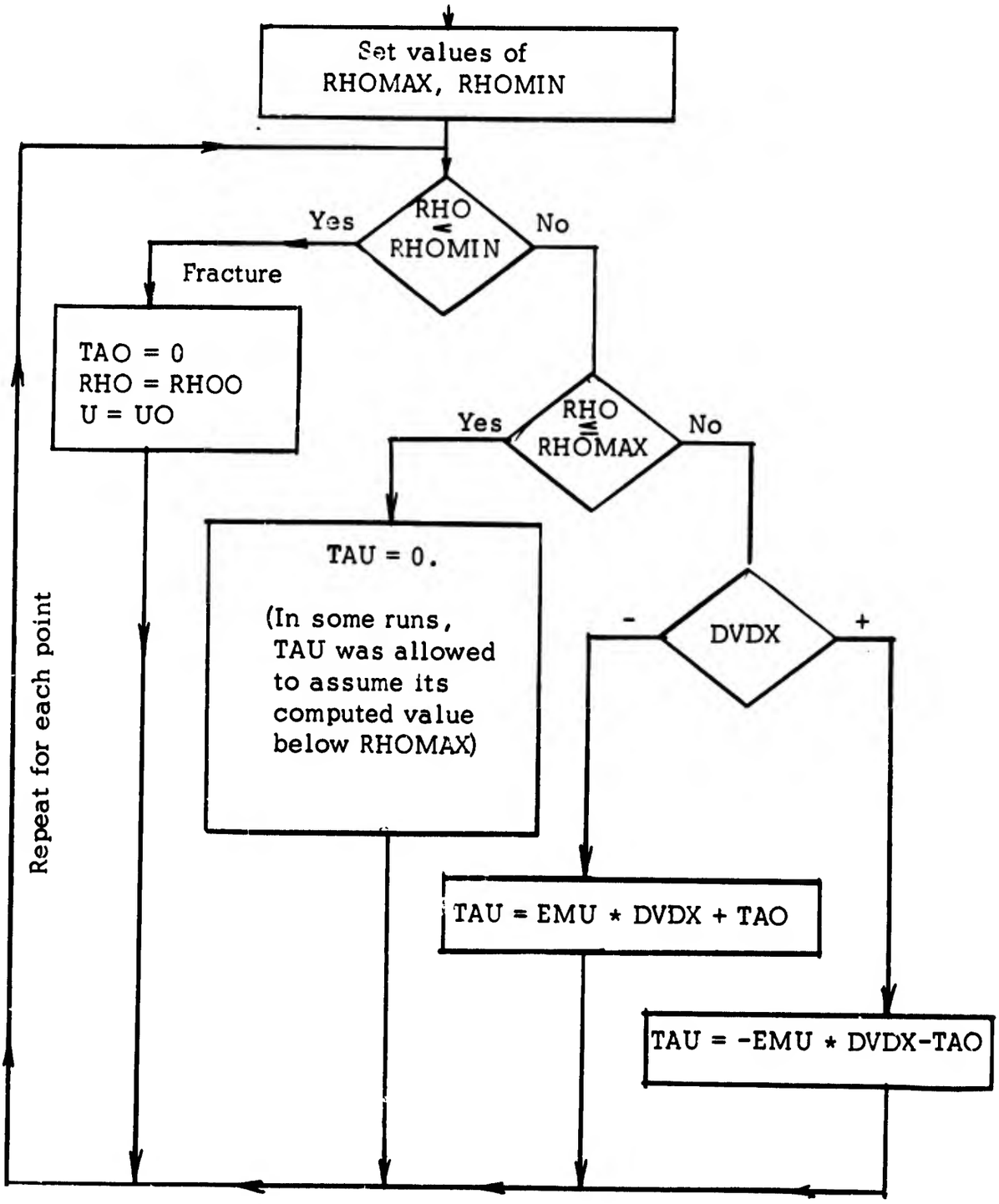

SUBROUTINE VGRAD, VGRADT, PGRAD, PGRADT, TGRAD, TGRADT

Linear interpolation was used to obtain gradients. Quadratic interpolation was tried but the improvement in results was only slight so the linear program was used to speed the computations.

SUBROUTINE PRNT

Quantities printed out and format are controlled in this subroutine.

SUBROUTINE PLOTP

This subroutine provides a rough plot of pressure versus particle number. It is produced by the regular printer rather than a plotter. It's purpose is to give a quick visual check on results.

In operation, the point with the highest pressure is found and the characteristic of the log of this number is found, NCH. This number plus 1 is used as the maximum on the logarithmic pressure scale on the plot. The pressure scale is divided into intervals and each pressure is tested with each interval to see where it fits. A line of print-out is generated for each interval consisting of a zero for each mass point (except a 1 every tenth number to provide a grid) except for a 4 whenever the pressure of a particular mass point falls in the interval. A sample of the print-out is shown.

rough plot of pressure →

```
10000000001000000001  12.0
10000000001000000001  11.9
10000000001000000001  11.8
10000000001000000001  11.7
10000000001000000001  11.6
10000000001040000001  11.5
10000000001000000001  11.4
44444444444040000001  11.3
10000000001000000001  11.2
10000000001000000001  11.1
```

SUBROUTINE PLOTP

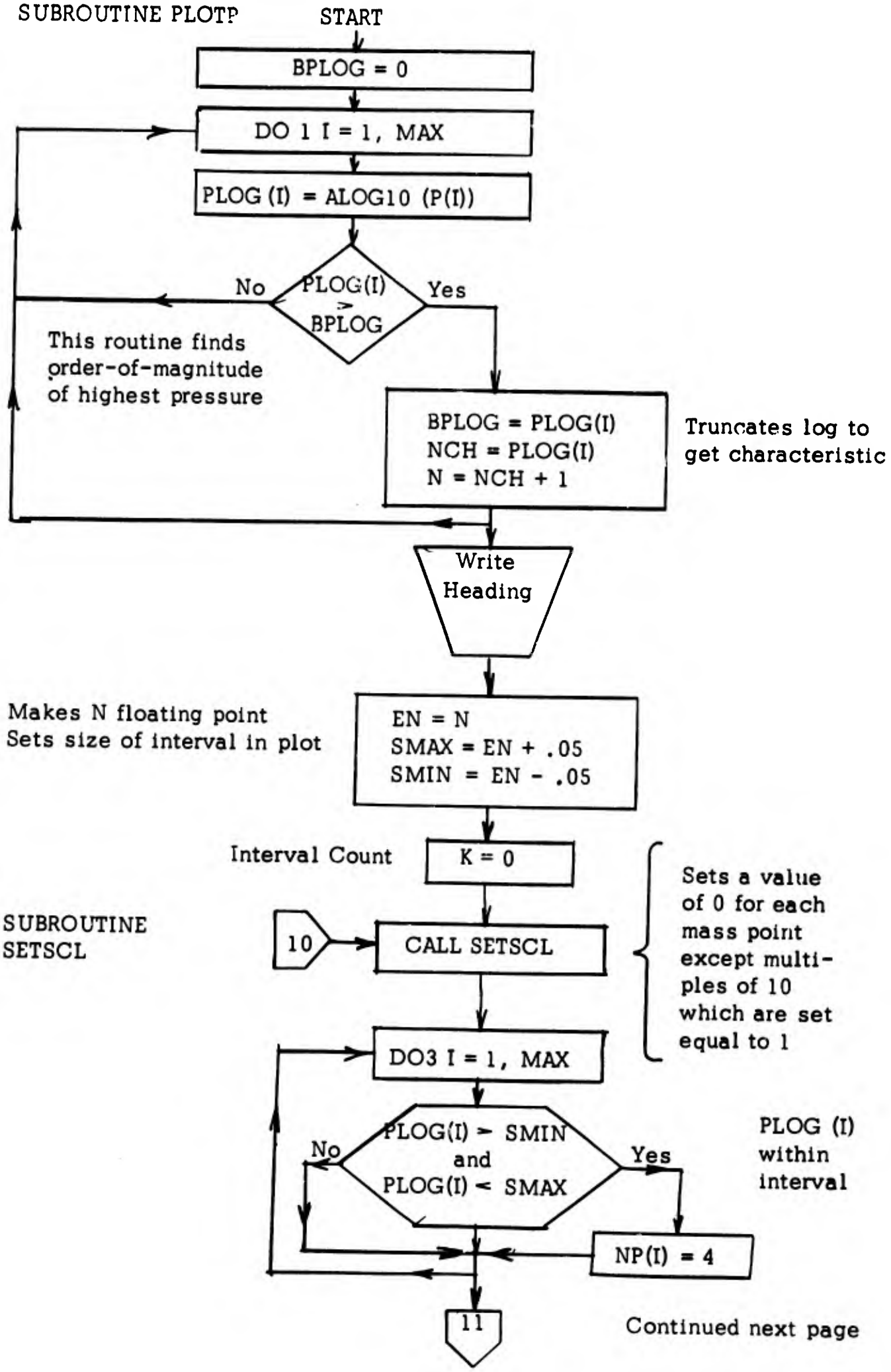

Continued next page

SUBROUTINE PLOTP (Continued)

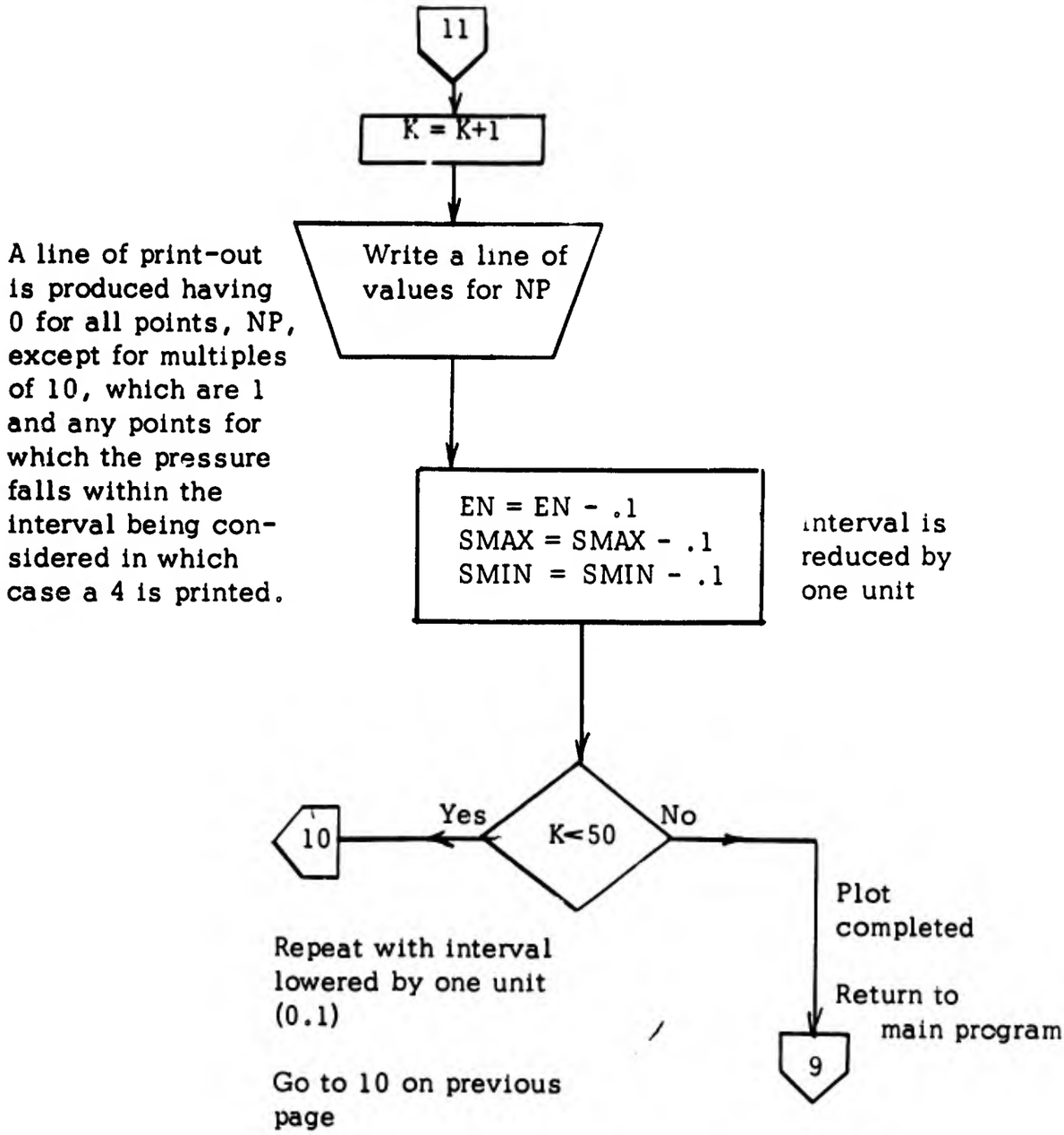

APPENDIX A

ONE-DIMENSIONAL PIF CODE; FORTRAN IV

```
   ONE DIMENSIONAL IMPACT, AL-AL, 2KM/SEC, MODIFIED MARCHING METHOD
   UTAH RESEARCH AND DEVELOPMENT CO
   CONTRACT DA-19-129-AMC-150(X)
   COMMON RHO(60),RHOT(60),DVDX(60),DVDXT(60),V(60),VT(60),
  1DPDX(60),DPDXT(60),DTDX(60),DTDXT(60),U(60),UT(60),Y(60),
  2P(60),PT(60),TAU(60),TAUT(60),X(60),XT(60),PLOG(60),NP(60),
  3MAX,DXO,DT,RHOO,EM,AK,TAO,EMU,UO,SMOM,SNRG,SU,T,NTORM,MM1
   READ(5,1)MAX,NPRNT,NPLOT,NCORM,MAXP,NPRNT2,NPLOT2
 1 FORMAT( I5)
   READ(5,2)DXO,DT,TMAX,RHOO,EM,AK,TAO,EMU,XO,VINP,VINT,TMAX2
 2 FORMAT(E15.8)
   UO= ((1.01325E6*EM)/(2.*RHOO))**(1./(1.-AK))
   X(1)=XO
   DO3 I=2,MAX
 3 X(I)=X(I-1)+DXO
   DO4 I=1,MAXP
 4 V(I)=VINP
   MINT=MAXP+1
   DO5 I=MINT,MAX
 5 V(I)=VINT
   SMOMO=0.
   SNRGO=0.
   MM1=MAX-1
   DO6 I=1,MAX
   P(I)=1.01325E6
   U(I)=UO
   TAU(I)=0.
   RHO(I)=RHOO
   SMOMO=SMOMO+V(I)*RHOO*DXO
   SNRGO=SNRGO+RHOO*DXO*(V(I)*V(I)/2.+U(I))
 6 CONTINUE
   WRITE(6,15)SMOMO,SNRGO
15 FORMAT(1H 2E18.8)
   WRITE(6,7)
 7 FORMAT(61H       MAX    NPRNT    NPLOT    NCORM     MAXP   NPRNT2   NPLOT
  12        )
   WRITE(6,8)MAX,NPRNT,NPLOT,NCORM,MAXP,NPRNT2,NPLOT2
 8 FORMAT(1H 7I8)
   WRITE(6,9)
 9 FORMAT(130H       DXO           DT           TMAX           RHOO           EM
  1             AK          TAO           EMU             XO             UO
  2    VINP     )
   WRITE(6,10)DXO,DT,TMAX,RHOO,EM,AK,TAO,EMU,XO,UO,VINP
10 FORMAT(1H 11E12.5)
   WRITE(6,11)
11 FORMAT(50H     SMOMO        SNRGO        VINT         TMAX2          )
   WRITE(6,12)SMOMO,SNRGO,VINT,TMAX2
12 FORMAT(1H 4E12.5)
```

```
      CALL VGRAD
      CALL STRSS
      CALL TGRAD
      CALL PGRAD
      T=0.
      CALL PRNT
      NPRINT=0
      NTINT=0
   13 CALL TRIAL
      CALL CHNGMM
      SMOM=0.
      SNRG=0.
      SU=0.
      DO14 I=1,MAX
      SMOM=SMOM+V(I)*RHOO*DXO
      SNRG=SNRG+RHOO*DXO*(V(I)*V(I)/2.+U(I))
      SU=SU+RHOO*DXO*U(I)
   14 CONTINUE
      T=T+DT
      IF(T-TMAX)16,17,17
   17 CALL PRNT
      CALL PLOTP                                                    $I
      TMAX=TMAX2
      NPRNT=NPRNT2
      NPLOT=NPLOT2
      IF(T-TMAX2)13,20,20
   20 CALL EXIT
   16 NTINT=NTINT+1
      IF(NTINT-NPRNT)13,18,18
   18 CALL PRNT
      NTINT=0
      NPRINT=NPRINT+1
      IF(NPRINT-NPLOT)13,19,19
   19 CALL PLOTP
      NPRINT=0
      GO TO 13
      END

$IBFTC TRIAL
      SUBROUTINE TRIAL
      COMMON RHO(60),RHOT(60),DVDX(60),DVDXT(60),V(60),VT(60),
     1DPDX(60),DPDXT(60),DTDX(60),DTDXT(60),U(60),UT(60),Y(60),
     2P(60),PT(60),TAU(60),TAUT(60),X(60),XT(60),PLOG(60),NP(60),
     3MAX,DXO,DT,RHOO,EM,AK,TAO,EMU,UO,SMOM,SNRG,SU,T,NTORM,MM1
      RHOT(1)=RHO(1)-RHO(1)*DVDX(1)*DT
      RHOT(MAX)=RHOO
      UT(1)=U(1)-(DT*DVDX(1)/RHO(1))*(P(1)+TAU(1))
      UT(MAX)=UO                                                    $IB
```

```
      VT(1)=V(1)-((DT*2.)/(RHO(1)+RHOO))*(DPDX(1)+DTDX(1))
      VT(MAX)=V(MAX)-((DT*2.)/(RHO(MM1)+RHOO))*(DPDX(MAX)+DTDX(MAX))
      XT(1)=X(1)+DT*V(1)
      XT(MAX)=X(MAX)+DT*V(MAX)
      DO1 I=2,MM1
      ROAV=(RHO(I)+RHO(I-1))/2.
      RHOT(I)=RHO(I)-RHO(I)*DVDX(I)*DT
      VT(I)=V(I)-(DT/ROAV)*(DPDX(I)+DTDX(I))
      UT(I)=U(I)-(DT*DVDX(I)/RHO(I))*(P(I)+TAU(I))
      XT(I)=X(I)+DT*V(I)
    1 CONTINUE
      NTORM=1
      CALL VGRADT
       CALL STRSST
      CALL PRESST
      CALL PGRADT
      CALL TGRADT
      NTORM=0
      RETURN
      END

$IBFTC CHNGMM
      SUBROUTINE CHNGMM
      COMMON RHO(60),RHOT(60),DVDX(60),DVDXT(60),V(60),VT(60),
     1DPDX(60),DPDXT(60),DTDX(60),DTDXT(60),U(60),UT(60),Y(60),
     2P(60),PT(60),TAU(60),TAUT(60),X(60),XT(60),PLOG(60),NP(60),
     3MAX,DXO,DT,RHOO,EM,AK,TAO,EMU,UO,SMOM,SNRG,SU,T,NTORM,MM1
      DO1 I=1,MAX
      RHO(I)=RHO(I)-(DT/2.)*(RHO(I)*DVDX(I)+RHOT(I)*DVDXT(I))
      X(I)=X(I)+(DT/2.)*(V(I)+VT(I))
      U(I)=U(I)-(DT/2.)*(DVDX(I)*(1./RHO(I))*(P(I)+TAU(I))+
     1DVDXT(I)*(1./RHOT(I))*(PT(I)+TAUT(I)))
    1 CONTINUE
      V(1)=V(1)-DT*((1./(RHO(1)+RHOO))*(DPDX(1)+DTDX(1))+
     1(1./(RHOT(1)+RHOO))*(DPDXT(1)+DTDXT(1)))
      DO2 I=2,MAX
      V(I)=V(I)-DT*((1./(RHO(I)+RHO(I-1)))*(DPDX(I)+DTDX(I))+
     1(1./(RHOT(I)+RHOT(I-1)))*(DPDXT(I)+DTDXT(I)))
    2 CONTINUE
      CALL VGRAD
      CALL STRSS
      CALL TGRAD
      CALL PRESS
      CALL PGRAD
      RETURN
      END

$IBFTC PRESS
```

```
      SUBROUTINE PRESS
      COMMON RHO(60),RHOT(60),DVDX(60),DVDXT(60),V(60),VT(60),
     1DPDX(60),DPDXT(60),DTDX(60),DTDXT(60),U(60),UT(60),Y(60),
     2P(60),PT(60),TAU(60),TAUT(60),X(60),XT(60),PLOG(60),NP(60),
     3MAX,DXO,DT,RHOO,EM,AK,TAO,EMU,UO,SMOM,SNRG,SU,T,NTORM,MM1
      G=1.-AK
      NEGU=0
      DO1 I=1,MAX
      URAT=ABS(U(I)/UO)
      P(I)=(1.01325E6*RHO(I)/RHOO)*URAT**G
      IF(U(I).LT.0.)GOTO 2
      GOTO 1
    2 NEGU=1
      P(I)=-P(I)
    1 CONTINUE
    5 RETURN
      END

$IBFTC STRSS
      SUBROUTINE STRSS
      COMMON RHO(60),RHOT(60),DVDX(60),DVDXT(60),V(60),VT(60),
     1DPDX(60),DPDXT(60),DTDX(60),DTDXT(60),U(60),UT(60),Y(60),
     2P(60),PT(60),TAU(60),TAUT(60),X(60),XT(60),PLOG(60),NP(60),
     3MAX,DXO,DT,RHOO,EM,AK,TAO,EMU,UO,SMOM,SNRG,SU,T,NTORM,MM1
      NFRAC=0
      RHOMAX=RHOO+.05*RHOO
      RHOMIN=RHOO-.05*RHOO
      DO1 I=1,MAX
      IF(RHO(I)-RHOMIN)5,5,6
    5 NFRAC=1
      TAU(I)=0.
      RHO(I)=RHOO
      U(I)=UO
      GOTO 1
    6 IF(RHO(I)-RHOMAX)7,7,8
    7 TAU(I)=0.
      GOTO 1
    8 IF(DVDX(I))2,3,4
    2 TAU(I)=-EMU*DVDX(I)+TAO
      GOTO 1
    3 TAU(I)=0.
      GOTO 1
    4 TAU(I)=-EMU*DVDX(I)-TAO
    1 CONTINUE
   12 RETURN
      END

$IBFTC VGRAD
```

```
      SUBROUTINE VGRAD
      COMMON RHO(60),RHOT(60),DVDX(60),DVDXT(60),V(60),VT(60),
     1DPDX(60),DPDXT(60),DTDX(60),DTDXT(60),U(60),UT(60),Y(60),
     2P(60),PT(60),TAU(60),TAUT(60),X(60),XT(60),PLOG(60),NP(60),
     3MAX,DXO,DT,RHOO,EM,AK,TAO,EMU,UO,SMOM,SNRG,SU,T,NTORM,MM1
      DVDX(MAX)=0.
      DO1 I=1,MM1
    1 DVDX(I)=(V(I+1)-V(I))/(X(I+1)-X(I))
      RETURN
      END

$IBFTC PGRAD
      SUBROUTINE PGRAD
      COMMON RHO(60),RHOT(60),DVDX(60),DVDXT(60),V(60),VT(60),
     1DPDX(60),DPDXT(60),DTDX(60),DTDXT(60),U(60),UT(60),Y(60),
     2P(60),PT(60),TAU(60),TAUT(60),X(60),XT(60),PLOG(60),NP(60),
     3MAX,DXO,DT,RHOO,EM,AK,TAO,EMU,UO,SMOM,SNRG,SU,T,NTORM,MM1
      PO=1.01325E6
      DPDX(1)=2.*(P(1)-PO)/(X(2)+DXO-X(1))
      DPDX(MAX)=2.*(PO-P(MM1))/(X(MAX)-X(MM1)+DXO)
      DO1 I=2,MM1
    1 DPDX(I)=2.*(P(I)-P(I-1))/(X(I+1)-X(I-1))
      RETURN
      END

$IBFTC TGRAD
      SUBROUTINE TGRAD
      COMMON RHO(60),RHOT(60),DVDX(60),DVDXT(60),V(60),VT(60),
     1DPDX(60),DPDXT(60),DTDX(60),DTDXT(60),U(60),UT(60),Y(60),
     2P(60),PT(60),TAU(60),TAUT(60),X(60),XT(60),PLOG(60),NP(60),
     3MAX,DXO,DT,RHOO,EM,AK,TAO,EMU,UO,SMOM,SNRG,SU,T,NTORM,MM1
      DTDX(1)=2.*TAU(1)/(X(2)-X(1)+DXO)
      DTDX(MAX)=-2.*TAU(MM1)/(X(MAX)-X(MM1)+DXO)
      DO1 I=2,MM1
    1 DTDX(I)=2.*(TAU(I)-TAU(I-1))/(X(I+1)-X(I-1))
      RETURN
      END

$IBFTC PRNT
      SUBROUTINE PRNT
      COMMON RHO(60),RHOT(60),DVDX(60),DVDXT(60),V(60),VT(60),
     1DPDX(60),DPDXT(60),DTDX(60),DTDXT(60),U(60),UT(60) Y(60),
     2P(60),PT(60),TAU(60),TAUT(60),X(60),XT(60),PLOG(60),NP(60),
     3MAX,DXO,DT,RHOO,EM,AK,TAO,EMU,UO,SMOM,SNRG,SU,T,NTORM,MM1
      WRITE(6,1)T
    1 FORMAT(3H T=, E12.5)
      WRITE(6,2)SMOM
    2 FORMAT(6H SMOM=, E12.5)
```

```
      WRITE(6,3)SNRG
    3 FORMAT(6H SNRG=, E12.5)
      WRITE(6,31)SU
   31 FORMAT(6H SU=  , E12.5 )
      WRITE(6,4)
    4 FORMAT(7H X(I)      )
      WRITE(6,5)X
    5 FORMAT(1H 10E13.4)
      WRITE(6,6)
    6 FORMAT(7H V(I)      )
      WRITE(6,5)V
      WRITE(6,9)
    9 FORMAT(7H U(I)      )
      WRITE(6,5)U
      WRITE(6,8)
    8 FORMAT(7H TAU(I)    )
      WRITE(6,5)TAU
      WRITE(6,13)
   13 FORMAT(9H DVDX(I)    )
      WRITE(6,5)DVDX
      WRITE(6,15)
   15 FORMAT(9H DTDX(I)    )
      WRITE(6,5)DTDX
      WRITE(6,14)
   14 FORMAT(9H DPDX(I)    )
      WRITE(6,5)DPDX
      WRITE(6,7)
    7 FORMAT(7H RHO(I)    )
      WRITE(6,5)RHO
      WRITE(6,10)
   10 FORMAT(7H P(I)      )
      WRITE(6,5)P
      WRITE(6,11)
   11 FORMAT(131H XXXXXXXXXXXXXXXXXXXXXXXXXXXXXXXXXXXXXXXXXXXXXXXXXXXXXX
     1XXXXXXXXXXXXXXXXXXXXXXXXXXXXXXXXXXXXXXXXXXXXXXXXXXXXXXXXXXXXXXXXXX
     2XXXXXXXXXX)
      RETURN
      END
$IBFTC PLOTP
      SUBROUTINE PLOTP
      COMMON RHO(60),RHOT(60),DVDX(60),DVDXT(60),V(60),VT(60),
     1DPDX(60),DPDXT(60),DTDX(60),DTDXT(60),U(60),UT(60),Y(60),
     2P(60),PT(60),TAU(60),TAUT(60),X(60),XT(60),PLOG(60),NP(60),
     3MAX,DXO,DT,RHOO,EM,AK,TAO,EMU,UO,SMOM,SNRG,SU,T,NTORM,MM1
      BPLOG=0.
      DO1 I=1,MAX
      IF(P(I).LT.0..OR.P(I).EQ.0.)GOTO 6
```

```
      PLOG(I)=ALOG10(P(I) )
      IF(PLOG(I).GT.BPLOG)GOTO 2
      GOTO 1
    6 PLOG(I)=1.0E-10
      GOTO 1
    2 BPLOG=PLOG(I)
      NCH=PLOG(I)
      N=NCH+1
    1 CONTINUE
      WRITE(6,15)
   15 FORMAT(30H PLOT OF POSITIVE PRESSURE            )
      WRITE(6,40) T
   40 FORMAT(3H T=, E12.5)
      EN=N
      SMAX=EN+.05
      SMIN=EN-.05
      K=0
    4 CALL SETSCL       (MAX,NP)
      DO3 I=1,MAX
      IF(PLOG(I).GE.SMIN.AND.PLOG(I).LT.SMAX)NP(I)=4
    3 CONTINUE
      K=K+1
      WRITE(6,60)(NP(I),I=1,MAX),EN
      EN=EN-.1
      SMAX=SMAX-.1
      SMIN=SMIN-.1
   60 FORMAT(1H 60I1,F6.1)
      IF(K-50)4,5,5
    5 RETURN
      END

$IBFTC SETSCL
      SUBROUTINE SETSCL
      COMMON RHO(60),RHOT(60),DVDX(60),DVDXT(60),V(60),VT(60),
     1DPDX(60),DPDXT(60),DTDX(60),DTDXT(60),U(60),UT(60),Y(60),
     2P(60),PT(60),TAU(60),TAUT(60),X(60),XT(60),PLOG(60),NP(60),
     3MAX,DXO,DT,RHOO,EM,AK,TAO,EMU,UO,SMOM,SNRG,SU,T,NTORM,MM1
      DO1 I=1,MAX
    1 NP(I)=0
      DO2 I=10,MAX,10
    2 NP(I)=1
      RETURN
      END
```

APPENDIX B

COMPUTER PROGRAM FOR ADIABATIC EXPANSION

```
C     ADIABATIC EXPANSION OF SOLIDS
C     UTAH RESEARCH AND DEVELOPMENT CO
C     CONTRACT DA-19-129-AMC-150(X)
      DIMENSION W(80),V(70),P(70)
    1 FORMAT (I2,F7.3,E9.4,F8.5,F7.2,F6.2,E10.4,F7.5,F7.2,E9.5)
    2 FORMAT(20H                    )
    3 FORMAT (57H ADIABATIC PRESSURE HUGONIOT PRESSURE   NORMALIZED VOLU
     1ME)
    4 FORMAT (3E20.7)
    5 READ (5,1) K,S,C,H,A,REALM,P(1),RVHU,RHO,ERROR
      READ (5,2)
      WRITE (6,2)
      WRITE (6,3)
      V(1)= RVHU/RHO
      WRITE (6,4) P(1), P(1), RVHU
   10 DO 19 J=2,K
      PADI = P(J-1)
      VOL= V(J-1)
      I = J
   11 DELV=1./RHO-VOL
      DENOM=1./RHO-S*DELV
      PHUG=(C**2  *DELV)/DFNOM**2
      DPHUG=(C**2  *(-DENOM-2.0*S*DELV))/DENOM**3
      DEHUG=0.5*(-PHUG+DELV*DPHUG)
   12 W(I)=H*((PHUG-PADI)*(A/(VOL*(A+(REALM*RHO)*VOL)))-((A+(REALM*RHO)
     1    *VOL)/VOL)*(PADI+DEHUG)+DPHUG)
      IF (VOL-V(J-1)) 14,13,14
   13 VOL=V(J-1)+0.5*H
      PADI=P(J-1)+0.5*W(I)
      I=J+1
      GO TO 11
   14 IF (I-J-2) 15,17,18
   15 PADI=P(J-1)+0.5*W(I)
      I=J+2
      GO TO 11
   17 VOL =V(J-1)+H
      PADI =P(J-1)+W(I)
      I=J+3
      GO TO 11
   18 P(J)=P(J-1)+(1./6.)*(W(J)+2.*W(J+1)+2.*W(J+2)+W(J+3))
      V(J)= V(J-1)+H
      RVVZ=V(J)*RHO
   19 WRITE (6,4) P(J),PHUG,RVVZ
      GO TO 5
      END
```

PART II. - MEASUREMENT OF MATERIAL PROPERTIES

1. INTRODUCTION

Little is known concerning the behavior of materials under impact conditions, particularly under conditions in which a projectile strikes another object and the material flows and is highly deformed. Such information is necessary in order to devise any theory to predict the amount and nature of the damage produced. The purpose of experimental research done under this contract was to develop a theoretical and experimental basis for analyzing and predicting the behavior of materials under impact conditions.

The experiments were primarily aimed at measuring the energy involved in flow and deformation. They involved pure metals, alloys, plastics, glass, wood, and composition materials. Rates of deformation were varied from a minimum of about 10^{-2} per second (in a testing machine) to about 10^{5} per second (by accelerating a projectile in a powder gun). Impact velocities ranged from about .010 to about 2.0 km/sec.

In Section 2, the manner in which deformation calculations were made is described, and procedures are outlined for the different experiments. Section 3 contains the results of the experiments. Graphs and tables are used to relate data from different materials and experiments. The results are discussed in Section 4 with main emphasis being placed on the disk-crushing experiment. Section 5 contains the derivation of the stress equation. Conclusions and recommendations are presented in Section 6. Section 7, the Appendix, contains a list of symbols.

2. EXPERIMENTAL PROCEDURE

A number of different experiments were conducted to measure material properties. Generally, these experiments were designed to determine properties, such as the strength of the material or the energy associated with its deformation, at strain rates which were varied from about 10^{-2} per second to about 10^{5} per second. This was done by deforming test specimens under essentially static conditions with a testing machine or under dynamic conditions by impacting them with a projectile.

2.1 Deformation Calculations

Equation 13 in Section 4.1, expresses the degree of deformation of a uniformly deformed disk as being $\ln z_f/z_o$; where z_o and z_f are the thicknesses of the disk before and after deformation. This logarithm is given the symbol, d. It is shown in Section 4.1 that d is proportional to the energy of deformation. It can be shown that d is also equal to $2 \ln (r_o/r_f)$; where r_o and r_f are the original and final radii of the disk. Total deformation of a uniformly deformed body is proportional to md; where m is the mass of the disk. This product is given the symbol, D.

In some experiments, deformation is not uniform throughout the deformed body. In these cases, the specimen is considered as being composed of an arbitrary number, i, of uniformly deformed segments, and total deformation is proportional to $\sum_1 m_i d_i$. In the case of non-uniform deformation of a rod, d is determined for each section by calculating an average radius; and for a thin plate by calculating an average thickness.

Unit deformation is defined as being that which deforms one gram of material to the extent that $\ln z_f/z_o$ or $2 \ln (r_o/r_f)$ is equal to one. These logarithms may be either positive or negative, depending upon the nature of the deforming forces.

The symbol, τ, is used for the proportionality constant relating energy to deformation and is defined by the equation, $\tau = E/D$; where E is the energy involved.

2.2 Experiments Made Under Dynamic Conditions

All impact experiments were made using a 50 caliber, smooth-bore gun with either compressed air or gunpowder as a propellant. Maximum projectile velocities achieved were about 0.2 km/sec with compressed air and about 2.0 km/sec with gunpowder. Different velocities were obtained by varying the air pressure or the amount of gunpowder used.

Three types of experiments were performed under impact

conditions. The first is referred to as the disk-crushing experiment, the second as the thin-plate impact experiment, and the third (actually two experiments) as the rod-to-rod impact experiment.

2.2.1 Disk-Crushing Experiment. This experiment was designed for the purpose of observing the manner in which a thin disk responds as it is deformed between two hardened-steel anvils; one of the anvils being in a fixed position and the other driven by a testing machine or shot from a gun. The arrangement using the testing machine is described in Section 2.3.1. Figure 1 is a sketch of the equipment used for driving the anvil with a gun. Compressed air was used at all times in this experiment giving projectile impact velocities ranging from 0.01 to 0.07 km/sec. The gun was fitted with a perforated barrel extension which permitted pressure behind the projectile to be released. This was done to stop acceleration of the projectile so that its impact velocity could be accurately determined. This was accomplished by measuring the time taken for the projectile to pass between two shorting probes in the gun-barrel extension. As a probe was shorted by the projectile, a pulse started or stopped an electronic timer.

In this experiment, it was desired that the rate of deformation of the disk be known. As shown in Figure 1, a beam of light passing through a narrow slit was cut off by the projectile as it impacted against the disk and deformed it. The output from a photomultiplier tube indicated the amount of light passing through the slit. This output varied linearly with the amount of light cut off by the projectile and thus, when photographed on an oscilloscope, gave a record of the rate at which the disk was crushed. Figure 2 is a sketch of an oscillograph of a typical shot. Part 1 of the curve represents light being cut off across the slit at a constant rate by the projectile before impact, part 2 represents the projectile being decelerated as the disk was deformed, and part 3 shows an increase in light intensity as the projectile rebounded.

The kinetic energy associated with the rebound of the projectile was always small. From slopes of the curve in Figure 2, it can be seen that, in this instance, rebound energy represents less than four per cent of the projectile's kinetic energy before impact. Because of this, it was assumed that all of the projectile's kinetic energy was used to deform the disk, that is the impact was completely elastic. Another assumption was that friction between the disk and the anvils was negligible. A check (discussed in Section 3.1.3) was made to see if this assumption is valid, and it was found that about 25 per cent of the energy was used in friction. A lubricant between the anvils and disk decreased the friction to some extent.

Deformation was determined, as described in Section 2.1, by relating the original disk dimensions to its dimensions after impact.

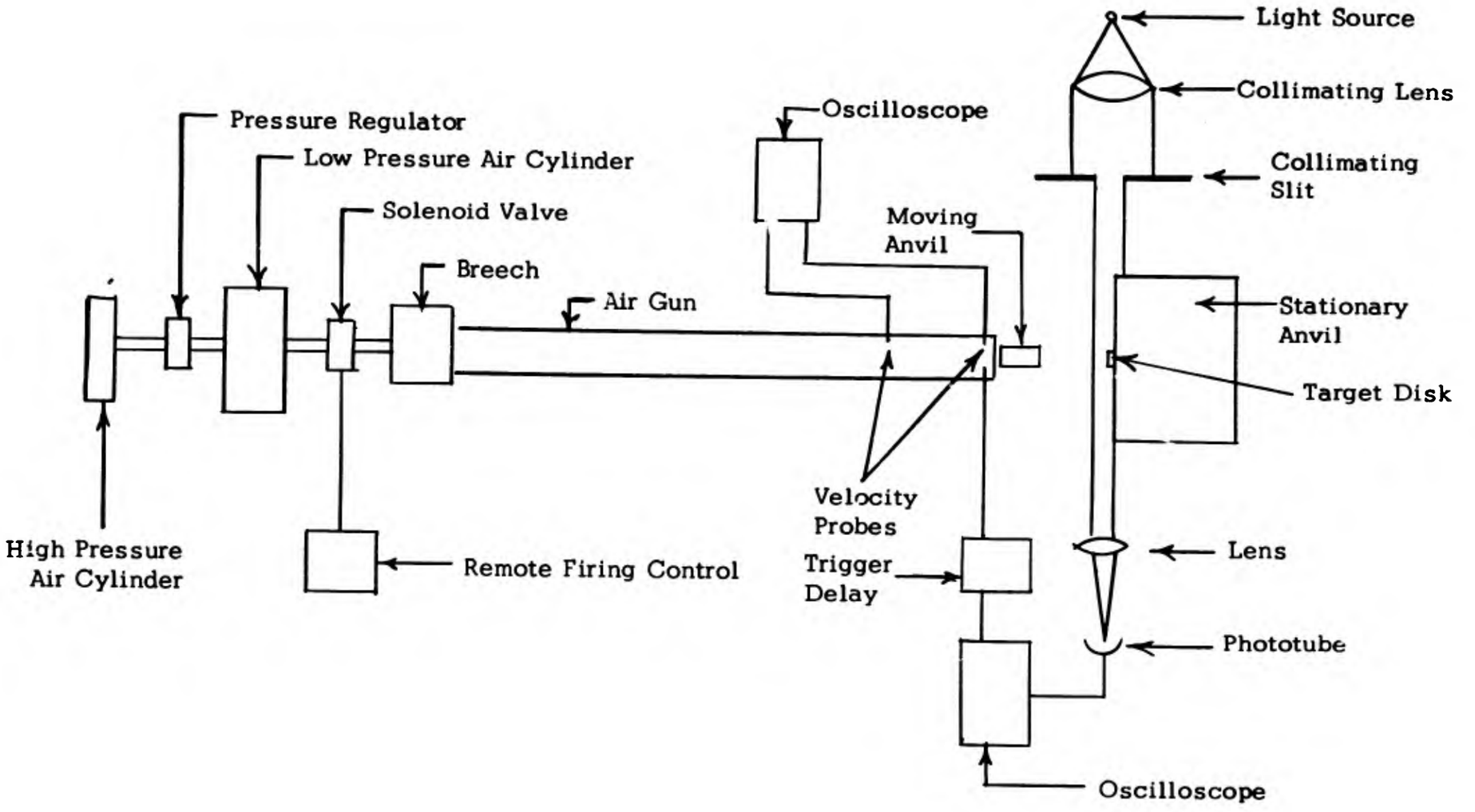

Figure 1. Diagram showing the system used in accelerating a projectile with compressed air, measuring its velocity, and determining its deceleration as it deforms a disk.

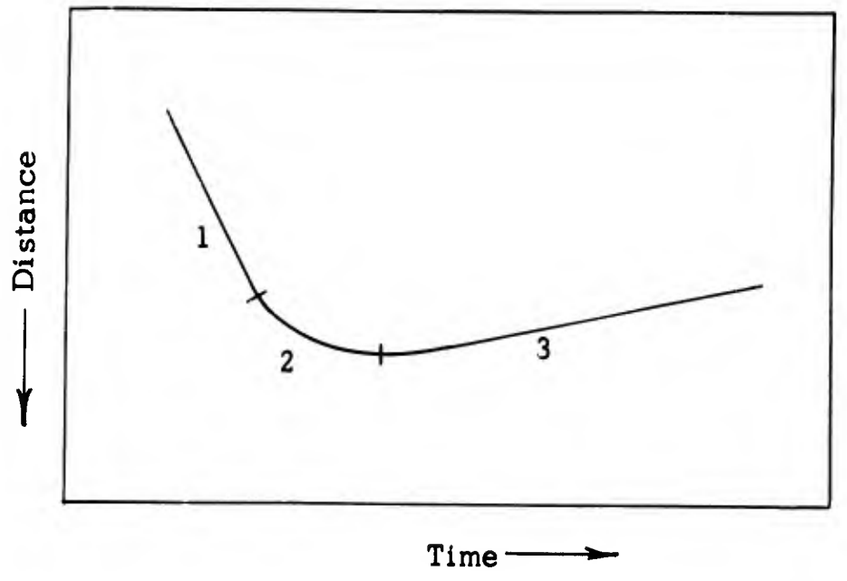

Figure 2. Oscillograph showing light intensity from a photomultiplier tube which indicates a projectile position as a function of time. Part 1 of the curve denotes a constant projectile velocity before impact, Part 2 represents the projectile being decelerated as the disk was deformed, and Part 3 shows an increase in light intensity as the projectile rebounded.

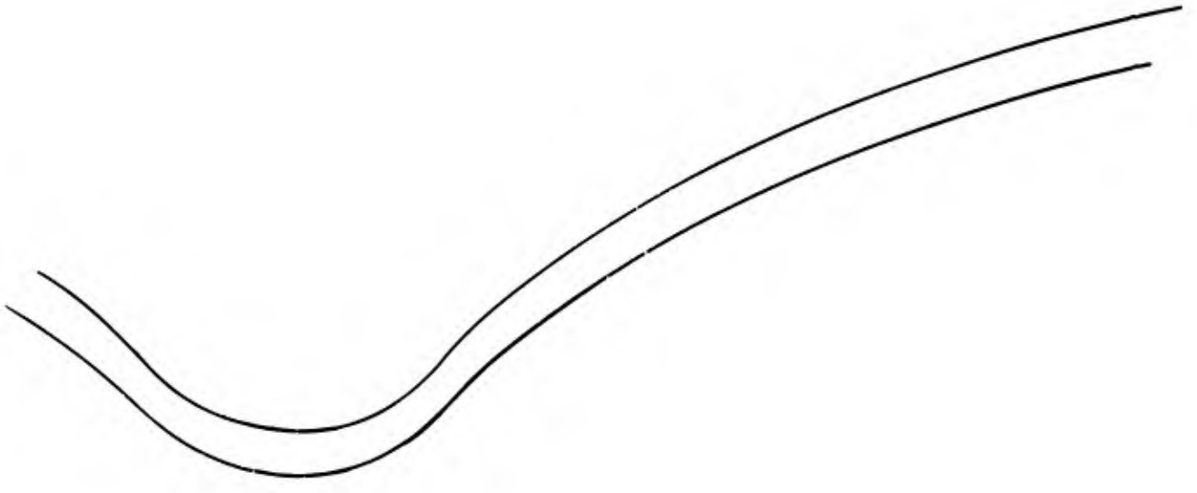

Figure 3. Sketch showing part of a cross section of a deformed copper plate. (x 4.6)

Average values were used when the deformation was not uniform.

Several materials were tested under these conditions. They are pure copper, pure aluminum, 6061-T4 aluminum, 6061-T6 aluminum, nylon, polypropylene, Lexan, polyethylene, and Teflon. Some tests were made with copper disks which had been annealed after fabrication. The annealing was done to remove work-hardening effects induced during machining and was accomplished by holding the disks at a temperature of 800°F for one hour and then cooling slowly to room temperature.

2.2.2 Thin-Plate Impact Experiment. Thin plates, one-sixteenth inch thick, of copper, polypropylene and Mylar were impacted with one-half-inch diameter steel balls at velocities up to about 0.16 km/sec. This was done to relate deformation and energy under these conditions and to compare the results with those from the disk-crushing experiment.

Compressed air was used to accelerate the projectiles and velocities were measured as described in the preceding section. No attempt was made to measure the deceleration of the projectile during the deformation process.

It was intended in this experiment that penetration of the plate would not occur and that target material around the point of impact would be plastically deformed. Then, on the assumption that all of the kinetic energy of the projectile was used in deformation, the ratio of energy to deformation could be determined. This assumption appeared to be reasonable with copper but not with the plastics as the projectile rebounded considerably with them. Also, it was found that the polypropylene fractured easily and that the Mylar showed little permanent deformation before the projectile sheared through. No quantitative information was obtained from the plastics for these reasons.

Total deformation in the copper plates was determined by considering a cross section of the deformed plate, calculating the average degree of deformation in each of several rings around the point of impact, multiplying these values by the masses of the corresponding rings, and then summing these products for all the rings. It was assumed that the degree of deformation was uniform throughout each ring. A sketch of a cross section of a deformed plate is shown in Figure 3.

2.2.3 Rod-to-Rod Impact Experiments. In the disk-crushing experiments, measurements were made on plastics with only a few materials under limited conditions. Deformation measurements usually were hindered by plastic recovery and shattering under impact. To obtain some measurement of the "strength of materials under impact conditions, a rod-to-rod impact experiment was devised in which a projectile rod was impacted against a stationary target rod and the acceleration of the rear

face of the target rod was measured. This gave a gross measurement of an effective pressure gradient.

As the impact velocity is increased in such an experiment, it is of interest to see whether the acceleration (pressure gradient) reaches a maximum, indicating the maximum effective strength of the material. This value can be used in a theoretical program or as a means of rating different materials for use under impact conditions. Work to determine this maximum was carried out with glass, polypropylene, nylon, plexiglass, polyethylene, wood (birch), aluminum and a compressed wood fiber called Benelex 70.

The system used to make the desired measurements was built up around devices which indicated the time-position history of the flat end of a rod from measurements of the total light intensity from an illuminated slit which was covered or uncovered by the moving rod. A schematic diagram of the system is shown in Figure 4. All possible measurements listed were not made on each shot. Rods were 0.5 inch in diameter and were either 0.75, 1.0, or 2.0 inch long.

The optical system was designed to permit the following measurements:

1. Velocity of the projectile at the time of impact with the target. This allows impact pressure to be determined.

2. Time of impact upon target. This gives wave-velocity data.

3. Time-position history of rear target face after impact. Differentiating this curve twice gives acceleration data and thus pressure-gradient data.

4. Velocity of target after acceleration. This allows calibration of the acceleration curve.

Of the four measurements required, it was found that determining the time of projectile impact upon the target was the most difficult. One method tried was to pass a beam of light in front of the target rod and observe its intensity as the projectile impacted the target. It was expected that when the projectile closed the gap in front of the target, the time of impact could be determined as being that moment when all the light was cut off. This method was useful at low velocities, but at high velocities it became difficult to determine just when the light was at zero, because the oscilloscope trace was rounded rather than

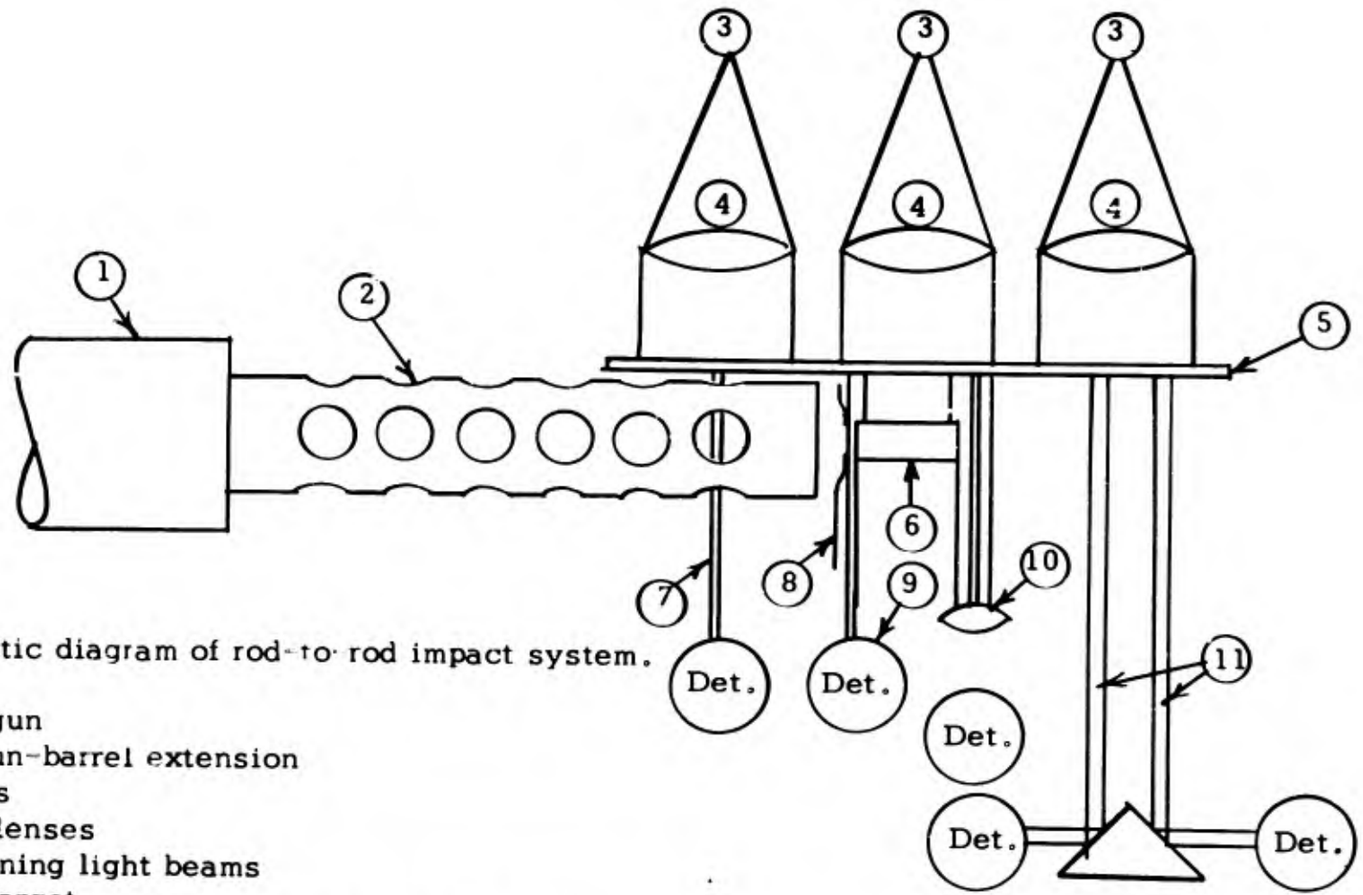

Figure 4. Schematic diagram of rod-to-rod impact system.

1. 50-cal. air gun
2. Perforated gun-barrel extension
3. Light sources
4. Collimating lenses
5. Slits for defining light beams
6. Cylindrical target
7. Light beam and detector for impact-velocity measurement
8. Make-wire circuit for impact-velocity measurement
9. Light beam and detector for impact-velocity measurement
10. Single or double light beam with collimator and detector for measuring target-rod acceleration and velocity
11. Double beam with prism and detector for measuring target-rod velocity

showing a sharp break. Later it was discovered that this was due to the generation of light at impact in the transparent plastics. Also, the target rod sometimes appeared to move from air shock and vibration before impact.

A simple wire make-circuit was substituted for the first light slit and gave better results. The impact end of the target was painted with conducting silver paint and two small bare wires were suspended in front of the target. When the projectile pushed the wires into the silver paint, the circuit was closed. At first a charged capacitor, discharged into a pulse-forming circuit, provided a pulse to the oscilloscope. This proved to be more reliable than the other methods tried, but still gave some trouble due to the high voltage across the break wires. Some premature discharging of the capacitor was experienced. This was improved by using a low voltage battery which shifted the oscilloscope trace when the make-wires were shorted.

The acceleration of the rear target face was measured using a light beam which was intercepted by the rear face. Figure 5 is a sketch of the oscilloscope trace produced as a target rod moves and cuts off a light beam.

The source of the pip of light represented on the oscilloscope trace, which occurred at or about the time of impact, was found by shooting a projectile into a target with all things normal except with no light present. The pip on the oscilloscope trace was still evident. Subsequent investigation revealed that a luminescence was taking place upon impact and increasing in intensity as the impact pressure increased. No further study was made to determine if the intensity of the light is directly proportional to impact pressure or where the upper and lower limits are.

At first it was believed that this luminescence could be used to indicate the time of impact; but after a number of shots were made it became evident that controlling it would be a problem and that it interferred with the acceleration curve in too many instances. It was eliminated by painting the target rod black.

Much difficulty was experienced at higher impact velocities in obtaining a target velocity. This was caused by the target rod breaking into small pieces before the velocity-measuring station was reached, thus giving erratic data. To overcome this problem, the single slit at the rear of the target rod was changed to a double slit to give a step in the oscilloscope trace. Knowing the distance between the two slits, the velocity of the target rod could be calculated, thereby obtaining a rod velocity before fragmentation could take place.

The linearity of the system was checked by shooting a projectile

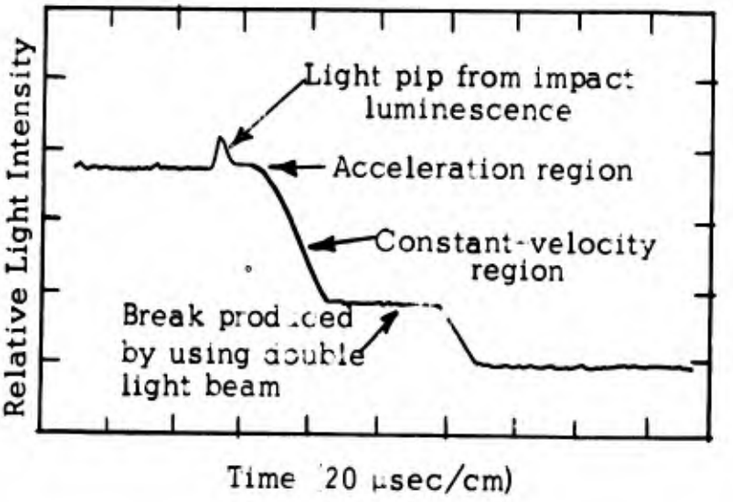

Figure 5. Oscilloscope trace from photomultiplier observing rear end of target rod. A double light beam of known spacing is used to give an internal velocity calibration so that an absolute velocity measurement is available for any slope on the trace. The light pip is ordinarily eliminated by painting rods.

through the light beam at a constant velocity with no target in place. It was found that some non-linearity was present in the photomultiplier tube. This was eliminated by focusing all light across the slit to a point on the tube which gave the best response.

The linearity of the photomultiplier and associated electronics was checked with a rotating disk. A slit was cut in the disk which would pass a beam of light into the photomultiplier once each revolution. By synchronizing the rotation of the disk with the sweep of an oscilloscope, a photograph of the rise and fall was obtained. This was determined to be about 0.1 μsec, which was well within the time requirements of the event being measured. The size and shape of the slit was also varied to show that these factors had little effect upon the shape and rise time of the light pulses.

A spark source with a known rise time of 0.5 μsec was used to check the response of the photomultiplier system. It was suspected that the target was moving before actual impact because of vibration caused by shock waves or by air pressure ahead of the projectile. This

was checked by shooting into a target firmly secured to the support platform. It was determined that some movement took place. A small amount of silicone grease between the target and its support platform prohibited this without decreasing the acceleration of the target significantly.

It was found that a maximum projectile velocity of about 0.2 km/sec could be obtained with compressed air as the propellant. Further increase in air pressure after this velocity was reached actually reduced the velocity of the projectile. This is believed to have been caused by turbulence resulting from a small opening between the gun and the air reservoir. Because of this, gunpowder was used to get higher projectile impact velocities. When using gunpowder, the velocity and acceleration measuring systems shown in Figure 4 were found to be unsatisfactory because light from the burning powder was picked up by the system and the signal was driven off scale. The problem was solved by using wire probes in the gun barrel to measure the projectile velocity, and by modifying the system for measuring target acceleration and knock-on velocity. A sketch of this arrangement is shown in Figure 6. The light source, lens arrangement, slits and photomultiplier tube were mounted in a light-tight box with the light source adjusted to give parallel light passing in front of the target rod. With this system, it was possible to differentiate between the parallel light of the system and the light coming from the muzzle flash.

If a cylindrical projectile is impacted against an identical target, the target being stationary but free to move, the target and projectile are equally deformed. Also, where the impact velocity is low enough to prevent mass loss from the target or projectile, a measurement of impact velocity and the knock-on velocity of either the target or projectile allows the amount of energy going into internal energy to be calculated. This can be seen from the following equations.

For a cylinder of mass m impacting against an identical cylinder, the momentum equation is

$$mv_1 = mu_1 + mu_2$$

where

v_1 = projectile velocity before impact
u_1 = projectile velocity after impact
u_2 = target velocity after impact.

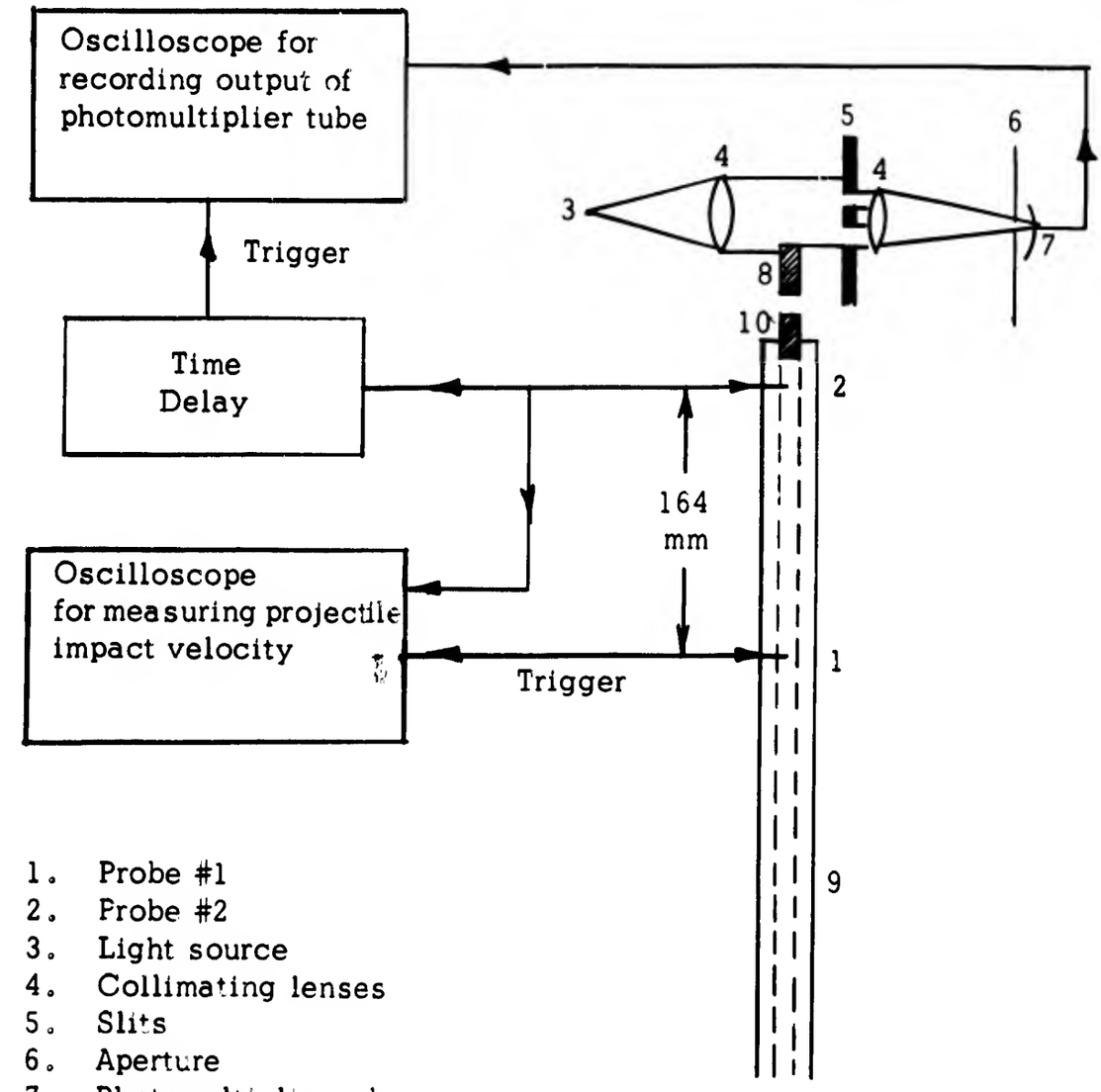

1. Probe #1
2. Probe #2
3. Light source
4. Collimating lenses
5. Slits
6. Aperture
7. Photomultiplier tube
8. Target rod
9. Gun
10. Projectile rod

Figure 6. Sketch showing the modified system used for determining projectile impact velocity and the acceleration and knock-on velocity of the target.

The energy equation is

$$\frac{1}{2} mv_1^2 = \frac{1}{2} mu_1^2 + \frac{1}{2} mu_2^2 + f\left(\frac{1}{2} mv_1^2\right)$$

where

f = the fraction of the kinetic energy of the projectile before impact which appears as internal energy of the target and the projectile.

By eliminating u_1 (using the momentum equation) we get

$$f = \frac{2u_2}{v_1} - \frac{2u_2^2}{v_1^2}$$

Thus we see that f can be calculated when v_1 and u_2 are known.

A system was developed which would accelerate the projectile cylinder, produce an aligned impact of the projectile against the target, and measure the projectile impact velocity and the target knock-on velocity. This system was similar to that shown in Figure 4. Both compressed air and gunpowder were used to accelerate the projectiles, depending on the velocity desired. Shorting probes were used in measuring projectile velocity when gunpowder was used. With compressed air, a light beam, as shown in Figure 4, was substituted for the probes.

2.3 Experiments Made under Low Strain-Rate Conditions

A Tinius-Olson testing machine, with which a constantly increasing force of from 0 to 120,000 pounds could be applied, was used in deforming specimens at strain rates of about 10^{-2} per second to about 1 per second. Two experiments, designated as the disk-crushing experiment and the rod-elongation experiment, were performed.

2.3.1 Disk-Crushing Experiment. Disks of the same materials and of the same sizes as those used in the impact experiment were deformed with the testing machine. Typical stress-strain curves were obtained. An example is shown in Figure 7. The energy going into deformation was determined for each test from the area under the curve. All of the materials listed in Section 3.2.1 were used in this experiment.

2.3.2 Rod-Elongation Experiment. In an attempt to determine the amount of energy used in friction between the disks and the anvils in

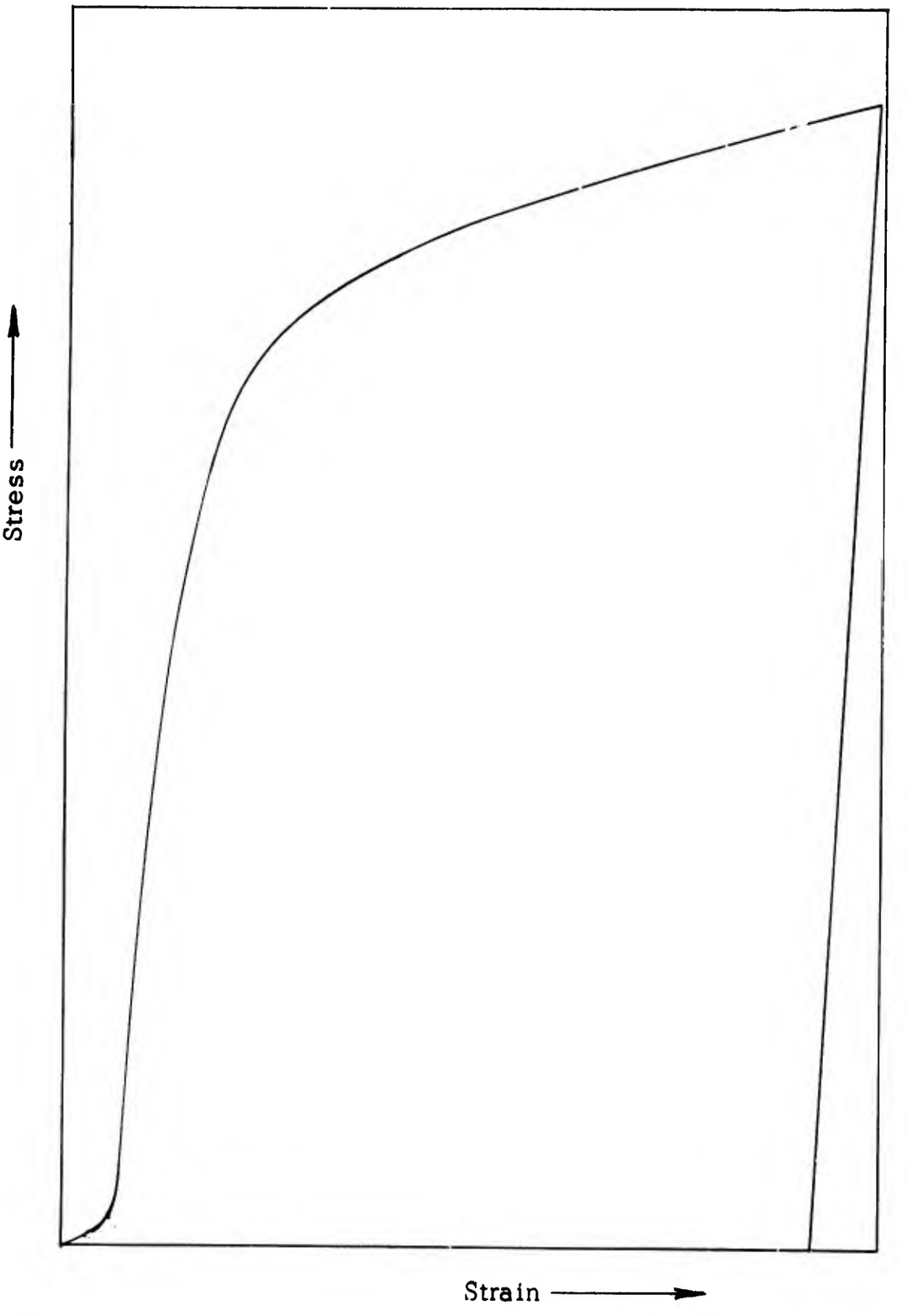

Figure 7. Stress as a function of strain plotted for the deformation of a copper disk with a testing machine.

the disk-crushing experiments, copper test specimens were prepared and deformed in tension in the testing machine. Total deformation was calculated for each specimen and compared with the deformation energy calculated from the stress-strain diagram.

3. RESULTS

The experimental results of this investigation are presented here in graphical and tabular form. Section 4.1 consists of a development of the differential equations governing the mechanisms associated with the disk-crushing experiment. This section should be referred to as a preface to the experimental results in order to better understand the manner in which the data are presented and compared. Also, Section 2.1 should be referred to for an understanding of the method used in calculating deformation.

Section 3.1 deals mainly with the disk-crushing experiments with sub-sections treating such subjects as the relationships of the degree of deformation to specific energy, the amount of energy used in friction between the disk and the anvils, and the comparison of values determined for the proportionality constant relating energy to deformation for different materials and experiments. Section 3.2 is concerned with the pressure gradients developed in different materials in the rod-to-rod impact experiments. In Section 3.3 the results of the thin-plate impact experiment are presented.

3.1 Results of Disk-Crushing Experiments

3.1.1 Degree of Deformation. Disks made of copper, aluminum and various plastics were deformed by impacting them at velocities of ten to seventy meters per second with a hardened-steel cylinder or by compressing them in a testing machine under static conditions. The deformation rate in experiments using these two methods varied by as much as a factor of 10^7. It was anticipated that such a variation would show any strain-rate dependency in the materials tested merely by observing variation in τ using Equation 13 of Section 4.1.

Most of the disks were of the same original size; 1/4 inch diameter by 1/8 inch thick. However, copper disks of other sizes were also used. Materials used were annealed and unannealed copper, 99.99 per cent pure aluminum, 6061-T4 and 6061-T6 aluminum alloys, nylon, Lexan, Teflon, polyethylene, and polypropylene.

The specific energy (energy per gram of material) and the degree of deformation (the logarithm of the ratio of the final disk thickness to its original thickness) have been determined for each impact shot and for each compression test. In Figures 8 to 14, the ratio of the final to the original disk thickness is plotted on a logarithmic scale versus specific energy. Figure 8 shows data for copper, Figure 9 shows data for aluminum, and Figures 10 to 14 show data for plastics. If the relationship expressed in Equation 13 is correct, lines drawn through the points in these figures will

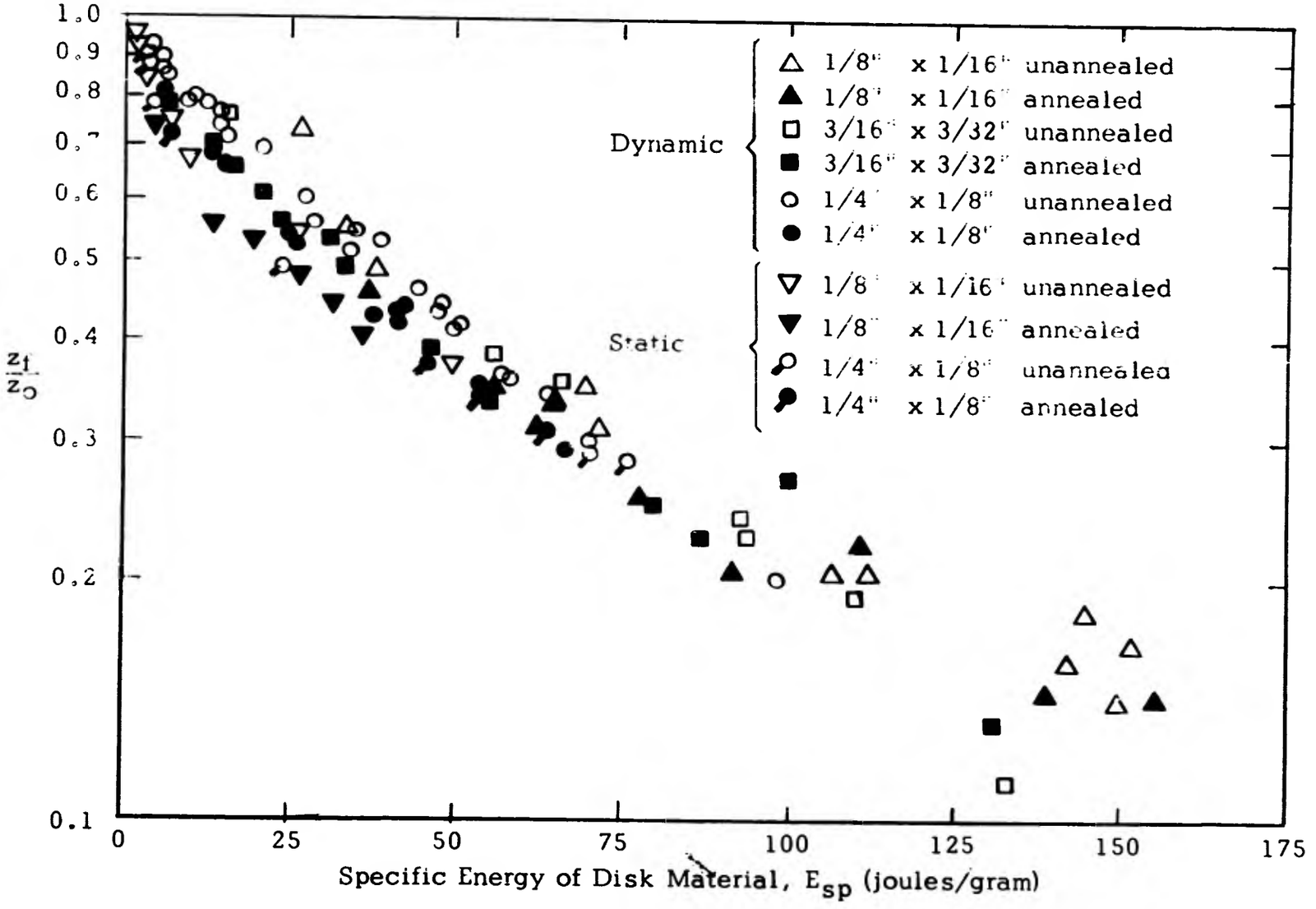

Figure 8. Copper

(See Figure 15 for separate curves for these data).

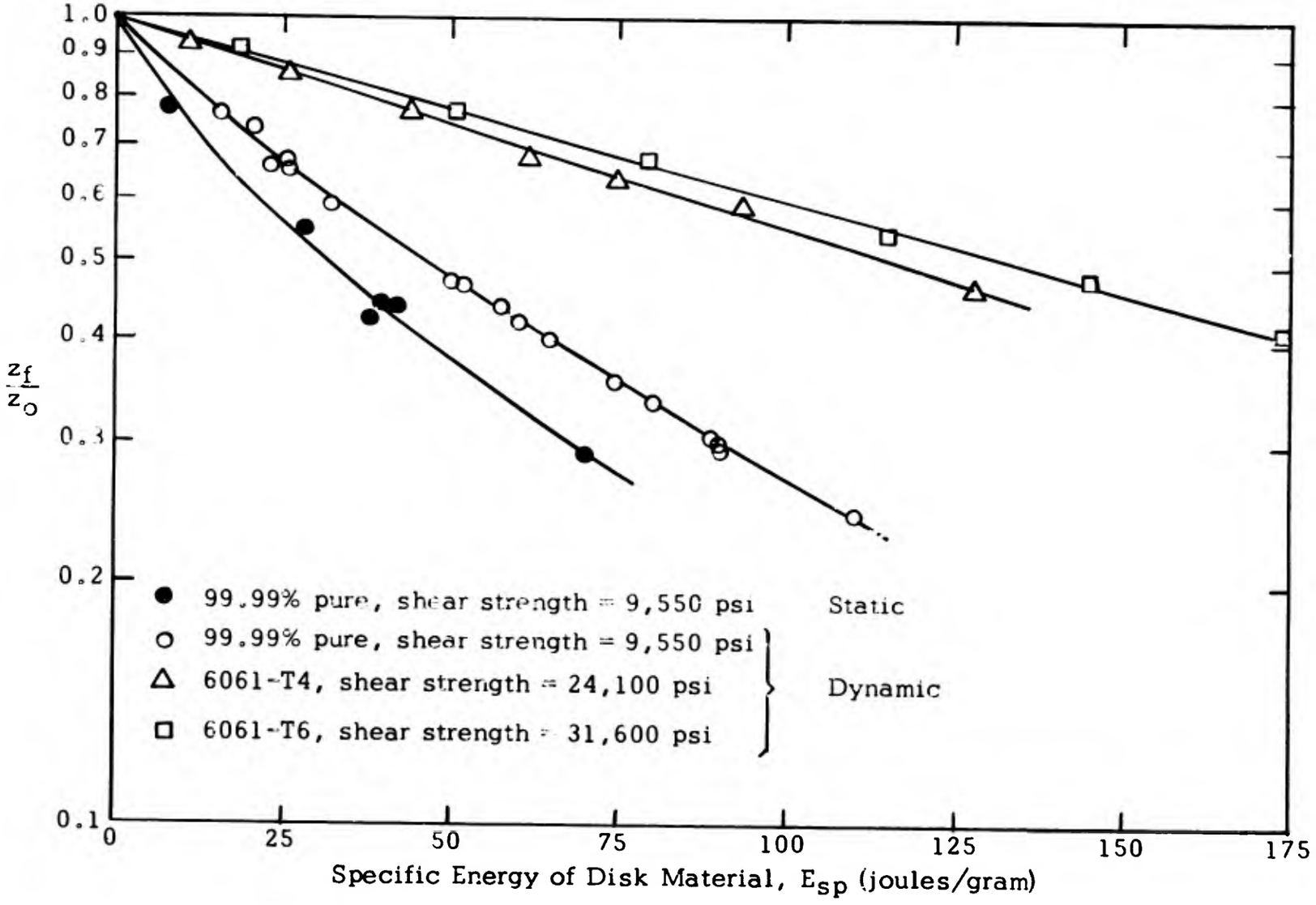

Figure 9. Aluminum

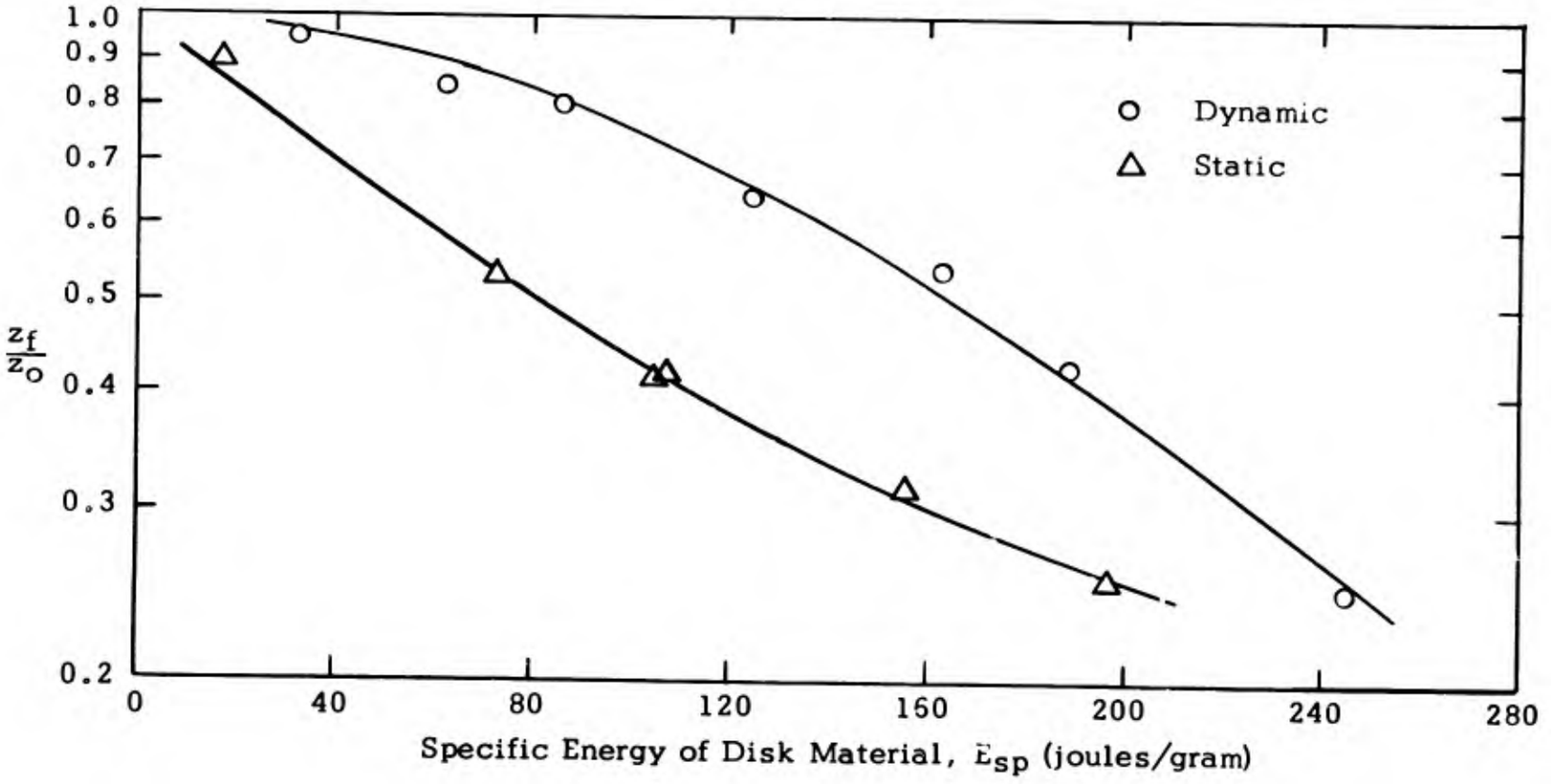

Figure 10. Nylon

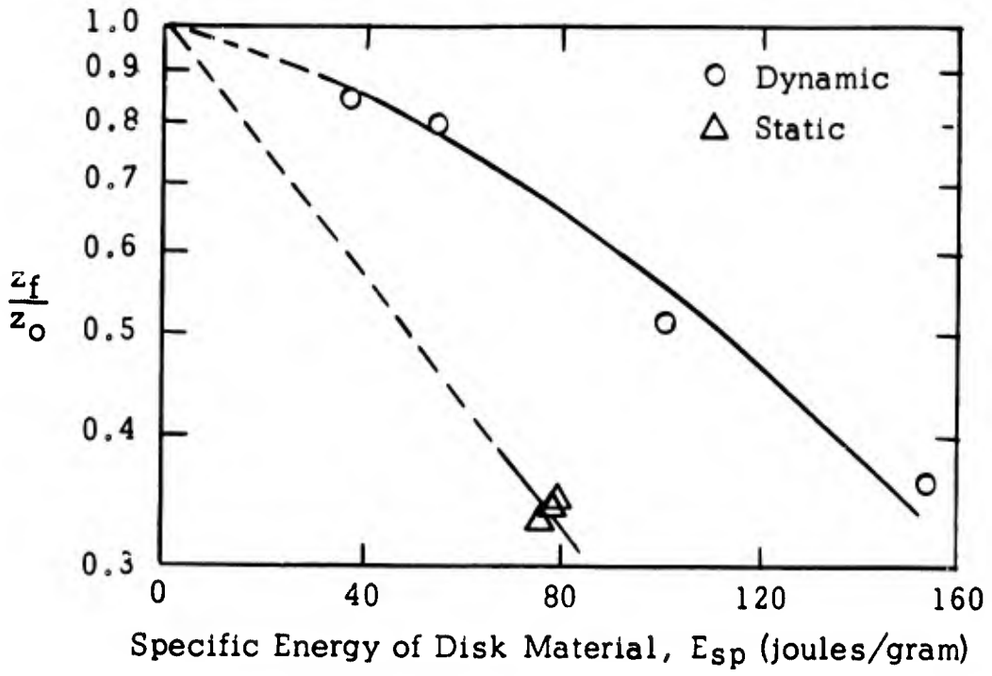

Figure 11. Polypropylene

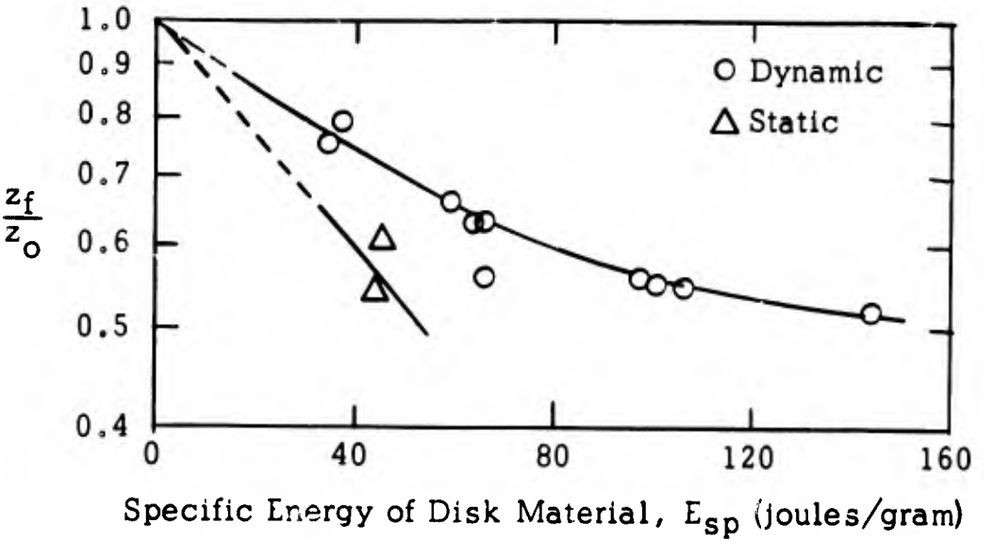

Figure 12. Lexan

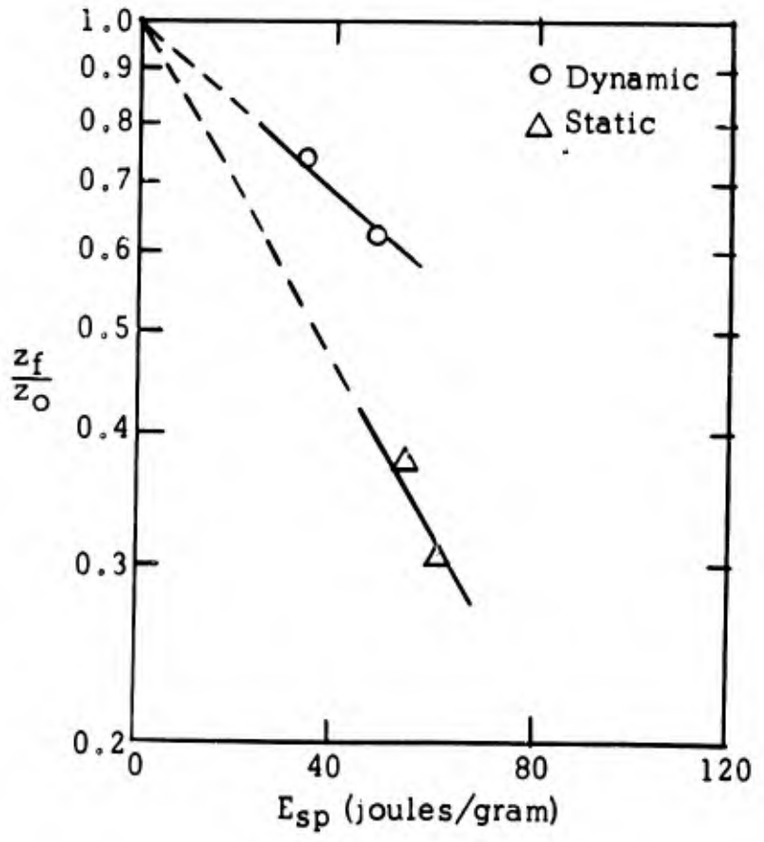

Figure 13. Polyethylene

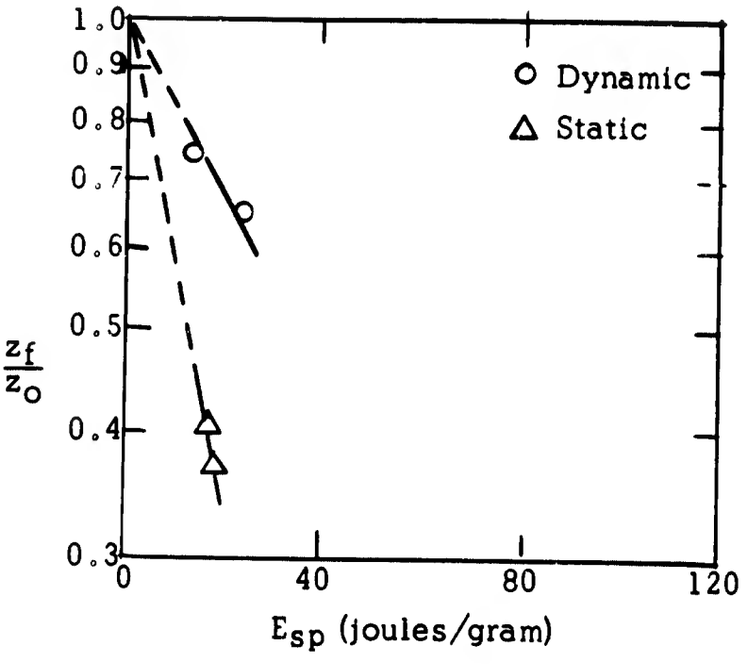

Figure 14. Teflon

be straight, indicating that specific energy is directly proportional to the logarithm of the final and original disk thickness ratio. This is seen to be approximately true for all cases.

In Figure 8, the data for copper show that there is no observable difference between disks of different sizes. This indicates that friction losses are proportional to mass for disks of the same relative dimentions. The best-fit curves to the copper data are shown in Figure 15. Data points are omitted for clarity. Differences are shown in Figure 15 between annealed and unannealed copper, indicating strain-hardening effects; and between static and impact data, indicating strain-rate effects.

The data for aluminum in Figure 9 show some effects of friction or strain hardening and show a large strain-rate effect. This is shown by the difference in position of the data points from static and impact tests.

In Figures 10 to 14, both static and dynamic data concerning five different plastics are shown. In each one, a strong rate dependency is exhibited showing that it is stronger under impact conditions than under static conditions. It is also shown that under impact conditions, an apparent "strain-softening" effect exists for nylon and polypropylene.

3.1.2 Friction in Disk Crushing. Experimental work was done to determine how much of the energy going into crushing of a disk was due to frictional loss with the anvil surfaces and how much was actually due to internal deformation of the disk. Tests were made by deforming a rod in tension in a testing machine, determining the energy involved, and measuring the deformation on the same basis as was used in the disk-crushing experiment. It was found that although friction required a fair-sized correction to be made in the results, it was not large enough to invalidate them. It was found that with the copper disks at large deformations, about 25 per cent of the energy was used in friction with the disk faces.

3.1.3 The Relationship of Energy to Deformation. Table I contains data comparing total deformation to the energy involved for copper and steel specimens. Data from the rod-elongation, thin-plate-impact, and rod-to-rod impact experiments are given. For copper, average values for τ in the rod-elongation experiment are considerably less than those in the other two experiments. This is considered to be due to a loss of energy through rebound of the projectile in the thin-plate experiment and to energy being used in friction between the impacting rods in the rod-to-rod experiment. The limited data show no obvious differences between the data from annealed and unannealed specimens in the rod-elongation experiment. This might be due to the low rate at which deformation occurred which made it possible for strain hardening to be

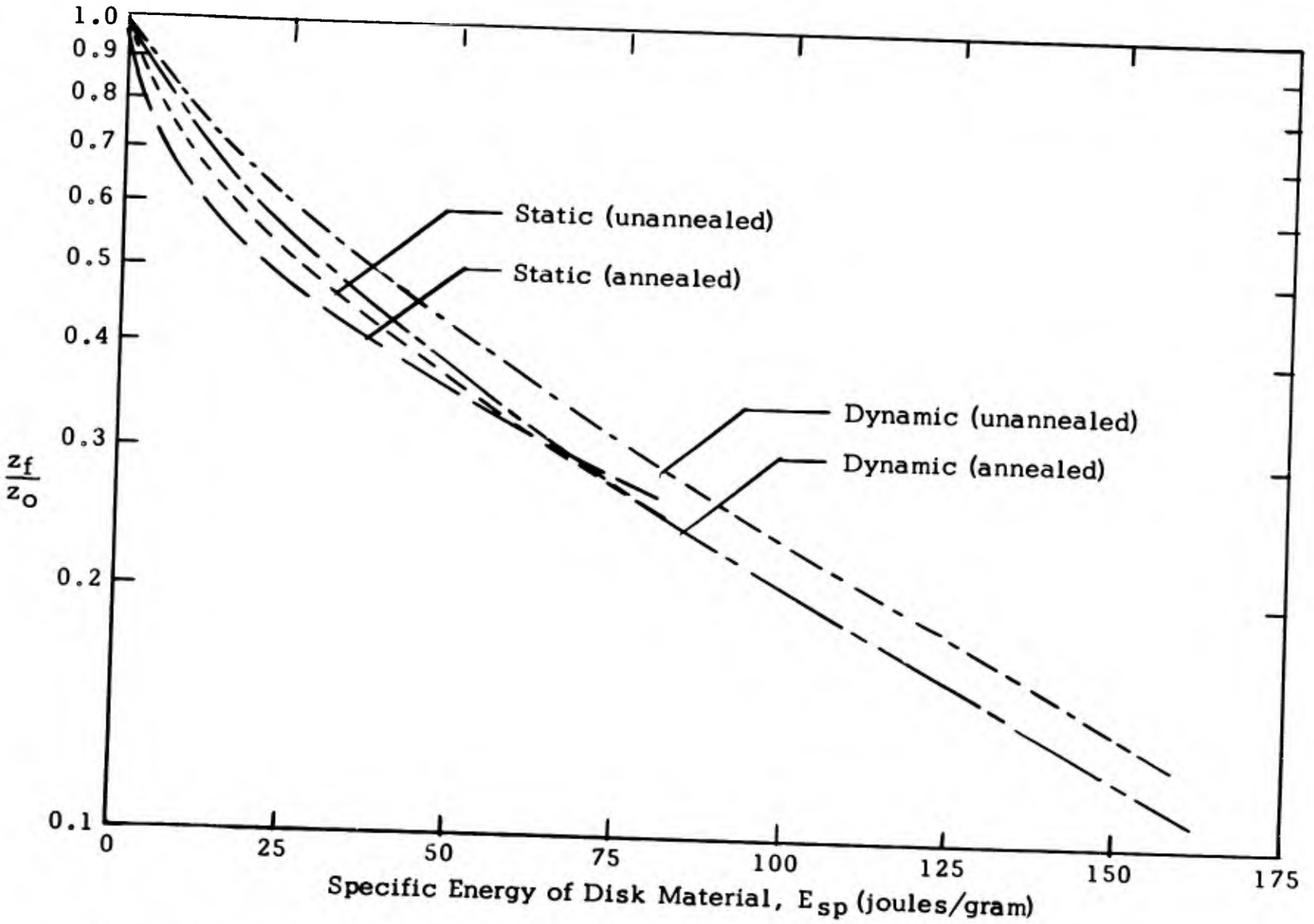

Figure 15. Best-fit curves through the data of Figure 1. Strain-rate effect is shown by the displacement between comparable static and dynamic curves.

TABLE I. Data comparing total deformation to the energy involved for copper and steel in different experiments.

Test No.	Experiment Type	Material	Total Energy, E (joules)	Total Deformation, D (units)	τ = E/D (joules/unit)	Specimen Dimensions (inch)
8	Rod Elongation	Copper	12.9	.359	36	dia = 1/8
13	Rod Elongation	Copper	13.2	.290	46	dia = 1/8
9	Rod Elongation	Copper (annealed)	19.8	.533	37	dia = 1/8
11	Rod Elongation	Copper (annealed)	12.8	.514	25	dia = 1/8
12	Rod Elongation	Copper (annealed)	16.7	.408	41	dia = 1/8
1	Thin-Plate Impact	Copper	103	2.00	52	thickness = 1/16
2	Thin-Plate Impact	Copper	48.5	.890	54	thickness = 1/16
107	Rod-to-Rod Impact	Copper	106	2.18	49	dia = 1/2
108	Rod-to-Rod Impact	Copper	119	2.37	50	length = 1/2 dia = 1/2
94	Rod-to-Rod Impact	Copper	59.5	1.05	57	length = 1/2 dia = 1/2
96	Rod-to-Rod Impact	Copper	31.0	.649	48	length = 1 dia = 1/2
97	Rod-to-Rod Impact	Copper	351	7.27	48	length = 1 dia = 1/2
32	Rod-to-Rod Impact	Copper	37.5	.633	55	length = 1 dia = 1/2
37	Rod-to-Rod Impact	Copper	158	2.74	58	length = 1-1/2 dia = 1/2
38	Rod-to-Rod Impact	Copper	502	11.8	43	length = 1-1/2 dia = 1/2 length = 1-1/2
78	Rod-to-Rod Impact	Steel	504	4.82	104	dia = 1/2
79	Rod-to-Rod Impact	Steel	805	7.43	108	length = 1-1/2 dia = 1/2
82	Rod-to-Rod Impact	Steel	319	2.90	110	length = 1-1/2 dia = 1/2 length = 1-1/2

reintroduced into the annealed specimens.

Table II contains average values of τ for the disk-crushing experiments. Copper is seen to be stronger under dynamic conditions and unannealed copper is stronger than annealed copper under dynamic conditions but not necessarily so under static conditions. Pure aluminum is stronger under dynamic conditions. The data from the aluminum alloys show the influence of strength. Under static conditions, the values of τ for all of the plastics are only about half those obtained under dynamic conditions.

3.2 Pressure Gradients

Dynamic strength measurements were made in which a projectile rod was impacted against a similar target rod and the acceleration of the end of the target rod, opposite the impacted end, was measured. This acceleration gave a measure of the combined pressure and stress gradient which reached the end of the rod.

Measurements were made at impact velocities of up to 0.2 km/sec with plexiglass, Benelex 70, polypropylene, glass, polyethylene, and wood (birch); and to 1.5 km/sec with nylon, phenolic, and aluminum. Also, measurements were made with nylon, glass, phenolic and aluminum specimens of different lengths to see if a variation in this parameter caused a change in the strength value. The results are plotted in Figure 16 where maximum pressure gradient is represented as a function of projectile impact velocity for each material tested. The curves are best-fit-by-eye lines drawn through the data points. As an example of a plot of actual data, the points for phenolic are shown in Figure 17. In a few of the materials, especially nylon, there was considerable scatter in the data. This is considered to be due to the specific material properties because scatter is not excessive with all materials.

Calculations were made concerning the fraction, f, of the kinetic energy of the projectile rod going into internal energy of the target and projectile. Values of f were plotted as a function of projectile velocity for all shots to see if some additional information might be obtained regarding the manner in which energy is utilized by different materials. The only significant features observed are that for all materials tested f approaches 0.5 at impact velocities in the range 0.1 - 0.2 km/sec, and becomes less than 0.5 at velocities of from 0.5 to 1.0 km/sec; the decrease caused by energy being used in the acceleration of projectile and target fragments as fracturing occurs.

TABLE II. Average values of τ (energy per unit deformation) for disks crushed under both static and dynamic conditions. Under disk dimensions, the diameter is given first, followed by the thickness.

Conditions	Material	Disk Dimensions (inch)	τ (joules/unit)
Dynamic	Copper	1/4 x 1/8	55
Dynamic	Copper (annealed)	1/4 x 1/8	41
Static	Copper	1/4 x 1/8	33
Static	Copper (annealed)	1/4 x 1/8	42
Dynamic	Copper	1/8 x 1/16	71
Dynamic	Copper (annealed)	1/8 x 1/16	61
Static	Copper	1/8 x 1/16	47
Static	Copper (annealed)	1/8 x 1/16	49
Dynamic	Copper	3/16 x 3/32	62
Dynamic	Copper (annealed)	3/16 x 3/32	52
Static	Copper	3/16 x 3/32	19
Dynamic	Copper	1/4 x 1/16	50
Dynamic	Copper	1/4 x 3/64	48
Dynamic	Aluminum (99.99% pure)	1/4 x 1/8	69
Static	Aluminum (99.99% pure)	1/4 x 1/8	49
Dynamic	Aluminum (6061-T4)	1/4 x 1/8	145
Dynamic	Aluminum (6061-T6)	1/4 x 1/8	199
Dynamic	Lexan	1/4 x 1/8	161
Static	Lexan	1/4 x 1/8	81
Dynamic	Polyethylene	1/4 x 1/8	108
Dynamic	Teflon	1/4 x 1/8	50
Static	Teflon	1/4 x 1/8	20
Dynamic	Polypropylene	1/4 x 1/8	205
Static	Polypropylene	1/4 x 1/8	73
Dynamic	Nylon	1/4 x 1/8	265
Static	Nylon	1/4 x 1/8	126
Static	Polyethylene	1/4 x 1/8	55

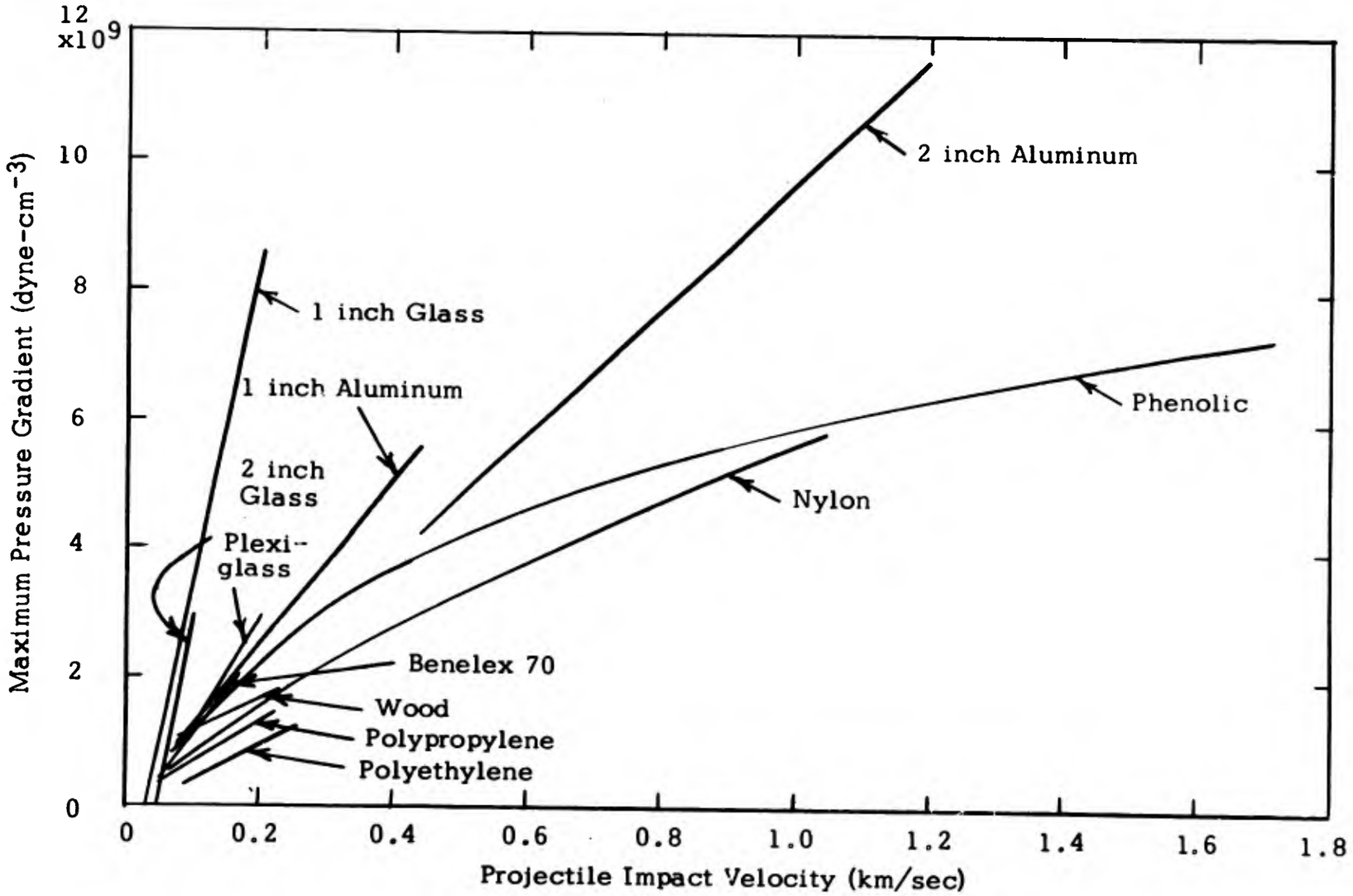

Figure 16. Maximum pressure gradient plotted as a function of projectile impact velocity for all materials tested.

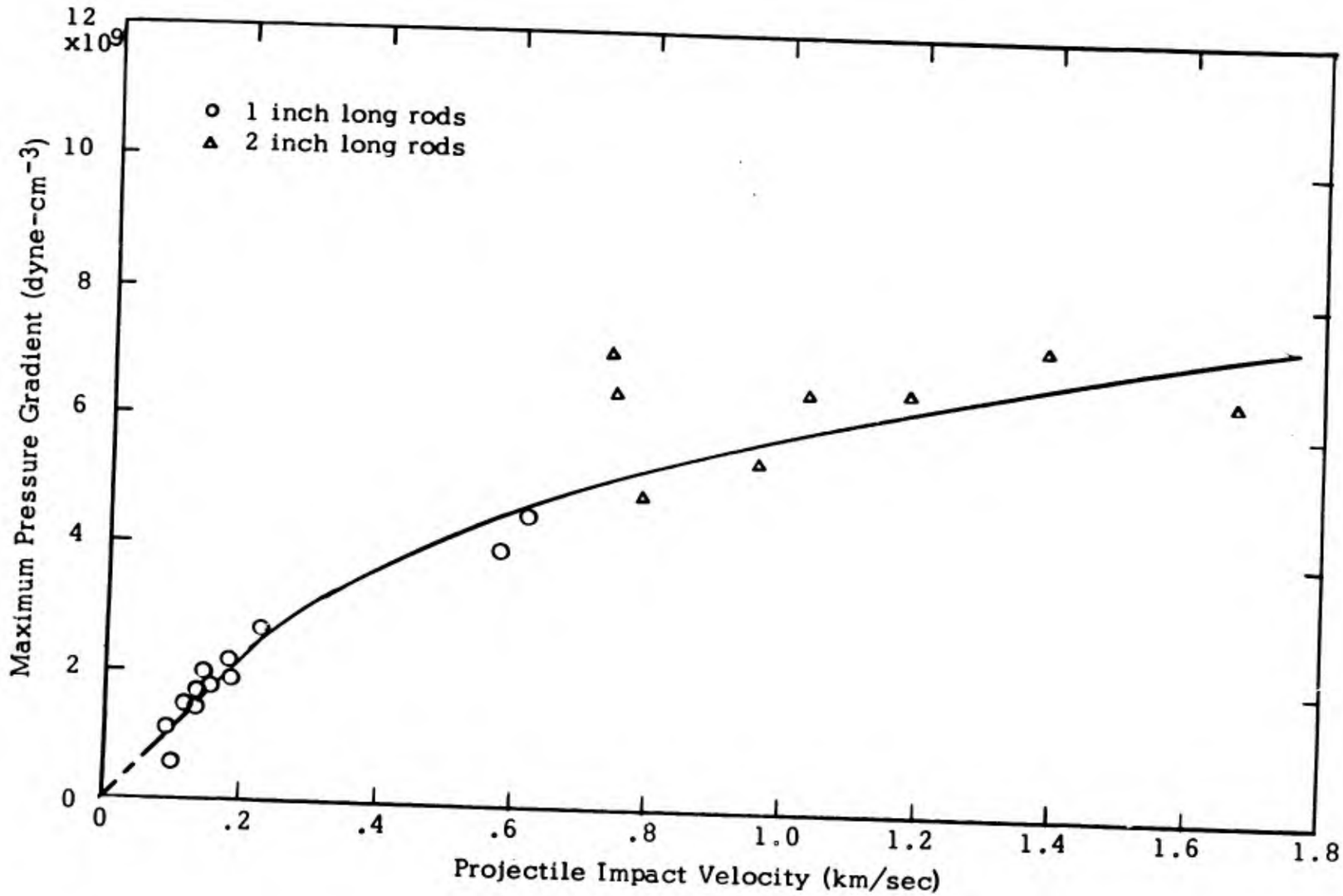

Figure 17. Maximum pressure gradient as a function of projectile impact velocity for phenolic.

3.3 Results of Thin-Plate-Impact Experiments

It was mentioned earlier that rebound of the projectile in the thin-plate-impact experiment might account for the values of τ in Table I being higher than those for the rod-elongation experiment. Rebound velocities were not measured, so it is not certain that this explanation is correct.

Figure 18 shows the degree of deformation plotted as a function of distance from the point of impact for two specimens. The plots show that maximum deformation occurs at a distance of about one-half the radius of the projectile from the point of impact.

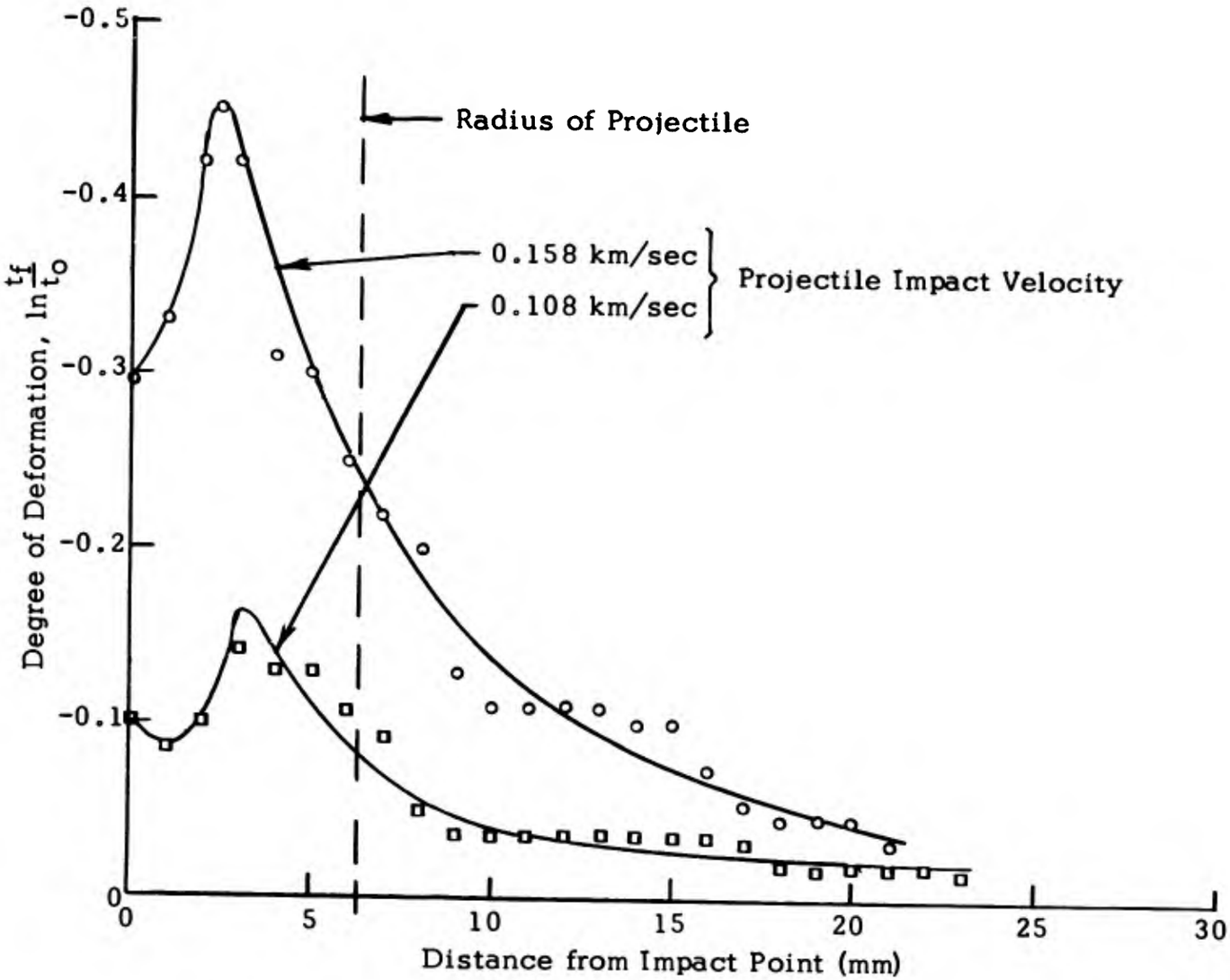

Figure 18. Degree of deformation as a function of distance from the point of impact for two 1/16 inch thick copper plates deformed by 1/2 inch diameter steel balls.

4. DISCUSSION OF RESULTS

4.1 Differential Equations of Disk Crushing

The disk-crushing experiment uses two hardened-steel anvils, one fixed and one driven by a testing machine or shot from a gun. The disk is placed on the fixed anvil and some lubricant used to reduce friction. If a relatively thin disk is crushed between two unyielding anvils at a velocity which is low compared with wave velocity in the material, we may assume that the material is incompressible, inelastic, and that flow is laminar without friction with the anvils. With unyielding anvils and no stored elastic energy, the energy of crushing can be determined by measuring the testing machine force and travel distance or by measuring velocity and mass of the anvil shot from a gun. The time history of the deformation can be determined as well as the total energy involved.

The geometry of the problem is as shown in Figure 19.

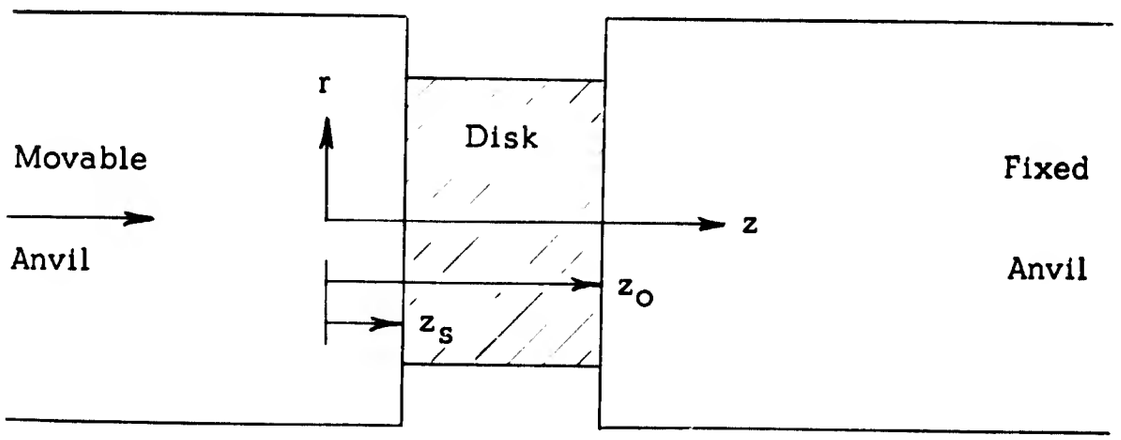

Figure 19. Geometry of the disk-crushing experiment.

The subscripts used are as follows: o = initial condition, f = final condition, s = measurement made at the moving surface.

Neglecting body forces, the equations of continuity, motion, and energy for the system may be written in cylindrical coordinates as follows:

Continuity

$$\frac{\partial \rho}{\partial t} + \frac{1}{r}\frac{\partial}{\partial r}(\rho r v_r) + \frac{1}{r}\frac{\partial}{\partial \theta}(\rho v_\theta) + \frac{\partial}{\partial z}(\rho v_z) = 0 \qquad (1)$$

Motion (r component)

$$\rho\left(\frac{\partial v_r}{\partial t} + v_r\frac{\partial v_r}{\partial r} + \frac{v_\theta}{r}\frac{\partial v_r}{\partial \theta} - \frac{v_\theta^2}{r} + v_z\frac{\partial v_r}{\partial z}\right) =$$

$$-\frac{\partial p}{\partial r} - \left[\frac{1}{r}\frac{\partial}{\partial r}(r\tau_{rr}) + \frac{1}{r}\frac{\partial \tau_{r\theta}}{\partial \theta} - \frac{\tau_{\theta\theta}}{r} + \frac{\partial \tau_{rz}}{\partial z}\right] \qquad (2)$$

(θ component)

$$\rho\left(\frac{\partial v_\theta}{\partial t} + v_r\frac{\partial v_\theta}{\partial r} + \frac{v_\theta}{r}\frac{\partial v_\theta}{\partial \theta} + \frac{v_r v_\theta}{r} + v_z\frac{\partial v_\theta}{\partial z}\right) =$$

$$-\frac{1}{r}\frac{\partial p}{\partial \theta} - \left[\frac{1}{r^2}\frac{\partial}{\partial r}(r^2\tau_{r\theta}) + \frac{1}{r}\frac{\partial \tau_{\theta\theta}}{\partial \theta} + \frac{\partial \tau_{\theta z}}{\partial z}\right] \qquad (3)$$

(z component)

$$\rho\left(\frac{\partial v_z}{\partial z} + v_r\frac{\partial v_z}{\partial r} + \frac{v_\theta}{r}\frac{\partial v_z}{\partial \theta} + v_z\frac{\partial v_z}{\partial z}\right) =$$

$$-\frac{\partial p}{\partial z} - \left[\frac{1}{r}\frac{\partial}{\partial r}(r\tau_{rz}) + \frac{1}{r}\frac{\partial \tau_{\theta z}}{\partial \theta} + \frac{\partial \tau_{zz}}{\partial z}\right] \qquad (4)$$

The τ terms are the components of the stress tensor.

Internal Energy U

$$\rho\frac{DU}{Dt} = \rho\left(\frac{\partial U}{\partial z} + v_r\frac{\partial U}{\partial r} + \frac{v_\theta}{r}\frac{\partial U}{\partial \theta} + v_z\frac{\partial U}{\partial z}\right) =$$

$$-\left(\frac{1}{r}\frac{\partial}{\partial r}(rq_r) + \frac{1}{r}\frac{\partial q_\theta}{\partial \theta} + \frac{\partial q_z}{\partial z}\right) - p\left[\frac{1}{r}\frac{\partial}{\partial r}(rv_r) + \frac{1}{r}\frac{\partial v_\theta}{\partial \theta} + \frac{\partial v_z}{\partial z}\right]$$

$$-\left[\tau_{rr}\frac{\partial v_r}{\partial r} + \tau_{\theta\theta}\left(\frac{1}{r}\frac{\partial v_\theta}{\partial \theta} + \frac{v_r}{r}\right) + \tau_{zz}\frac{\partial v_z}{\partial z}\right] \qquad (5)$$

$$-\tau_{r\theta}\left[r\frac{\partial}{\partial r}\left(\frac{v_\theta}{r}\right) + \frac{1}{r}\frac{\partial v_r}{\partial \theta}\right] \tau_{\theta z}\left(\frac{1}{r}\frac{\partial v_z}{\partial \theta} + \frac{\partial v_\theta}{\partial z}\right) - \tau_{rz}\left(\frac{\partial v_z}{\partial r} + \frac{\partial v_r}{\partial z}\right)$$

These equations may be simplified by the symmetry of the problem and by the assumptions mentioned.

One simple flow pattern assumes that the z velocity decreases linearly from that at the moving anvil to zero at the fixed anvil. We assume $\partial p/\partial z = 0$ during the time of interest after the first waves have passed through the disk. If the material is incompressible, the radial flow is then determined. The rate at which the piston displaces material at a portion of the circular disk of radius r is equal to the rate at which material flows out through the curved sides of the cylinder at r.

$$\pi r^2 v_s = 2\pi r (z_o - z_s) v_r \qquad (6)$$

$$v_r = \frac{r v_s}{2(z_o - z_s)}$$

$$v_z = \frac{v_s (z_o - z)}{(z_o - z_s)} \qquad z_o \geq z \geq z_s \qquad (7)$$

v_s is a function of time and describes the motion of the moving anvil.

By symmetry $\frac{\partial}{\partial\theta} = 0$, $v_\theta = 0$, $\tau_{r\theta} = 0$, $\tau_{z\theta} = 0$

The continuity equation (1), becomes

$$\frac{\partial v_r}{\partial r} + \frac{v_r}{r} + \frac{\partial v_z}{\partial z} = 0 \tag{8}$$

Equations 6 and 7 satisfy this continuity equation.

The θ component equation of motion is identically zero.

The r and z component equations become:

$$\rho\left(\frac{\partial v_r}{\partial t} + v_r\frac{\partial v_r}{\partial r}\right) = -\frac{\partial p}{\partial r} - \left[\frac{\partial \tau_{rr}}{\partial r} + \frac{\tau_{rr}}{r} - \frac{\tau_{\theta\theta}}{r}\right] \tag{9}$$

$$\rho\left(\frac{\partial v_z}{\partial t} + v_z\frac{\partial v_z}{\partial z}\right) = -\frac{\partial \tau_{zz}}{\partial z} \tag{10}$$

Considering these equations with 6 and 7, we see that by observing the dynamic deformation, v_s and $z_o - z_s$, we can make important deductions as to material properties. By the assumed flow, relative material motion in the z direction is uniform throughout the disk, so $\partial\tau_{zz}/\partial z = 0$. v_z and v_r can then be determined by observing v_s and z_s.

In the energy equation, the pressure term is zero, as is seen by substituting Equations 6 and 7 into it. This is a result of the assumption of incompressibility. Heat transfer is neglected so the q terms are zero. The energy equation then becomes

$$\rho\frac{DU}{Dt} = \rho\frac{\partial U}{\partial t} + \rho v_r\frac{\partial U}{\partial r} + \rho v_z\frac{\partial U}{\partial z} =$$

$$-\left(\tau_{rr}\frac{\partial v_r}{\partial r} + \tau_{\theta\theta}\frac{v_r}{r} + \tau_{zz}\frac{\partial v_z}{\partial z}\right) \tag{11}$$

This equation can be simplified further by using Equations 6 and 7.

$$\rho \frac{DU}{Dt} = - \frac{v_s}{z_o - z_s} \left(\frac{\tau_{rr}}{2} + \frac{\tau_{\theta\theta}}{2} + \tau_{zz} \right) \qquad (12)$$

Note that τ_{zz} is opposite in sign to τ_{rr} and $\tau_{\theta\theta}$ and $\partial v_z/\partial z$ is opposite to $\partial v_r/\partial r$ and v_r/r. The term in parenthesis may be lumped into one strength term τ.

Equation 12 provides a means of measuring τ and also τ_{rr}, $\tau_{\theta\theta}$ and τ_{zz} since when the material is deforming to a large degree, the three terms are probably about equal.

At low impact velocities, the strain is dominated by the dissipative τ term and is probably fairly uniform throughout the material. Under the assumptions, the dissipation is uniform throughout the disk so the substantial derivative can be replaced by dU/dt. Thus, the energy equation is of the simple form

$$\rho \frac{dU}{dt} = - \frac{\tau}{(z_o - z_s)} \frac{dz_s}{dt}$$

For τ constant,

$$\rho U = \tau \ln \frac{z_o}{z_f} \qquad (13)$$

where z_o and z_f are initial and final thickness of the disk.

The actual nature of τ can be investigated by measuring deviations from Equation 13 as strain rate or total strain is changed. Various useful approximate equations can be written based on experimental evidence. As an example, τ may be written with terms giving the strain-rate effect, the work-hardening effect and possible work-softening effects.

$$\tau = a + b\left(1 - e^{\frac{-\dot{z}/z}{c}}\right) + d\left(1 - e^{\frac{-U}{f}}\right) + g\left(1 + e^{\frac{-U}{h}}\right) \qquad (14)$$

The a coefficient is determined by static strength, the b term is determined by the magnitude of the strain-rate effect while c determines the strain-rate at which the effect becomes significant. Similarly, d and f determine the work-hardening effect depending on total energy dissipated

or U and g and h represent a work-softening effect which dominates at higher energies.

The functional relationship among these variables may be quite different from that indicated here for some materials and some impact conditions. Under the brief exploratory program conducted so far, using copper, aluminum, and some plastics, the ideas embodied in Equation 14 seem adequate since τ is only weakly dependent on strain or strain rate and the constant term, a, dominates.

The experimental difficulties of separating friction effects from strain-hardening effects make the determination of d and f difficult.

One approach to correcting for friction uses the following model. An infinitesimal area $2\pi r\, dr$ on the disk at radius r from the center moves with velocity $r\, v_s/2(z_o-z_s)$. The power going into heat due to friction on this area is

$$P_f = \frac{F\, C_f\, \pi\, r^2\, v_s\, dr}{Z_o - Z_s}$$

where F is the force per unit area under the test conditions and C_f is the coefficient of friction. Integrating from r = 0 to the outer radius R and multiplying by 2 to include both faces of the disk, gives the total power going into friction as

$$P_f = \frac{2\, F\, C_f\, \pi v_s\, R^3}{3\, (Z_o - Z_s)}$$

$v_s/(Z_o-Z_s)$ can be expressed in terms of R using Equation 6; P_f then becomes

$$P_f = \frac{4}{3} F\, C_f\, \pi\, v_r\, R^2$$

or

$$dW = \frac{4}{3} F\, C_f\, \pi R^2\, dR$$

where W is the frictional energy. Integrating from initial to final disk radius

$$W = \frac{4}{9} F C_f \pi (R^3 - R_o^3) \qquad (15)$$

Disk mass is proportional to R^3 for disks of the same relative dimensions, so energy per unit mass contributed by friction is independent of disk size for disks of the same relative length to diameter.

4.2 Analysis of a Disk-Crushing Experiment

Figure 20 shows an oscillogram of light intensity as a function of time as light passing through a slit is cut off by a projectile as it deforms a copper disk. Figure 21, which was obtained by differentiating the curve in Figure 20, shows a plot of projectile velocity as a function of time. A plot of acceleration as a function of time, obtained by differentiation of the velocity curve, is shown in Figure 22. All data for this shot are given in Table III. Data for a similar shot at higher velocity are shown in Table IV.

The energy going into the disk, computed from the dynamic data, agrees closely with that obtained from measurements of rod velocity and mass. The low rebound velocity of the rod indicates that less than 5 per cent of the kinetic energy of the rod goes into recoverable elastic energy of anvils and disk at these impact velocities.

A rough estimate of the ratio of power going into the acceleration of material to that being dissipated in the material is given by comparing the rate of change of kinetic energy of the material with the rate of change of internal energy. These energies are plotted in Figure 23 for the data of Table I. Note the different scales for internal energy and kinetic energy. The maximum slopes indicate that the maximum power going into internal energy is 60 times that going into kinetic energy. Impact velocity would have to go up from 3.52×10^3 cm/sec to about 2.8×10^4 cm/sec for power going into kinetic energy to equal that going into internal. Unfortunately, tests cannot be made to see how internal energy behaves at this impact velocity since the disk would be so thin that friction with the anvil faces would dominate the process; also, the anvils could not be considered rigid.

These dynamic measurements have been used to compare integrated power data with total impact energy as computed from rod velocity and mass, and to compare instantaneous pressure with static testing-machine pressure data. No effort has been made to find the time function which satisfies the equations of motion. It is interesting to note that the maximum pressures indicated by the two dynamic shots are 7.9×10^9 and 8.6×10^9 dyne/cm^2. The agreement between these two shots at different velocities allows a good estimate to be made of the strength of copper under flow conditions. A disk pressed to similar

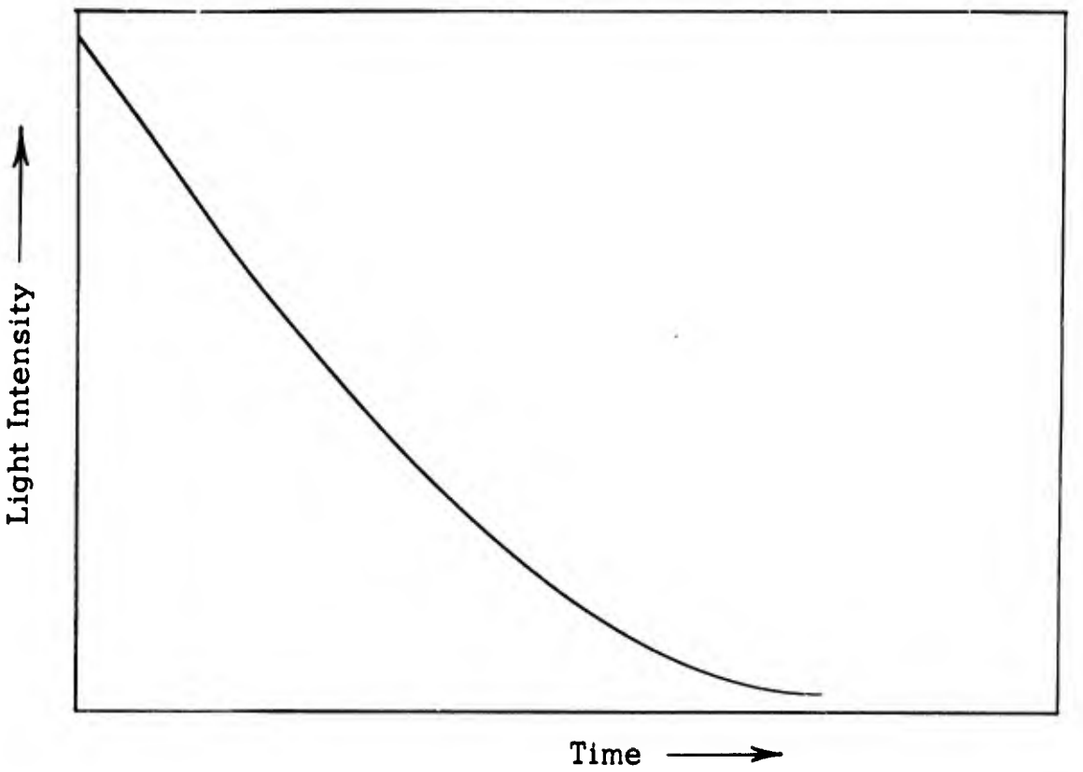

Figure 20. Sketch showing light intensity as a function of time as light passing through a slit is cut off by a projectile as it deforms a copper disk.

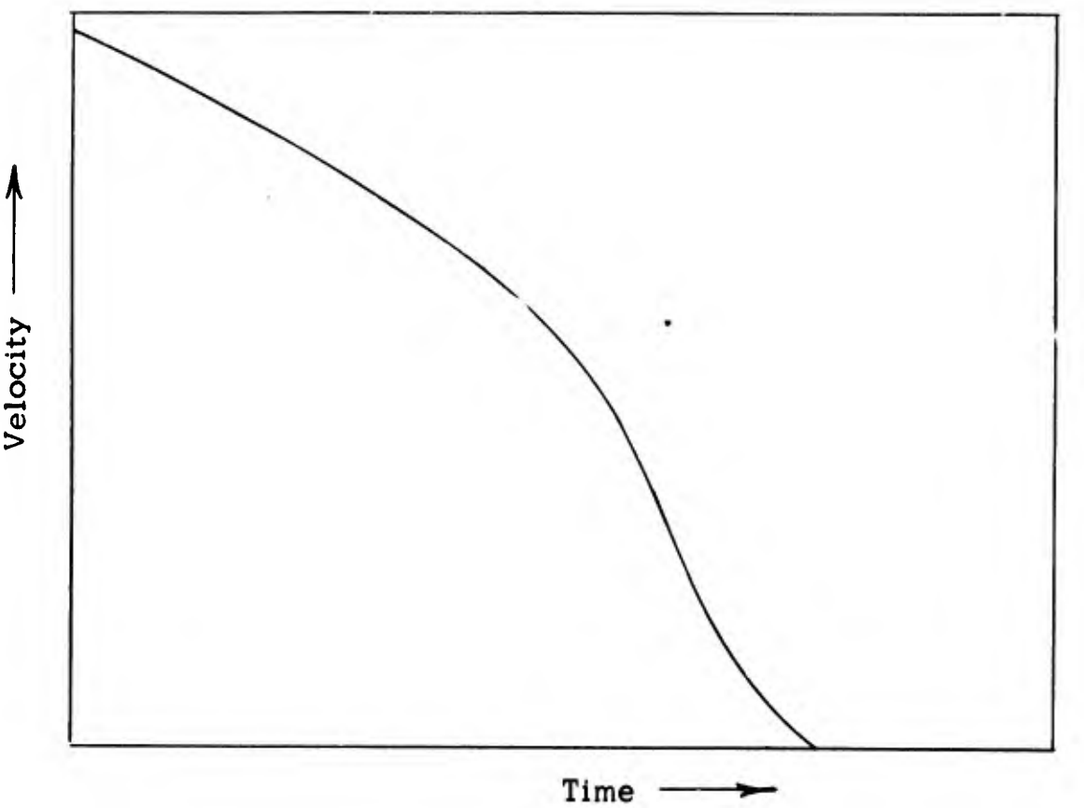

Figure 21. Plot of projectile velocity as a function of time obtained by differentiating the curve in Figure 20.

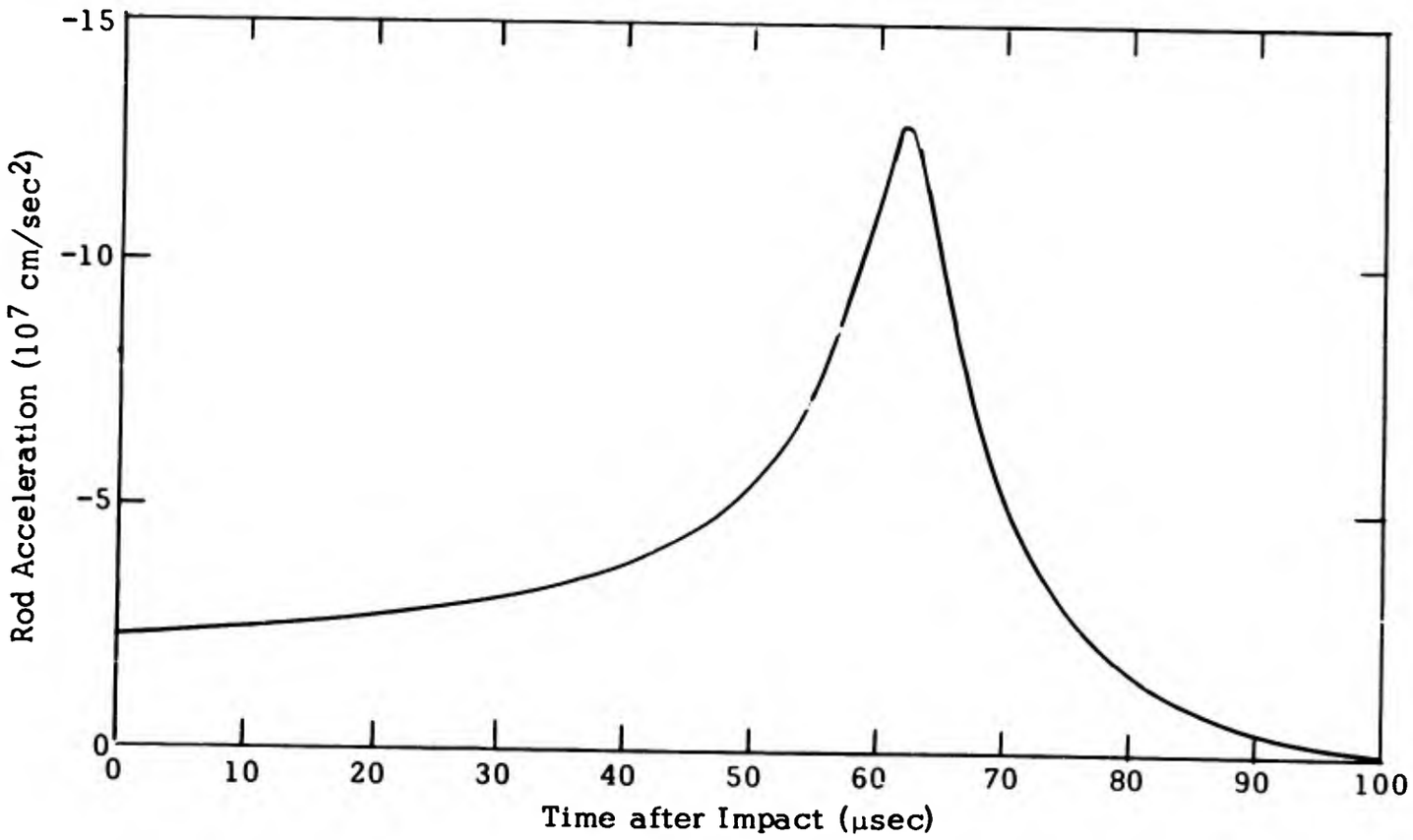

Figure 22. Acceleration of the moving-rod anvil as a function of time.

TABLE III. Data from Rod-Displacement Measurements for Impact of a Hardened-Steel Rod on a Copper Disk

Rod

Steel
1/2" diameter x 2" long
Mass = 49.9 g

Copper Disk

Initial Diameter = .470 cm
Initial Thickness = .213 cm
Final Diameter = .990 cm
Final Thickness = .048 cm
Mass = 0.330 g

Rod velocity 3.52×10^3 cm/sec
Kinetic energy 30.9 joule

Time After Impact (μsec)	Distance Moved After Impact (cm)	Disk Thickness (cm)	Disk Radius (cm)	Rod Velocity (10^3 cm/sec)	Rod Acceleration (10^7 cm/sec^2)	Axial Velocity Gradient $\left(\frac{10^3 \text{ cm/sec}}{\text{cm}}\right)$	Radial Velocity of Disk (10^3 cm/sec)
0	0	.213	.235	3.51	-2.2	16.5	1.94
8	.027	.186	.251	3.32	-2.4	17.8	2.24
16	.052	.161	.270	3.12	-2.2	19.3	2.61
24	.076	.137	.292	2.92	-2.8	21.3	3.08
32	.099	.114	.320	2.69	-3.2	23.4	3.72
40	.119	.094	.354	2.42	-3.8	25.8	4.48
48	.138	.075	.396	2.08	-4.9	27.8	5.43
56	.152	.061	.439	1.58	-8.2	25.9	6.19
64	.162	.051	.480	0.68	-11.4	13.3	6.03
72	.164	.049	.489	0.15	-4.0	3.1	3.09
76	.165	.048	.495	0	-2.5	0	0

TABLE III. (Continued)

Time After Impact (μsec)	Force (10^9 dyne)	Power (10^{12} erg/sec)	Integrated Energy (10^7 erg)	Pressure (10^9 dyne/cm^2)
0	1.10	3.86	0	6.33
8	1.20	3.98	3.12	6.06
16	1.30	4.05	6.28	5.67
24	1.40	4.08	9.51	5.22
32	1.60	4.30	12.89	4.96
40	1.90	4.60	16.44	4.82
48	2.44	5.08	20.28	4.95
56	4.09	6.46	24.75	6.76
64	5.68	3.86	29.50	7.85
72	2.00	.30	30.81	2.68
76	1.25	0	30.85	1.98

TABLE IV. Data from Rod-Displacement Measurements for Impact of a Hardened-Steel Rod on a Copper Disk

Rod

Steel
1/2" diameter x 2" long
Mass = 49.9 g

Copper Disk

Initial Thickness = 0.249 cm
Final Thickness = 0.026 cm
Change in Thickness = 0.223 cm

Impact velocity = 4.58×10^3 cm/sec
Kinetic energy of projectile = 52.4 joules

Time After Impact (μsec)	Distance Traveled by Rod (cm)	Disk Thickness (cm)	Disk Radius (cm)	Disk Area (cm^2)	Rod Velocity (10^3 cm/sec)	Rod Acceleration (10^7 cm/sec^2)	Velocity Gradient $\left(\frac{10^4 \text{ cm/sec}}{\text{cm}}\right)$
0	0	.249	.237	.177	4.58	-0.464	1.84
8	.039	.208	.259	.210	4.50	-1.10	2.16
11	.048				4.58	-1.43	
16	.074	.171	.286	.257	4.40	-2.10	2.57
24	.108	.135	.322	.326	4.20	-3.30	3.11
31	.136				3.81	-5.33	
32	.140	.102	.370	.430	3.81	-5.10	3.74
40	.167	.073	.439	.606	3.32	-7.60	4.55
44						-9.16	
48	.190	.049	.534	.896	2.58	-12.70	5.26
51	.198				2.12	-16.9	
54	.204	.034	.643	1.30	1.57	-21.0	4.62
55	.206	.032	.660	1.37	1.25	-2[illegible]	3.90
56	.206	.032	.660	1.37	1.15	-1[illegible]	3.59
60	.209	.029	.694	1.51	0.61	-9.86	2.10
64	.211	.027	.720	1.63	0.30	-6.60	1.11
70	.212	.026	.734	1.69	0	-4.01	0

TABLE IV. (Continued)

Time After Impact (μsec)	Force (10^9 dyne)	Power (10^{12} erg/sec)	Pressure (10^9 dyne/cm^2)
0	.231	1.06	1.31
8	.548	2.46	2.61
11			
16	1.04	3.51	4.05
24	1.64	6.88	5.04
31			
32	2.54	9.69	5.40
40	3.78	12.6	6.23
44			
48	6.33	16.3	7.08
51	8.41	17.8	
54	10.5	16.5	8.09
55	11.78	14.7	8.60
56	9.51	10.9	6.95
60	4.92	3.00	3.26
64	3.29	0.987	2.02
70	2.00	0	1.18

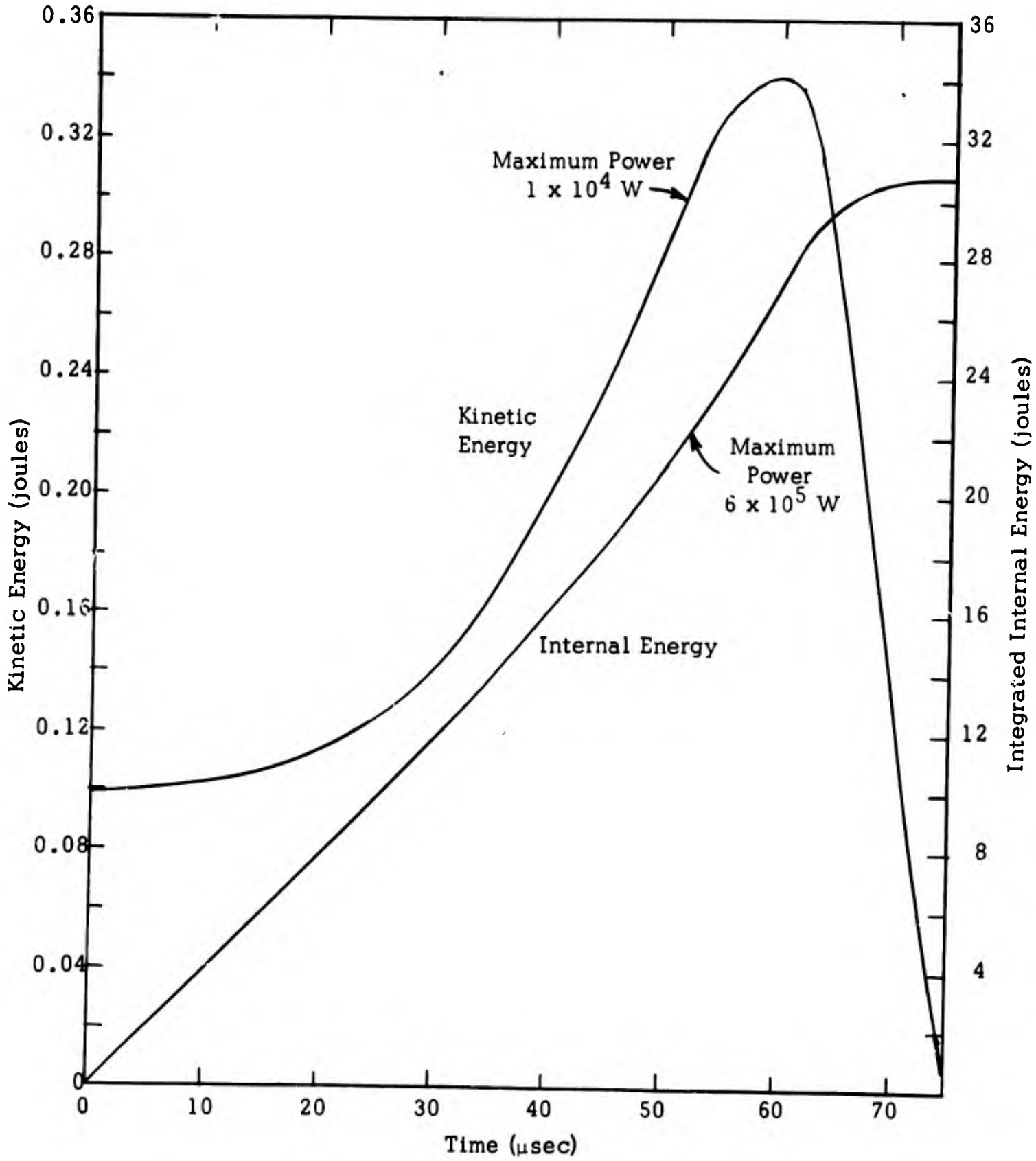

Figure 23. Kinetic energy of disk material compared with internal energy of material for the data of Table I.

thickness in a testing machine shows higher pressure, about 12×10^9 dyne/cm^2. The machine-tested disks were barrel-shaped after compression while those tested at high velocity were nearly right cylinders with straight sides. This probably indicates greater friction in the testing machine.

5. DERIVATION OF STRESS EQUATION

The stress or strength equation used in PART I

$$\tau = \mu_o \frac{\partial v}{\partial x} \pm \tau_o \qquad \text{(Eq. 5, Part I)}$$

describes a Bingham material. This simple model was found to be adequate in the theoretical program as far as it was developed.

The equation for aluminum, used in all computations, was derived from Figure 9. The results in Figure 9 are adequately described by the equation

$$\rho U = \tau \ln (z_o/z_f)$$

where τ is given by Equation 5 above. τ_o comes directly from the initial slope of the curve. (In this case the slope changes only slightly over the entire range). τ_o was determined to be 5.4×10^9 for 6061 Al and 2.1×10^9 for pure Al. (cgs units are used). The value 5.43×10^9 was used as the nominal value in most calculations. μ_o was determined from the difference between static and dynamic curves. The value of $\partial v/\partial x$ was approximately 3×10^4, obtained by dividing disk thickness by impact velocity for a shot which produced $z_f/z_o = 0.3$. A static test producing the same thickness ratios was compared with this. With all terms known in the above two equations except μ_o, this can be calculated. The value obtained was 1.0×10^4 (cgs units). Thus Equation 5 becomes

$$\tau = (1.0 \times 10^4) \frac{\partial v}{\partial x} \pm 5.4 \times 10^9$$

6. CONCLUSIONS

The disk-crushing experiment gives quantitative measurements of the energy involved in the flow of solid materials and is useful where the material to be tested is less rigid than the anvils. The assumptions made in the simplified analysis are adequate for small deformations and can be corrected from the experimental results. Dynamic measurements can be made and the effects of strain rate and strain hardening on the strength of materials can be determined. These data make it possible to compare materials as to their resistance to flow deformation, and they provide necessary data for a theoretical analysis of the impact problem.

The rod-to-rod-impact experiment gives comparative data concerning the maximum pressure gradients developed during impact. These data indicate the relative strengths of materials, including brittle substances such as glass, under the specific conditions involved.

7. APPENDIX

Section 7.1 contains a list of symbols used in the text and in the tables in Section 7.2. These tables contain all data concerning the disk-crushing experiments.

7.1 List of Symbols

Symbol	Units	Description
r_o	cm	Original radius of a test specimen
r_f	cm	Final radius of a test specimen
z_o	cm	Original thickness of a test specimen
z_f	cm	Final thickness of a test specimen
m	g	Mass
t_o	cm	Original thickness of a thin-plate specimen
t_f	cm	Final thickness of a thin-plate specimen
v_p	km/sec	Impact velocity of a projectile
E	joules	Deformation energy
E_k	joules	Kinetic energy of a projectile
E_{sp}	joules/gram	Specific energy of a deformed specimen
d	---	The natural logarithm of $(r_o/r_f)^2$, z_f/z_o or t_f/t_o in a deformed specimen. This is called the degree of deformation.
D	units	In a uniformly deformed specimen, D is the product of the mass and the degree of deformation. In a non-uniformly deformed specimen, $D = \sum_i m_i d_i$; where the specimen is divided into an arbitrary number, i, of uniformly deformed units.
τ	joules/unit	The proportionality constant relating energy to deformation

7.2 Tables of Data

Tables A-1 to A-19.

TABLE A-1. Data concerning the crushing of unannealed copper disks under dynamic conditions. The original nominal dimensions of the disks were 1/4-inch diameter by 1/8-inch thick.

Shot No.	r_o (cm)	z_o (cm)	r_f (cm)	z_f (cm)	m (g)	v_p (km/sec)	E_k (joules)	E_{sp} (joules)	(z_f/z_o)	d $\lvert \ln z_f/z_o \rvert$	D (units)	τ (joules/unit)
24	.317	.310	.332	.292	.87	.0173	3.78	4.35	.943	.059	.051	74
25	.315	.310	.332	.264	.86	.0195	4.80	5.59	.870	.139	.119	40
26	.315	.305	.353	.241	.84	.0274	9.50	11.3	.791	.234	.196	48
27	.317	.312	.368	.233	.88	.0318	12.8	14.6	.748	.290	.255	50
28	.312	.320	.384	.224	.87	.0377	18.0	20.6	.699	.358	.317	58
29	.315	.302	.419	.170	.84	.0434	23.8	28.5	.563	.574	.481	50
31	.317	.312	.439	.170	.88	.0490	30.4	34.6	.545	.606	.533	57
32	.317	.305	.449	.157	.86	.0480	29.2	34.0	.516	.662	.570	51
33	.317	.305	.502	.135	.89	.0577	42.1	47.5	.441	.819	.728	58
34	.320	.307	.534	.112	.88	.0625	49.4	56.3	.364	1.01	.890	56
35	.317	.302	.556	.104	.85	.0654	54.0	63.4	.344	1.07	.910	59
36	.310	.307	.330	.267	.83	.0207	5.41	6.54	.868	.141	.117	46
37	.315	.317	.353	.251	.88	.0286	10.7	12.1	.791	.234	.205	52
38	.310	.320	.358	.246	.85	.0310	12.2	14.3	.770	.262	.223	55
39	.310	.307	.381	.221	.82	.0318	12.8	15.6	.719	.329	.270	47
40	.307	.310	.396	.188	.82	.0416	21.9	26.8	.606	.500	.410	54
41	.310	.317	.441	.170	.85	.0506	32.4	38.4	.535	.625	.531	62
44	.307	.310	.524	.112	.82	.0614	47.6	58.2	.360	1.02	.835	57
120	.322	.317	.338	.287	.915	.0143	5.10	5.55	.904	.101	.092	56
121	.322	.307	.363	.249	.890	.0192	9.19	10.3	.810	.210	.187	49
122	.322	.307	.505	.142	.890	.0396	39.0	43.9	.462	.771	.686	57
124	.325	.320	.505	.140	.943	.0422	44.5	47.1	.436	.830	.782	57
126	.317	.317	.490	.132	.898	.0424	44.6	49.8	.416	.876	.786	57
127	.322	.320	.505	.135	.934	.0435	47.1	50.4	.420	.866	.809	58
128	.322	.320	.556	.096	.934	.0512	65.4	70.0	.302	1.20	1.12	58
129	.322	.315	.701	.064	.915	.0600	89.8	97.9	.202	1.60	1.46	62

TABLE A-2. Data concerning the crushing of annealed copper disks under dynamic conditions. The original nominal dimensions of the disks were 1/4-inch diameter by 1/8-inch thick.

Shot No.	r_o (cm)	z_o (cm)	r_f (cm)	z_f (cm)	m (g)	v_p (km/sec)	E_k (joules)	E_{sp} (joules)	(z_f/z_o)	d $\lvert \ln z_f/z_o \rvert$	D (units)	τ (joules/unit)
46	.315	.320	.381	.221	.890	.0302	11.5	13.0	.691	.370	.329	35
47	.317	.320	.350	.261	.900	.0139	4.81	5.35	.826	.191	.172	28
48	.315	.325	.388	.216	.900	.0233	13.6	15.1	.664	.410	.369	37
50	.317	.325	.434	.173	.916	.0306	23.3	25.4	.531	.632	.578	40
52	.315	.330	.353	.264	.909	.0209	5.52	6.09	.800	.223	.203	27
53	.315	.328	.421	.180	.909	.0416	22.0	24.6	.550	.598	.544	41
54	.312	.320	.482	.140	.864	.0533	36.0	41.7	.436	.830	.716	50
55	.315	.330	.539	.117	.909	.0618	48.4	53.4	.354	1.04	.944	51
56	.312	.325	.477	.140	.900	.0367	33.6	37.4	.430	.844	.759	44
58	.317	.330	.488	.140	.916	.0389	37.8	41.4	.423	.860	.788	48
135	.320	.312	.358	.249	.890	.0150	5.61	6.30	.797	.226	.201	28
136	.320	.317	.488	.137	.900	.0385	37.0	41.1	.432	.839	.754	49
137	.322	.317	.615	.094	.916	.0495	61.1	66.6	.296	1.22	1.12	55

TABLE A-3. Data concerning the crushing of unannealed copper disks under static conditions. The original nominal dimensions of the disks were 1/4-inch diameter by 1/8-inch thick.

Test No.	r_o (cm)	z_o (cm)	r_f (cm)	z_f (cm)	m (g)	E (joules)	E_{sp} (joules)	(z_f/z_o)	d $\lvert \ln z_f/z_o \rvert$	D (units)	τ (joules/unit)
1	.322	.312	.617	.089	.908	53.8	59.3	.284	1.26	1.14	47
2	.312	.322	.594	.094	.881	60.0	68.1	.291	1.23	1.08	55
3	.312	.332	.594	.098	.908	64.1	70.6	.290	1.24	1.12	57
4	.315	.325	.604	.091	.899	50.6	56.4	.281	1.27	1.14	44
5	.320	.322	.330	.302	.916	1.98	2.16	.937	.065	.595	33
7	.317	.322	.322	.315	.908	.502	.554	.976	.024	.218	23
8	.312	.325	.358	.259	.890	8.05	9.05	.798	.226	.201	40
9	.317	.322	.330	.290	.899	3.23	3.60	.898	.108	.097	33
10	.317	.322	.330	.294	.899	3.30	3.67	.913	.091	.082	40
11	.312	.322	.330	.287	.881	3.59	4.07	.890	.117	.103	35
21	.322	.317	.325	.315	.916	.024	.026	.992	.008	.007	4
22	.317	.317	.322	.302	.890	.311	.350	.952	.049	.044	8
23	.322	.315	.373	.236	.908	6.29	6.93	.750	.288	.261	24

TABLE A-4. Data concerning the crushing of annealed copper disks under static conditions. The original nominal dimensions of the disks were 1/4-inch diameter by 1/8-inch thick.

Test No.	r_o (cm)	z_o (cm)	r_f (cm)	z_f (cm)	m (g)	E (joules)	E_{sp} (joules)	(z_f/z_o)	d $\lvert \ln z_f/z_o \rvert$	D (units)	τ (joules/unit)
31	.317	.322	.597	.092	.908	68.3	76.3	.283	1.26	1.14	61
32	.317	.320	.584	.099	.908	57.9	63.8	.310	1.17	1.06	55
33	.317	.320	.551	.109	.908	48.7	53.7	.341	1.06	.963	51
34	.317	.320	.530	.119	.908	41.4	45.5	.373	.986	.895	46
35	.315	.322	.456	.130	.908	32.3	35.6	.401	.914	.829	39
36	.317	.317	.451	.158	.890	21.3	23.9	.496	.703	.625	34
37	.317	.315	.371	.228	.875	6.51	7.45	.726	.321	.281	23
38	.317	.322	.356	.256	.908	4.20	4.63	.795	.229	.208	25

TABLE A-5. Data concerning the crushing of unannealed copper disks under dynamic conditions. The original nominal dimensions of the disks were 1/8-inch diameter by 1/16-inch thick.

Shot No.	r_o (cm)	z_o (cm)	r_f (cm)	z_f (cm)	m (g)	v_p (km/sec)	E_k (joules)	E_{sp} (joules)	(z_f/z_o)	d $\lvert \ln z_f/z_o \rvert$	D (units)	τ (joules/unit)
18	.160	.160	.234	.079	.113	.0184	4.28	37.8	.492	.709	.080	53
19	.158	.163	.297	.051	.113	.0253	8.10	71.7	.312	1.16	.131	62
20	.160	.163	.401	.033	.116	.0320	12.9	112.	.203	1.59	.184	71
21	.160	.163	.185	.119	.113	.0155	3.04	26.9	.735	.308	.035	84
22	.160	.163	.363	.033	.113	.0309	12.1	107	.203	1.59	.180	67
23	.160	.160	.444	.025	.115	.0359	16.3	142	.159	1.77	.204	80
115	.165	.160	.292	.056	.122	.0184	8.43	69.3	.350	1.05	.128	66
116	.165	.168	.398	.030	.127	.0272	18.4	145	.182	1.70	.216	85
117	.165	.165	.254	.092	.125	.0130	4.21	33.6	.555	.589	.074	57
130	.165	.153	.434	.025	.126	.0266	17.6	152	.167	1.79	.208	85
131	.165	.163	.452	.023	.124	.0273	18.5	150	.141	1.96	.243	77

TABLE A-6. Data concerning the crushing of annealed copper disks under dynamic conditions. The original nominal dimensions of the disks were 1/8-inch diameter by 1/16-inch thick.

Shot No.	r_o (cm)	z_o (cm)	r_f (cm)	z_f (cm)	m (g)	v_p (km/sec)	E_k (joules)	E_{sp} (joules)	(z_i/z_o)	d $\lvert \ln z_f/z_o \rvert$	D (units)	τ (joules/unit)
61	.160	.160	.234	.079	.113	.0173	3.79	33.6	.492	.709	.080	48
62	.163	.163	.290	.051	.118	.0242	7.40	62.5	.312	1.16	.137	54
63	.160	.160	.358	.033	.112	.0286	10.3	91.9	.206	1.58	.175	58
64	.160	.158	.452	.023	.111	.0350	15.5	139	.145	1.93	.214	72
65	.168	.160	.284	.056	.123	.0166	6.87	56.0	.350	1.05	.129	53
66	.163	.160	.294	.053	.116	.0181	8.16	70.6	.334	1.10	.128	64
67	.160	.160	.358	.036	.114	.0222	12.3	113	.222	1.50	.171	75
68	.160	.160	.439	.023	.112	.0265	17.5	156	.143	1.94	.217	81
138	.165	.160	.246	.074	.122	.0135	4.54	37.3	.460	.776	.095	48
139	.165	.160	.320	.041	.122	.0195	9.48	77.8	.254	1.37	.167	57

TABLE A-7. Data concerning the crushing of unannealed copper disks under static conditions. The original nominal dimensions of the disks were 1/8-inch diameter by 1/16-inch thick.

Test No.	r_o (cm)	z_o (cm)	r_f (cm)	z_f (cm)	m (g)	E (joules)	E_{sp} (joules)	(z_f/z_o)	d $\lvert \ln z_f/z_o \rvert$	D (units)	τ (joules/unit)
12	.158	.157	.280	.073	.108	5.28	48.9	.371	.990	.108	49
13	.160	.163	.338	.089	.116	3.08	26.6	.547	.602	.070	44
14	.170	.163	.173	.157	.132	.187	1.42	.970	.030	.004	47
15	.163	.163	.165	.152	.120	.098	.82	.938	.064	.008	13
16	.165	.163	.168	.157	.122	.042	.35	.969	.031	.004	9

TABLE A-8. Data concerning the crushing of annealed copper disks under static conditions. The original nominal dimensions of the disks were 1/8-inch diameter by 1/16-inch thick.

Test No.	r_o (cm)	z_o (cm)	r_f (cm)	z_f (cm)	m (g)	E (joules)	E_{sp} (joules)	(z_f/z_o)	d $\lvert \ln z_f/z_o \rvert$	D (units)	τ (joules/unit)
39	.161	.160	.234	.119	.116	5.07	43.8	.746	.293	.034	150
40	.161	.163	.248	.112	.118	1.11	9.40	.688	.374	.044	25
41	.163	.163	.267	.092	.118	1.59	13.5	.564	.562	.066	24
42	.163	.163	.276	.086	.118	2.35	19.9	.531	.633	.075	32
43	.163	.163	.274	.079	.118	3.15	26.7	.484	.726	.086	36
44	.164	.160	.253	.071	.122	3.91	32.1	.444	.812	.099	40
45	.161	.163	.256	.066	.118	4.27	36.2	.406	.900	.106	40

TABLE A-9. Data concerning the crushing of unannealed copper disks under dynamic conditions. The original nominal dimensions of the disks were 3/16-inch diameter by 3/32-inch thick.

Shot No.	r_o (cm)	z_o (cm)	r_f (cm)	z_f (cm)	m (g)	v_p (km/sec)	E_k (joules)	Esp (joules)	(z_f/z_o)	d $\lvert \ln z_f/z_o \rvert$	D (units)	τ (ioules/unit)
119	.232	.224	.273	.170	.337	.0144	5.16	15.3	.761	.273	.092	56
132	.236	.221	.481	.053	.345	.0359	32.1	93.0	.241	1.42	.490	66
133	.235	.213	.511	.048	.329	.0352	30.9	93.8	.226	1.49	.490	63
134	.237	.249	.724	.028	.392	.0458	52.3	133	.112	2.18	.853	61

TABLE A-10. Data concerning the crushing of annealed copper disks under dynamic conditions. The original nominal dimensions of the disks were 3/16-inch diameter by 3/32-inch thick.

Shot No.	r_o (cm)	z_o (cm)	r_f (cm)	z_f (cm)	m (g)	v_p (km/sec)	E_k (joules)	E_{sp} (joules)	(z_f/z_o)	d $\lvert \ln z_f/z_o \rvert$	D (units)	τ (joules/unit)
69	.248	.244	.301	.170	.419	.0212	5.69	13.6	.698	.360	.151	38
70	.248	.242	.333	.147	.414	.0258	8.41	20.3	.610	.494	.204	41
71	.249	.236	.351	.127	.419	.0318	12.8	30.6	.537	.621	.260	49
72	.250	.239	.386	.094	.394	.0376	17.9	45.3	.394	.931	.367	49
73	.249	.239	.427	.081	.414	.0428	23.2	56.0	.340	1.08	.447	52
74	.246	.234	.500	.053	.394	.0521	34.4	87.1	.228	1.48	.583	59
75	.239	.239	.296	.158	.380	.0155	6.00	15.8	.660	.415	.158	38
76	.240	.239	.323	.132	.384	.0191	9.10	23.7	.553	.592	.227	40
77	.240	.242	.349	.120	.388	.0230	13.2	33.0	.495	.703	.273	47
78	.240	.236	.432	.084	.377	.0314	24.6	65.2	.355	1.04	.392	63
79	.235	.236	.480	.064	.363	.0379	35.9	99.0	.269	1.31	.475	80
80	.235	.236	.404	.091	.362	.0283	19.9	55.1	.387	.949	.343	58
81	.234	.239	.571	.043	.362	.0399	39.7	110	.181	1.71	.619	64
141	.238	.246	.369	.165	.388	.0158	6.23	16.0	.670	.400	.155	40
142	.238	.254	.483	.064	.400	.0358	31.9	79.8	.250	1.39	.556	57
143	.238	.249	.693	.033	.392	.0453	51.1	131	.133	2.02	.792	60

TABLE A-11. Data concerning the crushing of unannealed copper disks under static conditions. The original nominal dimensions of the disks were 3/16-inch diameter by 3/32-inch thick.

Test No.	r_o (cm)	z_o (cm)	r_f (cm)	z_f (cm)	m (g)	E_k (joules)	E_{sp} (joules)	(z_f/z_o)	d $\lvert \ln z_f/z_o \rvert$	D (units)	τ (joules/unit)
17	.231	.241	.236	.226	.359	.554	1.54	.936	.066	.024	23
18	.234	.238	.233	.236	.360	.082	.228	.990	.010	.004	23
19	.234	.231	.236	.228	.353	.045	.128	.990	.010	.004	13
24	.238	.231	.264	.196	.364	1.04	2.86	.846	.167	.061	17
25	.238	.238	.241	.234	.376	.007	.019	.979	.022	.008	1

TABLE A-12. Data concerning the crushing of unannealed copper disks under dynamic conditions. The original nominal dimensions of the disks were 1/4-inch diameter by 1/16-inch thick.

Shot No.	r_o (cm)	z_o (cm)	r_f (cm)	z_f (cm)	m (g)	v_p (km/sec)	E_k (joules)	Esp (joules)	(z_f/z_o)	d $\lvert \ln z_f/z_o \rvert$	D (units)	τ (joules/unit)
1	.318	.190	.378	.122	.54	.0250	7.80	14.4	.640	.446	.24	32
2	.318	.175	.336	.155	.50	.0148	2.78	5.56	.884	.123	.062	45
3	.318	.175	.465	.081	.51	.0410	21.2	41.6	.464	.767	.39	54
4	.318	.165	.543	.061	.46	.0500	31.6	68.7	.369	.996	.46	68
5	.320	.170	.561	.058	.49	.0525	34.8	71.0	.343	1.07	.52	67
6	.318	.173	.707	.033	.48	.0593	44.5	92.8	.191	1.65	.79	56
7	.318	.157	.429	.086	.45	.0319	12.9	28.9	.549	.600	.27	49
16	.317	.163	.353	.132	.45	.0155	3.04	6.76	.813	.207	.093	33
17	.318	.160	.338	.142	.45	.0140	2.48	5.51	.890	.116	.052	48

TABLE A-13. Data concerning the crushing of unannealed copper disks under dynamic conditions. The original nominal dimensions of the disks were 1/4-inch diameter by 3/64-inch thick.

Shot No.	r_o (cm)	z_o (cm)	r_f (cm)	z_f (cm)	m (g)	v_p (km/sec)	E_k (joules)	E_{sp} (joules)	(z_f/z_o)	d $\lvert \ln z_f/z_o \rvert$	D (units)	τ (joules/unit)
8	.320	.130	.386	.086	.37	.0226	6.45	17.3	.666	.406	.15	43
9	.320	.132	.419	.074	.37	.0258	8.41	22.6	.558	.583	.22	39
10	.318	.127	.456	.061	.36	.0312	12.3	34.4	.480	.734	.26	47
11	.320	.124	.508	.051	.36	.0360	16.4	46.4	.408	.896	.32	52
12	.320	.124	.556	.041	.36	.0425	22.8	64.6	.326	1.12	.40	58
13	.320	.135	.579	.038	.38	.0458	26.6	68.9	.283	1.26	.48	55
14	.318	.124	.609	.099	.35	.0162	3.32	9.48	.796	.228	.080	42

TABLE A-14. Data concerning the crushing of 99.99 percent pure aluminum disks under dynamic conditions. The original nominal dimensions of the disks were 1/4-inch diameter by 1/8-inch thick.

Shot No.	r_o (cm)	z_o (cm)	r_f (cm)	z_f (cm)	m (g)	v_p (km/sec)	E_k (joules)	E_{sp} (joules)	(z_f/z_o)	d $\lvert \ln z_f/z_o \rvert$	D (units)	τ (joules/unit)
83	.320	.307	.404	.203	.265	.0218	6.01	22.6	.660	.415	.110	55
84	.320	.307	.434	.183	.267	.0260	8.56	32.1	.595	.519	.317	62
85	.320	.302	.483	.142	.260	.0328	13.6	52.1	.470	.755	.196	69
86	.320	.328	.487	.132	.286	.0381	18.4	64.3	.403	.908	.260	71
87	.320	.317	.590	.097	.275	.0430	23.4	88.5	.304	1.19	.327	74
88	.320	.302	.665	.074	.260	.0475	28.6	110	.244	1.41	.367	78
89	.320	.330	.381	.244	.286	.0218	6.01	21.0	.739	.302	.086	70
90	.320	.317	.406	.208	.275	.0236	7.05	25.6	.656	.421	.116	61
92	.320	.320	.495	.142	.278	.0356	16.0	57.5	.444	.811	.226	71
93	.320	.320	.554	.114	.278	.0403	20.6	74.1	.357	1.03	.286	72
94	.320	.320	.664	.094	.278	.0445	25.0	90.0	.294	1.22	.339	74
95	.317	.320	.368	.244	.270	.0181	4.14	15.3	.761	.273	.074	69
96	.312	.320	.394	.216	.265	.0234	6.91	26.0	.675	.392	.104	66
97	.317	.315	.465	.150	.269	.0325	13.4	49.8	.475	.744	.200	67
98	.317	.317	.508	.135	.270	.0358	16.2	60.0	.424	.858	.231	69
99	.317	.320	.569	.107	.270	.0411	21.4	79.3	.334	1.10	.296	72
100	.317	.312	.608	.094	.264	.0431	23.6	89.5	.301	1.20	.317	75

TABLE A-15. Data concerning the crushing of 99.99 percent pure aluminum disks under static conditions. The original nominal dimensions of the disks were 1/4-inch diameter by 1/8-inch thick.

Test No.	r_o (cm)	z_o (cm)	r_f (cm)	z_f (cm)	m (g)	E (joules)	E_{sp} (joules)	(z_f/z_o)	d $\lvert \ln z_f/z_o \rvert$	D (units)	τ (joules/unit)
66	.315	.322	.470	.142	.260	10.9	42	.441	.820	.213	51
67	.307	.325	.470	.140	.254	9.7	38	.429	.850	.216	45
68	.312	.317	.465	.142	.248	9.8	39	.447	.806	.200	48
74	.307	.325	.353	.250	.255	2.2	8.6	.772	.258	.066	33
75	.312	.322	.422	.175	.253	7.0	28	.546	.605	.153	63
77	.310	.327	.587	.095	.263	18.3	70	.291	1.24	.326	56

TABLE A-16. Data concerning the crushing of 6061-T4 aluminum disks under dynamic conditions. The original nominal dimensions of the disks were 1/4-inch diameter by 1/8-inch thick.

Shot No.	r_o (cm)	z_o (cm)	r_f (cm)	z_f (cm)	m (g)	v_p (km/sec)	Ek (joules)	Esp (joules)	(z_f/z_o)	d $\lvert \ln z_f/z_o \rvert$	D (units)	τ (joules/unit)
101	.320	.322	.335	.300	.281	.0157	3.12	11.1	.930	.073	.020	153
102	.320	.317	.348	.272	.276	.0238	7.15	26.0	.856	.155	.043	168
103	.322	.315	.373	.244	.276	.0309	12.1	44.0	.774	.256	.071	172
104	.317	.317	.391	.216	.270	.0362	16.6	61.5	.680	.386	.104	159
105	.317	.317	.404	.203	.270	.0400	20.2	74.8	.640	.446	.120	167
106	.322	.317	.427	.188	.278	.0452	25.9	93.0	.592	.524	.146	178
107	.320	.320	.480	.150	.276	.0528	35.2	128	.468	.759	.209	169

TABLE A-17. Data concerning the crushing of 6061-T6 aluminum disks under dynamic conditions. The original nominal dimensions of the disks were 1/4-inch diameter by 1/8-inch thick.

Shot No.	r_o (cm)	z_o (cm)	r_f (cm)	z_f (cm)	m (g)	v_p (km/sec)	E_k (joules)	E_{sp} (joules)	(z_f/z_o)	d $\lvert \ln z_f/z_o \rvert$	D (units)	τ (joules/unit)
108	.315	.315	.327	.290	.267	.0197	4.91	18.5	.920	.083	.022	222
109	.315	.299	.376	.229	.251	.0318	12.8	51.0	.763	.270	.068	189
110	.317	.320	.396	.216	.273	.0412	21.5	78.9	.675	.393	.107	200
111	.315	.310	.439	.170	.261	.0486	30.0	115	.549	.599	.156	192
112	.317	.317	.465	.152	.268	.0555	39.0	145	.480	.733	.197	198
113	.317	.320	.500	.132	.273	.0611	47.4	174	.4[illegible]	.886	.242	196

TABLE A-18. Data concerning the crushing of disks of various plastics under dynamic conditions. The original nominal dimensions of the disks were 1/4-inch diameter by 1/8-inch thick.

Shot No.	r_o (cm)	z_o (cm)	r_f (cm)	z_f (cm)	m (g)	v_p (km/sec)	E_k (joules)	E_{sp} (joules)	(z_f/z_o)	d $\lvert \ln z_f/z_o \rvert$	D (units)	τ (joules/unit)	Material
145	.322	.327	.436	.185	.129	.0184	8.46	65.6	.565	.571	.074	115	Lexan
146	.325	.320	.411	.203	.127	.0183	8.37	66.0	.635	.455	.058	145	Lexan
147	.322	.325	.451	.183	.128	.0224	12.5	97.8	.562	.575	.074	170	Lexan
148	.320	.327	.436	.183	.126	.0226	12.7	101	.555	.590	.074	171	Lexan
149	.322	.330	.436	.183	.130	.0228	13.1	101	.554	.590	.077	171	Lexan
150	.322	.325	.401	.216	.128	.0175	7.65	59.8	.664	.410	.052	146	Lexan
151	.322	.322	.373	.241	.125	.0132	4.35	34.8	.755	.281	.035	124	Lexan
152	.325	.322	.465	.168	.128	.0271	18.4	144	.520	.655	.084	220	Lexan
160	.327	.315	.416	.201	.134	.0186	8.65	64.5	.637	.450	.060	143	Lexan
161	.325	.322	.441	.178	.127	.0232	13.5	106	.550	.595	.076	178	Lexan
163	.322	.320	.366	.254	.127	.0144	5.19	40.9	.794	.230	.029	178	Lexan
155	.322	.320	.409	.201	.100	.0138	4.76	47.6	.627	.466	.047	102	Polyethylene
156	.320	.322	.376	.241	.100	.0116	3.36	33.6	.746	.294	.029	114	Polyethylene
158	.317	.330	.399	.216	.241	.0152	5.77	24.0	.654	.424	.102	54	Teflon
159	.317	.322	.378	.241	.238	.0113	3.19	13.4	.748	.290	.069	46	Teflon
179	.320	.325	.346	.280	.092	.0118	3.48	37.8	.859	.152	.014	249	Polypropylene
180	.320	.322	.363	.262	.092	.0142	5.04	54.8	.810	.210	.019	261	Polypropylene
181	.320	.302	.460	.158	.087	.0194	9.41	101	.520	.651	.057	155	Polypropylene
183	.320	.322	.561	.117	.094	.0238	14.5	154	.363	1.01	.095	153	Polypropylene
184	.317	.320	.327	.307	.115	.0120	3.55	30.9	.960	.041	.005	754	Nylon
185	.317	.320	.353	.264	.114	.0169	7.15	62.8	.845	.168	.019	374	Nylon
188	.317	.320	.406	.208	.116	.0241	14.4	125	.650	.430	.050	291	Nylon
190	.317	.325	.450	.175	.113	.0275	18.9	163	.540	.617	.070	264	Nylon
192	.317	.330	.510	.140	.118	.0295	22.3	189	.423	.860	.102	220	Nylon
193	.317	.327	.596	.081	.118	.0341	28.9	245	.248	1.39	.164	176	Nylon

TABLE A-19. Data concerning the crushing of disks of various plastics under static conditions. The original nominal dimensions of the disks were 1/4-inch diameter by 1/8-inch thick.

Test No.	r_o (cm)	z_o (cm)	r_f (cm)	z_f (cm)	m (g)	E (joules)	E_{sp} (joules)	(z_f/z_o)	d $\lvert \ln z_f/z_o \rvert$	D (units)	τ (joules/unit)	Material
47	.317	.325	.505	.132	.236	4.16	17.7	.406	.901	.212	20	Teflon
50	.317	.325	.515	.122	.238	4.69	19.7	.375	.981	.234	20	Teflon
48	.325	.322	.545	.122	.100	5.62	56.2	.378	.973	.097	58	Polyethylene
51	.322	.325	.568	.099	.102	6.32	62.1	.304	1.19	.121	52	Polyethylene
49	.322	.327	.464	.200	.129	5.77	44.8	.611	.493	.064	91	Lexan
52	.322	.327	.444	.177	.129	5.53	42.9	.541	.614	.079	70	Lexan
64	.317	.335	.500	.140	.118	12.8	108	.416	.875	.103	123	Nylon
65	.317	.327	.501	.137	.116	12.7	110	.418	.871	.101	126	Nylon
72	.320	.320	.340	.287	.118	2.00	17.0	.895	.155	.018	110	Nylon
73	.320	.310	.446	.165	.110	8.20	74.6	.532	.630	.069	118	Nylon
78	.320	.320	.574	.102	.112	17.9	159	.318	1.14	.128	139	Nylon
79	.320	.322	.644	.081	.114	22.8	200	.253	1.27	.145	138	Nylon
69	.320	.320	.553	.112	.092	7.30	79.5	.349	1.06	.097	75	Polypropylene
70	.320	.327	.563	.109	.094	7.10	75.5	.334	1.10	.104	69	Polypropylene
71	.320	.317	.555	.109	.091	7.20	79.1	.344	1.07	.097	74	Polypropylene

Unclassified
Security Classification

DOCUMENT CONTROL DATA - R&D
(Security classification of title, body of abstract and indexing annotation must be entered when the overall report is classified)

1. ORIGINATING ACTIVITY *(Corporate author)*
Utah Research & Development Co., Inc.
1820 South Industrial Road
Salt Lake City, Utah 84104

2a. REPORT SECURITY CLASSIFICATION
Unclassified

2b GROUP

3 REPORT TITLE
THEORETICAL AND EXPERIMENTAL STUDY OF LOW-VELOCITY PENETRATION PHENOMENA

4. DESCRIPTIVE NOTES *(Type of report and inclusive dates)*
Final Report May 1964 - August 1966

5. AUTHOR(S) *(Last name, first name, initial)*
Cannon, Emerson T., Palmer, E. Paul

6. REPORT DATE	7a. TOTAL NO. OF PAGES	7b. NO. OF REFS
November 1966	147	23

8a. CONTRACT OR GRANT NO.	9a. ORIGINATOR'S REPORT NUMBER(S)
DA19-129-AMC-150(X)	
b. PROJECT NO. ARPA Order No. 267	
c.	9b. OTHER REPORT NO(S) *(Any other numbers that may be assigned this report)*
d.	

10. AVAILABILITY/LIMITATION NOTICES
Distribution of this document is unlimited. Release to CFSTI is authorized.

11. SUPPLEMENTARY NOTES	12. SPONSORING MILITARY ACTIVITY
	U. S. Army Natick Laboratories Natick, Massachusetts 01760

13. ABSTRACT This final report on Contract DA19-129-AMC-150(X) reports the development of a computer code for solving impact problems. The code uses moving mass points which have all the field variables such as pressure, energy, and stress associated with the points. The fields and their gradients determine the forces on the masses and change as the points move. The code was tested in a one-dimensional problem where it was found to produce correct results. The ideas embodied in this work appear to have sufficient value to justify research to extend them to three-dimensional impact problems.

An investigation was carried out on equations of state for materials of interest in armor development. A summary of existing data is given. A simple equation is given for the shock compression of metals and other materials and a computer code is given for calculating adiabatic expansions from a shock-compressed state.

A complete report is given on an experimental program to measure material properties. The emphasis in the work is on measuring the energy involved in large-scale deformation of materials. Measurements were made by crushing disks of the test material in testing machines and by ballistic impacts. Measurements were also made on rod-to-rod impacts and on impacts of steel balls on thin plates of the test materials. Ultimate strength of materials was measured by measuring maximum acceleration of a free surface in rod-to-rod impact. Techniques and results of the research are reported.

DD FORM 1 JAN 64 1473

Unclassified
Security Classification

Unclassified
Security Classification

14 KEY WORDS	LINK A		LINK B		LINK C	
	ROLE	WT	ROLE	WT	ROLE	WT
Development	8					
Mathematical models	9					
Coding	9		10			
Computers	9		10			
Determination	4					
Impact strength	4					
Materials	4		9			
Armor	4		4			
Prediction			8			
Penetration			9			
Low-velocity			0			

INSTRUCTIONS

1. ORIGINATING ACTIVITY: Enter the name and address of the contractor, subcontractor, grantee, Department of Defense activity or other organization *(corporate author)* issuing the report.

2*a*. REPORT SECURITY CLASSIFICATION: Enter the overall security classification of the report. Indicate whether "Restricted Data" is included. Marking is to be in accordance with appropriate security regulations.

2*b*. GROUP: Automatic downgrading is specified in DoD Directive 5200.10 and Armed Forces Industrial Manual. Enter the group number. Also, when applicable, show that optional markings have been used for Group 3 and Group 4 as authorized.

3. REPORT TITLE: Enter the complete report title in all capital letters. Titles in all cases should be unclassified. If a meaningful title cannot be selected without classification, show title classification in all capitals in parenthesis immediately following the title.

4. DESCRIPTIVE NOTES: If appropriate, enter the type of report, e.g., interim, progress, summary, annual, or final. Give the inclusive dates when a specific reporting period is covered.

5. AUTHOR(S): Enter the name(s) of author(s) as shown on or in the report. Enter last name, first name, middle initial. If military, show rank and branch of service. The name of the principal author is an absolute minimum requirement.

6. REPORT DATE: Enter the date of the report as day, month, year, or month, year. If more than one date appears on the report, use date of publication.

7*a*. TOTAL NUMBER OF PAGES: The total page count should follow normal pagination procedures, i.e., enter the number of pages containing information.

7*b*. NUMBER OF REFERENCES: Enter the total number of references cited in the report.

8*a*. CONTRACT OR GRANT NUMBER: If appropriate, enter the applicable number of the contract or grant under which the report was written.

8*b*, 8*c*, & 8*d*. PROJECT NUMBER: Enter the appropriate military department identification, such as project number, subproject number, system numbers, task number, etc.

9*a*. ORIGINATOR'S REPORT NUMBER(S): Enter the official report number by which the document will be identified and controlled by the originating activity. This number must be unique to this report.

9*b*. OTHER REPORT NUMBER(S): If the report has been assigned any other report numbers *(either by the originator or by the sponsor)*, also enter this number(s).

10. AVAILABILITY/LIMITATION NOTICES: Enter any limitations on further dissemination of the report, other than those imposed by security classification, using standard statements such as:

(1) "Qualified requesters may obtain copies of this report from DDC."

(2) "Foreign announcement and dissemination of this report by DDC is not authorized."

(3) "U. S. Government agencies may obtain copies of this report directly from DDC. Other qualified DDC users shall request through

_____."

(4) "U. S. military agencies may obtain copies of this report directly from DDC. Other qualified users shall request through

_____."

(5) "All distribution of this report is controlled. Qualified DDC users shall request through

_____."

If the report has been furnished to the Office of Technical Services, Department of Commerce, for sale to the public, indicate this fact and enter the price, if known.

11. SUPPLEMENTARY NOTES: Use for additional explanatory notes.

12. SPONSORING MILITARY ACTIVITY: Enter the name of the departmental project office or laboratory sponsoring *(paying for)* the research and development. Include address.

13. ABSTRACT: Enter an abstract giving a brief and factual summary of the document indicative of the report, even though it may also appear elsewhere in the body of the technical report. If additional space is required, a continuation sheet shall be attached.

It is highly desirable that the abstract of classified reports be unclassified. Each paragraph of the abstract shall end with an indication of the military security classification of the information in the paragraph, represented as *(TS)*, *(S)*, *(C)*, *or (U)*.

There is no limitation on the length of the abstract. However, the suggested length is from 150 to 225 words.

14. KEY WORDS: Key words are technically meaningful terms or short phrases that characterize a report and may be used as index entries for cataloging the report. Key words must be selected so that no security classification is required. Identifiers, such as equipment model designation, trade name, military project code name, geographic location, may be used as key words but will be followed by an indication of technical context. The assignment of links, rules, and weights is optional

Unclassified
Security Classification